



# (De/Re)-Composition of Data-Parallel Computations via Multi-Dimensional Homomorphisms

ARI RASCH, University of Muenster, Germany

Data-parallel computations, such as linear algebra routines and stencil computations, constitute one of the most relevant classes in parallel computing, e.g., due to their importance for deep learning. Efficiently de-composing such computations for the memory and core hierarchies of modern architectures and re-composing the computed intermediate results back to the final result—we say *(de/re)-composition* for short—is key to achieve high performance for these computations on, e.g., GPU and CPU. Current high-level approaches to generating data-parallel code are often restricted to a particular subclass of data-parallel computations and architectures (e.g., only linear algebra routines on only GPU or only stencil computations), and/or the approaches rely on a user-guided optimization process for a well-performing (de/re)-composition of computations, which is complex and error prone for the user.

We formally introduce a systematic (de/re)-composition approach, based on the algebraic formalism of Multi-Dimensional Homomorphisms (MDHs). Our approach is designed as general enough to be applicable to a wide range of data-parallel computations and for various kinds of target parallel architectures. To efficiently target the deep and complex memory and core hierarchies of contemporary architectures, we exploit our introduced (de/re)-composition approach for a correct-by-construction, parametrized cache blocking, and parallelization strategy. We show that our approach is powerful enough to express, in the same formalism, the (de/re)-composition strategies of different classes of state-of-the-art approaches (scheduling-based, polyhedral, etc.), and we demonstrate that the parameters of our strategies enable systematically generating code that can be fully automatically optimized (auto-tuned) for the particular target architecture and characteristics of the input and output data (e.g., their sizes and memory layouts). Particularly, our experiments confirm that via auto-tuning, we achieve higher performance than state-of-the-art approaches, including hand-optimized solutions provided by vendors (such as NVIDIA cuBLAS/cuDNN and Intel oneMKL/oneDNN), on real-world datasets and for a variety of data-parallel computations, including linear algebra routines, stencil and quantum chemistry computations, data mining algorithms, and computations that recently gained high attention due to their relevance for deep learning.

CCS Concepts: • **Computing methodologies** → **Parallel computing methodologies**; *Machine learning*; • **Theory of computation** → **Program semantics**; • **Software and its engineering** → **Compilers**;

Additional Key Words and Phrases: Code generation, data parallelism, auto-tuning, GPU, CPU, OpenMP, CUDA, OpenCL, linear algebra, stencils computation, quantum chemistry, data mining, deep learning

A full version of this article is provided by Rasch [2024], which presents our novel concepts with all of their formal details. In contrast to the full version, this article relies on a simplified formal foundation for better illustration and easier understanding. We often refer the interested reader to Rasch [2024] for formal details that should not be required for understanding the basic ideas and concepts of our approach.

This work was funded by the Deutsche Forschungsgemeinschaft (DFG, German Research Foundation)—project PPP-DL (470527619).

Author's Contact Information: Ari Rasch (Corresponding author), University of Muenster, Muenster, Germany; e-mail: a.rasch@uni-muenster.de.

Permission to make digital or hard copies of all or part of this work for personal or classroom use is granted without fee provided that copies are not made or distributed for profit or commercial advantage and that copies bear this notice and the full citation on the first page. Copyrights for components of this work owned by others than the author(s) must be honored. Abstracting with credit is permitted. To copy otherwise, or republish, to post on servers or to redistribute to lists, requires prior specific permission and/or a fee. Request permissions from [permissions@acm.org](mailto:permissions@acm.org).

© 2024 Copyright held by the owner/author(s). Publication rights licensed to ACM.

ACM 1558-4593/2024/10-ART10

<https://doi.org/10.1145/3665643>

### ACM Reference format:

Ari Rasch. 2024. (De/Re)-Composition of Data-Parallel Computations via Multi-Dimensional Homomorphisms. *ACM Trans. Program. Lang. Syst.* 46, 3, Article 10 (October 2024), 74 pages.  
<https://doi.org/10.1145/3665643>

## 1 Introduction

Data-parallel computations constitute one of the most relevant classes in parallel computing. Important examples of such computations include linear algebra routines [Whaley and Dongarra, 1998], various kinds of stencil computations (e.g., Jacobi method and convolutions) [Hagedorn et al., 2018], quantum chemistry computations [Kim et al., 2019], and data mining algorithms [Rasch et al., 2019b]. The success of many application areas critically depends on achieving high performance for their data-parallel building blocks, on a variety of parallel architectures. For example, highly optimized linear algebra routines implementations combined with the computational power of modern GPUs currently enable deep learning to significantly outperform other existing machine learning approaches (e.g., for speech recognition and image classification).

Data-parallel computations are characterized by applying the same function (a.k.a *scalar function*) to each point in a multi-dimensional grid of data (a.k.a. *array*) and combining the obtained intermediate results in the grid's different dimensions using so-called *combine operators*.

Figures 1 and 2 illustrate data parallelism using as examples two popular computations: (1) linear algebra routine *Matrix-Vector multiplication* (MatVec) and (2) stencil computation *Jacobi* (Jacobi1D). In the case of MatVec, the grid is two-dimensional and consists of pairs, each pointing to one element of the input matrix  $M_{i,k}$  and the vector  $v_k$ . To each pair, scalar function  $f(M_{i,k}, v_k) := M_{i,k} * v_k$  (multiplication) is applied, and results in the  $i$ -dimension are combined using combine operator  $\otimes_1((x_1, \dots, x_n), (y_1, \dots, y_m)) := (x_1, \dots, x_n, y_1, \dots, y_m)$  (concatenation) and in  $k$ -dimension using operator  $\otimes_2((x_1, \dots, x_n), (y_1, \dots, y_n)) := (x_1 + y_1, \dots, x_n + y_n)$  (point-wise addition). Similarly, the scalar function of Jacobi1D is  $f(v_{i+0}, v_{i+1}, v_{i+2}) := c * (v_{i+0} + v_{i+1} + v_{i+2})$  which computes the Jacobi-specific function for an arbitrary but fixed constant  $c$ ; Jacobi1D's combine operator  $\otimes_1$  is concatenation. We formally define scalar functions and combine operators later in this article.

Achieving high performance for data-parallel computations is considered important in both academia and industry but has proven to be challenging. In particular, achieving *high performance* that is *portable* (i.e., the same program code achieves a consistently high level of performance across different architectures and characteristics of the input/output data, e.g., their size and memory layout) and in a *user-productive* way is identified as an ongoing, major research challenge. This is because for high performance, an efficient *(de/re)-composition* of computations (illustrated in Figure 3 and discussed thoroughly in this article) is required to efficiently break down a computation for the deep and complex memory and core hierarchies of state-of-the-art architectures, via efficient cache blocking and parallelization strategies. Moreover, to achieve performance that is portable across architectures, the programmer has to consider that architectures often differ significantly in their characteristics [Sun et al., 2019]—depth of memory and core hierarchies, automatically managed caches (as in CPUs) vs. manually managed caches (as in GPUs), and so on—which poses further challenges on identifying an efficient *(de/re)-composition* of computations. Productivity is often also hampered: state-of-the-art programming models (such as OpenMP [OpenMP, 2022] for CPU, CUDA [NVIDIA, 2022g] for GPU, and OpenCL [Khronos, 2022b] for multiple kinds of architectures) operate on a low abstraction level; thereby, the models require from the programmer explicitly implementing a well-performing *(de/re)-composition*, which involves complex and error-prone index computations, explicitly managing memory and threads on multiple layers, and so on.

Current high-level approaches to generating data-parallel code usually struggle with addressing in one combined approach all three challenges: *performance*, *portability*, and *productivity*. For

$$\begin{pmatrix} M_{1,1} & \dots & M_{1,K} \\ \vdots & \ddots & \vdots \\ M_{I,1} & \dots & M_{I,K} \end{pmatrix}, \begin{pmatrix} v_1 \\ \vdots \\ v_K \end{pmatrix} \xrightarrow{\text{MatVec}} \begin{array}{c} \xrightarrow{\oplus_2} \\ \begin{pmatrix} f(M_{1,1}, v_1) & \dots & f(M_{1,K}, v_K) \\ \vdots & \ddots & \vdots \\ f(M_{I,1}, v_1) & \dots & f(M_{I,K}, v_K) \end{pmatrix} \\ \downarrow \oplus_1 \end{array} = \begin{pmatrix} M_{1,1} * v_1 + \dots + M_{1,K} * v_K \\ \vdots \\ M_{I,1} * v_1 + \dots + M_{I,K} * v_K \end{pmatrix} = \begin{pmatrix} w_1 \\ \vdots \\ w_I \end{pmatrix}$$

Fig. 1. Data parallelism illustrated using the example *Matrix-Vector Multiplication* (MatVec).

$$\begin{pmatrix} v_1 \\ \vdots \\ v_N \end{pmatrix} \xrightarrow{\text{Jacobi1D}} \begin{array}{c} \begin{pmatrix} f(v_1, v_2, v_3) \\ f(v_2, v_3, v_4) \\ \vdots \end{pmatrix} \\ \downarrow \oplus_1 \end{array} = \begin{pmatrix} c * (v_1 + v_2 + v_3) \\ c * (v_2 + v_3 + v_4) \\ \vdots \end{pmatrix} = \begin{pmatrix} w_1 \\ \vdots \\ w_{N-2} \end{pmatrix}$$

Fig. 2. Data parallelism illustrated using the example *Jacobi 1D* (Jacobi1D).

example, approaches such as Halide [Ragan-Kelley et al., 2013], Apache TVM [Chen et al., 2018a], Fireiron [Hagedorn et al., 2020a], and LoopStack [Wasti et al., 2022] achieve high performance but incorporate the user into the optimization process—by requiring from the user explicitly expressing optimizations in a so-called *scheduling language*—which is error prone and needs expert knowledge about low-level code optimizations, thus hindering user’s productivity. In contrast, *polyhedral approaches*, such as Pluto [Bondhugula et al., 2008b], PPCG [Verdoolaee et al., 2013], and Facebook’s TC [Vasilache et al., 2019], are often fully automatic and thus productive but usually specifically designed toward a particular architecture (e.g., only GPU as TC and PPCG, or only CPU as Pluto) and thus not portable. *Functional approaches*, e.g., Lift [Steuer et al., 2015], are productive for functional programmers (e.g., with experience in *Haskell* [Haskell.org, 2022] programming, which relies on small, functional building blocks for expressing computations), but the approaches often have difficulties in automatically achieving the full performance potential of architectures [Rasch et al., 2019a]. Furthermore, many of the existing approaches are specifically designed toward a particular subclass of data-parallel computations only, e.g., only tensor operations (as LoopStack and TC) or only matrix multiplication (as Fireiron), or they require significant extensions for new subclasses (as Lift for matrix multiplication [Rommelg et al., 2016] and stencil computations [Hagedorn et al., 2018]), which further hinders the productivity of the user.

In this article, we formally introduce a systematic (de/re)-composition approach for data-parallel computations targeting state-of-the-art parallel architectures. We express computations via *high-level functional expressions* (specifying *what* to compute), in the form of easy-to-use higher-order functions, based on the algebraic formalism of **Multi-Dimensional Homomorphisms (MDHs)**<sup>1</sup> [Rasch and Gorlatch, 2016].<sup>2</sup> Our higher-order functions are capable of expressing various kinds of data-parallel computations (linear algebra, stencils, etc.), in the same formalism and on a high level of abstraction, independently of hardware and optimization details, thereby contributing to user’s productivity.<sup>3</sup> As target for our high-level expressions, we introduce *functional low-level expressions* (specifying *how* to compute) to formally reason about (de/re)-compositions of data-parallel computations; our low-level expressions are designed such that they can be straightforwardly transformed to executable program code (e.g., in OpenMP, CUDA, and OpenCL). To systematically lower our high-level expressions to low-level expressions, we introduce a formally sound, parameterized *lowering process*. The parameters of our lowering process enable automatically computing low-level expressions that are optimized (auto-tuned [Balaprakash et al., 2018]) for the particular target architecture and characteristics of the input/output data, thereby achieving fully automatically

<sup>1</sup><https://mdh-lang.org><sup>2</sup>We thoroughly compare to the existing MDH work in Section 6.6.<sup>3</sup>We consider as main users of our approach compiler engineers and library designers. Rasch et al. [2020b] show that our approach can also take straightforward, sequential code as input, which makes our approach attractive also to end users.

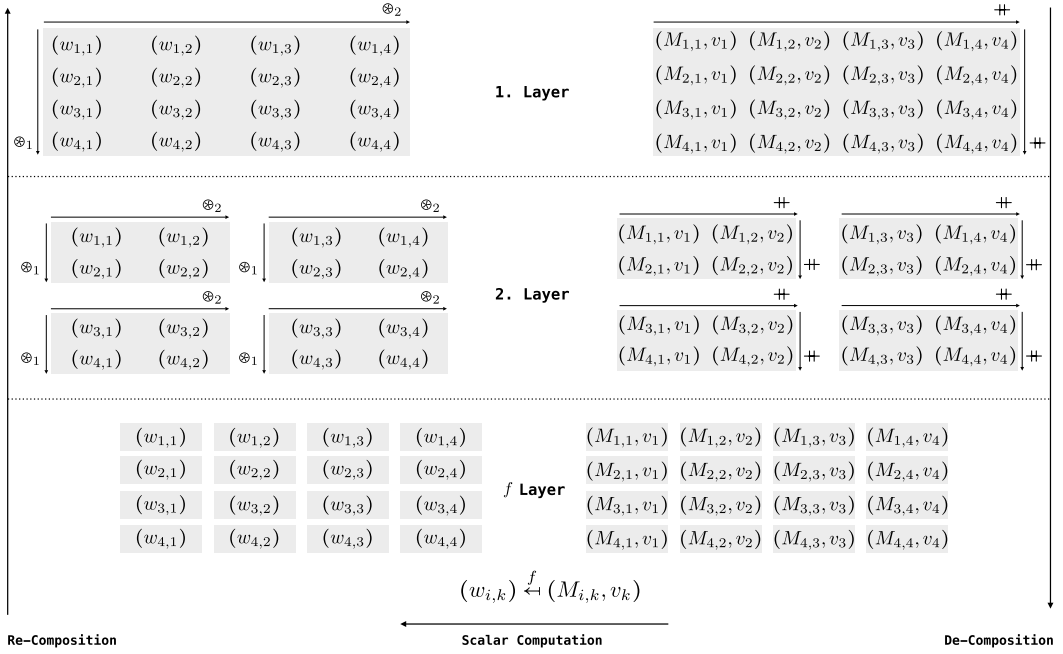


Fig. 3. Example (de/re)-composition of MatVec (Figure 1) on a  $4 \times 4$  input matrix  $M$  and a 4-sized vector  $v$ : (1) the *de-composition phase* (right part of the figure) partitions the concatenated input data into parts (a.k.a. *tiles* in programming), where  $\oplus$  denotes the concatenation operator; (2) to each part, scalar function  $f$  is applied in the *scalar phase* (bottom part of figure), which is defined for MatVec as multiplying matrix element  $M_{i,k}$  with vector element  $v_k$ , resulting in element  $w_{i,k}$ ; (3) the *re-composition phase* (figure's left part) combines the computed parts to the final result, using combine operator  $\otimes_1$  for the first dimension (defined as *concatenation* in the case of MatVec) and operator  $\otimes_2$  (point-wise *addition*) for the second dimension. All basic building blocks (*scalar function*, *combine operator*, ...) and concepts (e.g., *partitioning*) are defined in this article, based on algebraic concepts. For simplicity, this example presents a (de/re)-composition on two layers only, and we partition the input for this example into parts that have straightforward, equal sizes. Optimized values of semantics-preserving parameters (a.k.a. *tuning parameters*), such as the number of parts and the application order of combine operators, are crucial for achieving high performance, as we discuss in this article. Phases are arranged from right to left, inspired by the application order of function composition, as we also discuss later.

high, portable performance. For example, we formally introduce parameters for flexibly choosing the target memory regions for de-composed and re-composed computations and also parameters for flexibly setting an optimized data access pattern.

We show that our high-level representation is capable of expressing various kinds of data-parallel computations, including computations that recently gained high attention due to their relevance for deep learning [Barham and Isard, 2019]. For our low-level representation, we show that it can express the cache blocking and parallelization strategies of state-of-the-art parallel implementations—as generated by scheduling approach TVM and polyhedral compilers PPCG and Pluto—in one uniform formalism. Moreover, we present experimental results to confirm that based on our parameterized lowering process in combination with auto-tuning, we are able to achieve higher performance than the state of the art, including hand-optimized implementations provided by vendors (e.g., NVIDIA cuBLAS and Intel oneMKL for linear algebra routines, and NVIDIA cuDNN and Intel oneDNN for deep learning computations).

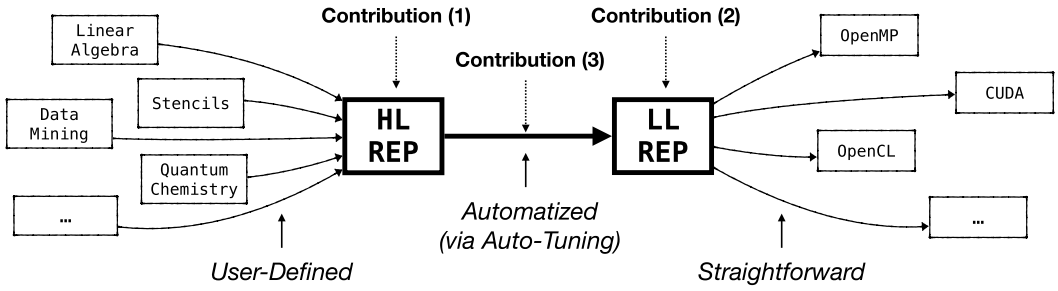


Fig. 4. Overall structure of our approach (contributions highlighted in bold).

Summarized, we make the following three major contributions (illustrated in Figure 4):

- (1) We introduce a functional **High-Level Representation (HL REP)**, based on the algebraic formalism of MDHs, that enables uniformly expressing data-parallel computations on a high level of abstraction.
- (2) We introduce a functional **Low-Level representation (LL REP)** that enables formally expressing and reasoning about (de/re)-compositions of data-parallel computations; our low-level representation is designed such that it can be straightforwardly transformed to executable program code in state-of-practice parallel programming models, including OpenMP, CUDA, and OpenCL.
- (3) We introduce a *systematic lowering process* to fully automatically lower an expression in our high-level representation to a device- and data-optimized expression in our low-level representation, in a formally sound manner, based on auto-tuning.

Our three contributions aim to answer the following questions:

- (1) *How can data parallelism be formally defined, and how can data-parallel computations be uniformly expressed via higher-order functions that are agonistic from hardware and optimization details while still capturing all information relevant for generating high-performing, executable program code?* (Contribution 1)
- (2) *How can optimizations for the memory and core hierarchies of state-of-the-art parallel architectures be formally expressed and generalized such that they apply to arbitrary data-parallel computations?* (Contribution 2)
- (3) *How can optimizations for data-parallel computations be expressed and structured so that they can be automatically identified (auto-tuned) for a particular target architecture and characteristics of the input and output data?* (Contribution 3)

The rest of the article is structured as follows. We introduce our functional HL REP (Contribution 1) in Section 2, and we show how this representation is used for expressing various kinds of popular data-parallel computations. In Section 3, we discuss our functional LL REP (Contribution 2) which is powerful enough to express the optimization decisions of state-of-practice approaches (e.g., scheduling approach TVM and polyhedral compilers PPCG and Pluto) and beyond. Section 4 shows how we systematically lower a computation expressed in our high-level representation to an expression in our low-level representation, in a formally sound and auto-tunable manner (Contribution 3). We present experimental results in Section 5, discuss related work in Section 6, conclude in Section 7, and we present our ideas for future work in Section 8.

We provide a full version of this paper [Rasch, 2024] that contains details for the interested reader that should not be required for understanding the basic concepts introduced in this article.

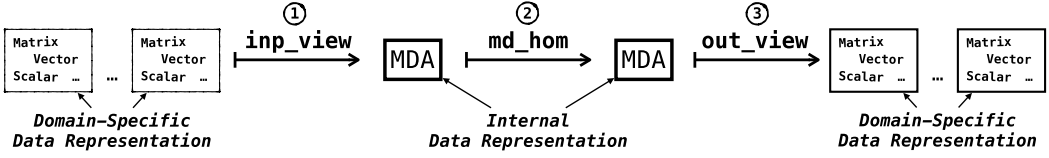


Fig. 5. High-level representation (overview).

In particular, our full version contains formal details—for all the following definition, examples, and theorems in Sections 2–4—whereas the formalism in this article is simplified for better illustration and easier understanding of our basic ideas and concepts.

## 2 High-Level Representation for Data-Parallel Computations

We introduce functional building blocks, in the form of higher-order functions, that express data-parallel computations on a high abstraction level. The goal of our high-level abstraction is to express computations agnostic from hardware and optimization details, and thus in a user-productive manner, while still capturing all information relevant for generating high-performance program code. The building blocks of our abstraction are based on the algebraic MDH formalism which is an approach toward formalizing data parallelism (we compare in detail to the existing work on MDHs in Section 6.6).

Figure 5 shows a basic overview of our high-level representation. We express data-parallel computations using exactly three higher-order functions only (a.k.a. *patterns* or *skeletons* [Gorlatch and Cole, 2011] in programming terminology): (1) `inp_view` transforms the domain-specific input data (e.g., a matrix and a vector in the case of matrix-vector multiplication) to a **Multi-Dimensional Array (MDA)** which is our internal data representation and defined later in this section; (2) `md_hom` expresses the data-parallel computation; (3) `out_view` transforms the computed MDA back to the domain-specific data representation.

In the following, after informally discussing an introductory example in Section 2.1, we formally define and discuss each higher-order function in detail in Section 2.2 (function `md_hom`) and Section 2.3 (functions `inp_view` and `out_view`). Sections 2.2 and 2.3 introduce and present the internals and formal details of our approach, which are not relevant for the end user of our system—the user only needs to operate on the abstraction level discussed in Section 2.1.

### 2.1 Introductory Example

Figure 6 shows how our high-level representation is used for expressing the example of matrix-vector multiplication `MatVec`<sup>4</sup> (Figure 1). Computation `MatVec` takes as input a matrix  $M \in T^{I \times K}$  and vector  $v \in T^K$  of arbitrary scalar type<sup>5</sup>  $T$  and sizes  $I \times K$  (matrix) and  $K$  (vector), for arbitrary but fixed positive natural numbers  $I, K \in \mathbb{N}$ .<sup>6</sup> In the figure, based on index function  $(i, k) \rightarrow (i, k)$  and  $(i, k) \rightarrow (k)$ , high-level function `inp_view` computes a function that takes  $M$  and  $v$  as input and maps them to a two-dimensional array of size  $I \times K$  (referred to as *input MDA* in the following and defined formally in the next subsection). The MDA contains at each point  $(i, k)$  the pair  $(M_{i,k}, v_k) \in T \times T$  comprising element  $M_{i,k}$  within matrix  $M$  (first component) and element  $v_k$  within vector  $v$  (second component). The input MDA is then mapped via function `md_hom` to an output MDA of size  $I \times 1$ , by applying multiplication  $*$  to each pair  $(M_{i,k}, v_k)$  within the input

<sup>4</sup>The expression in Figure 6 can also be extracted from straightforward, annotated sequential code [Rasch et al., 2020b,c].

<sup>5</sup>We consider as *scalar types* integers  $\mathbb{Z}$  (a.k.a. `int` in programming), floating point numbers  $\mathbb{Q}$  (a.k.a. `float` or `double`), any fixed collection of types (a.k.a. *record* or *struct*), and so on. We denote the set of scalar types as `TYPE` in the following.

<sup>6</sup>We denote by  $\mathbb{N}$  the set of positive natural number  $\{1, 2, \dots\}$ , and we use  $\mathbb{N}_0$  for the set of natural numbers including 0.



$$\text{MatVec}^{\langle T \in \text{TYPE} \mid I, K \in \mathbb{N} \rangle} := \text{out\_view}^{\langle T \rangle} (w : (i, k) \mapsto (i)) \circ \\ \text{md\_hom}^{\langle I, K \rangle} (\ast, (\ast, \ast)) \circ \\ \text{inp\_view}^{\langle T, T \rangle} (M : (i, k) \mapsto (i, k), v : (i, k) \mapsto (k))$$
Fig. 6. High-level expression for Matrix-Vector Multiplication (MatVec).<sup>7</sup>

MDA, and combining the obtained intermediate results within the MDA's first dimension via  $\ast$  (concatenation—also defined formally in the next subsection) and in second dimension via  $+$  (point-wise addition). Finally, function `out_view` computes a function that straightforwardly maps the output MDA, of size  $I \times 1$ , to `MatVec`'s result vector  $w \in T^I$ , which has scalar type  $T$  and is of size  $I$ . For the example of `MatVec`, the output view is trivial, but it can be used in other computations (such as matrix multiplication) to conveniently express more advanced variants of computations (e.g., computing the result matrix of matrix multiplication as transposed, as demonstrated later).<sup>7</sup>

## 2.2 Function `md_hom`

Higher-order function `md_hom` is introduced by Rasch and Gorlatch [2016] to express *MDH functions*—a formal representation of data-parallel computations—in a convenient and structured way. In the following, we recapitulate the definition of MDHs and function `md_hom`, but in a more general and formally more precise setting than done in the original MDH work.

To define MDH functions, we first need to introduce two central building blocks used in the definition of MDHs: (1) *MDAs*—the data type on which MDHs operate and which uniformly represent domain-specific input and output data (scalar, vectors, matrices, ...), and (2) *combine operators* which we use to combine elements within a particular dimension of an MDA.

### MDAs

*Definition 1 (MDA).* An MDA  $\alpha$  that has dimensionality  $D \in \mathbb{N}$ , size  $N \in \mathbb{N}^D$ , index sets  $I_1, \dots, I_D \subset \mathbb{N}_0$ , and scalar type  $T \in \text{TYPE}$  is a function with the following signature:

$$\alpha : I_1 \times \dots \times I_D \rightarrow T$$

We refer to  $I_1 \times \dots \times I_D \rightarrow T$  as the *type* of MDA  $\alpha$ .

*Notation 1.* For better readability, we denote MDAs' types and accesses to them using a notation close to programming. We often write:

- $\alpha \in T[I_1, \dots, I_D]$  instead of  $\alpha : I_1 \times \dots \times I_D \rightarrow T$  to denote the type of MDA  $\alpha$ ;
- $\alpha \in T[N_1, \dots, N_D]$  instead of  $\alpha : [0, N_1]_{\mathbb{N}_0} \times \dots \times [0, N_D]_{\mathbb{N}_0} \rightarrow T$ ;<sup>8</sup>
- $\alpha[i_1, \dots, i_D]$  instead of  $a(i_1, \dots, i_D)$  to access MDA  $\alpha$  at position  $(i_1, \dots, i_D)$ .

Figure 7 shows six MDAs for illustration. For example, the left part of the figure shows MDA  $\alpha$  which is of type  $\alpha : I_1 \times I_2 \rightarrow T$ , for  $I_1 = \{0, 1\}$ ,  $I_2 = \{0, 1, 2, 3\}$ , and  $T = \mathbb{Z}$  (integer numbers). Note that MDAs named  $\alpha^{(1,1)}$ ,  $\alpha^{(1,2)}$ ,  $\alpha^{(2,1)}$ ,  $\alpha^{(2,2)}$ ,  $\alpha^{(2,3)}$  in Figure 7 can be considered as *parts* (a.k.a. *tiles* in programming) of MDA  $\alpha$ : the MDA named  $\alpha^{(1,1)}$  represents the first row of  $\alpha$ , MDA  $\alpha^{(2,2)}$  the third column of  $\alpha$ , etc. We formally define and use *partitionings* of MDAs in Section 3.

<sup>7</sup> Our technical implementation takes as input a representation that is equivalent to Figure 6, expressed via straightforward program code (see Rasch [2024], Section A.4).

<sup>8</sup> We denote by  $[L, U]_{\mathbb{N}_0} := \{n \in \mathbb{N}_0 \mid L \leq n < U\}$  the half-open interval of natural numbers (including 0) between  $L$  (incl.) and  $U$  (excl.).

$$\begin{aligned}
\mathbf{a} &= \begin{bmatrix} \underbrace{1}_{\mathbf{a}[0,0]} & \underbrace{2}_{\mathbf{a}[0,1]} & \underbrace{3}_{\mathbf{a}[0,2]} & \underbrace{4}_{\mathbf{a}[0,3]} \\ \underbrace{5}_{\mathbf{a}[1,0]} & \underbrace{6}_{\mathbf{a}[1,1]} & \underbrace{7}_{\mathbf{a}[1,2]} & \underbrace{8}_{\mathbf{a}[1,3]} \end{bmatrix} \in T[ I_1 := \{0,1\}, I_2 := \{0,1,2,3\} ] \\
\mathbf{a}^{(1,1)} &= \begin{bmatrix} \underbrace{1}_{\mathbf{a}[0,0]} & \underbrace{2}_{\mathbf{a}[0,1]} & \underbrace{3}_{\mathbf{a}[0,2]} & \underbrace{4}_{\mathbf{a}[0,3]} \end{bmatrix} \in T[ I_1^{(1,1)} := \{0\}, I_2^{(1,1)} := \{0,1,2,3\} ] \\
\mathbf{a}^{(1,2)} &= \begin{bmatrix} \underbrace{5}_{\mathbf{a}[1,0]} & \underbrace{6}_{\mathbf{a}[1,1]} & \underbrace{7}_{\mathbf{a}[1,2]} & \underbrace{8}_{\mathbf{a}[1,3]} \end{bmatrix} \in T[ I_1^{(1,2)} := \{1\}, I_2^{(1,2)} := \{0,1,2,3\} ] \\
\mathbf{a}^{(2,1)} &= \begin{bmatrix} \underbrace{1}_{\mathbf{a}[0,0]} & \underbrace{2}_{\mathbf{a}[0,1]} \\ \underbrace{5}_{\mathbf{a}[1,0]} & \underbrace{6}_{\mathbf{a}[1,1]} \end{bmatrix} \in T[ I_1^{(2,1)} := \{0,1\}, I_2^{(2,1)} := \{0,1\} ] \\
\mathbf{a}^{(2,2)} &= \begin{bmatrix} \underbrace{3}_{\mathbf{a}[0,2]} \\ \underbrace{7}_{\mathbf{a}[1,2]} \end{bmatrix} \in T[ I_1^{(2,2)} := \{0,1\}, I_2^{(2,2)} := \{2\} ] \\
\mathbf{a}^{(2,3)} &= \begin{bmatrix} \underbrace{4}_{\mathbf{a}[0,3]} \\ \underbrace{8}_{\mathbf{a}[1,3]} \end{bmatrix} \in T[ I_1^{(2,3)} := \{0,1\}, I_2^{(2,3)} := \{3\} ]
\end{aligned}$$

Fig. 7. MDA examples.

### Combine Operators

A central building block in our definition of MDHs is a *combine operator*. Intuitively, we use a combine operator to combine all elements within a particular dimension of an MDA. For example, in Figure 1 (matrix-vector multiplication), we combine elements of the two-dimensional MDA via combine operator *concatenation* in MDA's first dimension and via operator *point-wise addition* in the second dimension. Technically, combine operators are functions that take as input two MDAs and yield a single MDA as their output.

We now define *combine operators* formally, and we illustrate this formal definition afterward using the example operators *concatenation* and *point-wise combination*.

**Definition 2 (Combine Operator).** We refer to any binary function  $\otimes$  of type

$$\otimes : T[ I_1, \dots, \underset{\uparrow d}{P}, \dots, I_D ] \times T[ I_1, \dots, \underset{\uparrow d}{Q}, \dots, I_D ] \rightarrow T[ I_1, \dots, \underset{\uparrow d}{R}, \dots, I_D ]$$

as *combine operator* that has *scalar type*  $T \in \text{TYPE}$ , *dimensionality*  $D \in \mathbb{N}$ , and *operating dimension*  $d \in [1, D]_{\mathbb{N}}$ . We denote combine operator's type concisely as CO.

**Example 1 (Concatenation).** We define *concatenation* (in dimension  $d$ ) as function  $\#_d$  of type

$$\#_d : T[ I_1, \dots, \underset{\uparrow d}{P}, \dots, I_D ] \times T[ I_1, \dots, \underset{\uparrow d}{Q}, \dots, I_D ] \rightarrow T[ I_1, \dots, \underset{\uparrow d}{P \cup Q}, \dots, I_D ]$$

and that is computed as

$$\#_d(\mathbf{a}_1, \mathbf{a}_2)[i_1, \dots, i_d, \dots, i_D] := \begin{cases} \mathbf{a}_1[i_1, \dots, i_d, \dots, i_D], & i_d \in P \\ \mathbf{a}_2[i_1, \dots, i_d, \dots, i_D], & i_d \in Q \end{cases}$$

The function is well defined when  $P$  and  $Q$  are disjoint. We usually use an infix notation for  $\#_d$ , i.e., we write  $\mathbf{a}_1 \#_d \mathbf{a}_2$  instead of  $\#_d(\mathbf{a}_1, \mathbf{a}_2)$ , and we refrain from  $\#_d$ 's subscript  $d$  when it is clear from the context.



$$\begin{aligned}
h\left(\underbrace{\begin{bmatrix} 1 & 2 & 3 & 4 \\ 5 & 6 & 7 & 8 \\ 9 & 10 & 11 & 12 \\ 13 & 14 & 15 & 16 \end{bmatrix}}_{\alpha_1 \mathrel{++}_1 \alpha_2}\right) &= h\left(\begin{array}{c} \overbrace{\begin{bmatrix} 1 & 2 & 3 & 4 \\ 5 & 6 & 7 & 8 \end{bmatrix}}^{\alpha_1} \\ \otimes_1 \\ \underbrace{\begin{bmatrix} 9 & 10 & 11 & 12 \\ 13 & 14 & 15 & 16 \end{bmatrix}}_{\alpha_2} \end{array}\right) \\
h\left(\underbrace{\begin{bmatrix} 1 & 2 & 3 & 4 \\ 5 & 6 & 7 & 8 \\ 9 & 10 & 11 & 12 \\ 13 & 14 & 15 & 16 \end{bmatrix}}_{\alpha_3 \mathrel{++}_2 \alpha_4}\right) &= h\left(\underbrace{\begin{bmatrix} 1 & 2 \\ 5 & 6 \\ 9 & 10 \\ 13 & 14 \end{bmatrix}}_{\alpha_3}\right) \otimes_2 h\left(\underbrace{\begin{bmatrix} 3 & 4 \\ 7 & 8 \\ 11 & 12 \\ 15 & 16 \end{bmatrix}}_{\alpha_4}\right)
\end{aligned}$$

Fig. 8. MDH property illustrated on a two-dimensional example computation.

*Example 2 (Point-Wise Combination).* We define *point-wise combination* (in dimension  $d$ ), according to a binary function  $\oplus : T \times T \rightarrow T$  (e.g., addition), as function  $\vec{\bullet}_d$  of type

$$\begin{array}{c}
\vec{\bullet}_d : \underbrace{T \times T}_{\oplus} \rightarrow \underbrace{T[I_1, \dots, \underbrace{\{0\}}_d, \dots, I_D] \times T[I_1, \dots, \underbrace{\{0\}}_d, \dots, I_D]}_{\text{point-wise combination (according to } \oplus \text{)}} \rightarrow T[I_1, \dots, \underbrace{\{0\}}_d, \dots, I_D]
\end{array}$$

that is computed as

$$\vec{\bullet}_d(\oplus)(\alpha_1, \alpha_2)[i_1, \dots, \underbrace{0}_d, \dots, i_D] := \alpha_1[i_1, \dots, \underbrace{0}_d, \dots, i_D] \oplus \alpha_2[i_1, \dots, \underbrace{0}_d, \dots, i_D].$$

The input MDAs are assumed to have index set  $\{0\}$  in the operating dimension  $d$ ; otherwise,  $\vec{\bullet}(\oplus)$  is undefined. We refrain from  $\vec{\bullet}_d(\oplus)$ 's subscript  $d$  when it is clear from the context. For brevity, we often write  $\oplus$  only, instead of  $\vec{\bullet}_d(\oplus)$ , and we usually use an infix notation for  $\oplus$ .

## MDHs

Now that we have defined MDAs (Definition 1) and combine operators (Definition 2), we can define *MDH functions*. Intuitively, a function  $h$  operating on MDAs is an MDH iff we can apply the function independently to parts of its input MDA and combine the obtained intermediate results to the final result using combine operators; this can be imagined as a typical divide-and-conquer pattern. Compared to classical approaches, e.g., *list homomorphisms* [Bird, 1989; COLE, 1995; Gorlatch, 1999], a major characteristic of MDH functions is that they allow (de/re)-composing computations in multiple dimensions (e.g., in Figure 1, in both the concatenation dimension as well as in the point-wise addition dimensions), rather than being limited to a particular dimension only (e.g., only the concatenation dimension or only point-wise addition dimension, respectively). We will see later in this article that a multi-dimensional (de/re)-composition approach is essential to efficiently exploit the hardware of modern architectures which require fine-grained cache blocking and parallelization strategies to achieve their full performance potential.

Figure 8 illustrates the MDH property informally on a simple, two-dimensional input MDA. In the left part of the figure, we split the input MDA in dimension 1 (i.e., horizontally) into two parts  $\alpha_1$  and  $\alpha_2$ , apply the MDH function  $h$  independently to each part, and combine the obtained intermediate results to the final result using the MDH function  $h$ 's combine operator  $\otimes_1$ . Similarly, in the right part of Figure 8, we split the input MDA in dimension 2 (i.e., vertically) into parts and combine the results via MDH function  $h$ 's second combine operator  $\otimes_2$ .

Figure 9 shows an artificial example in which we apply the MDH property (illustrated in Figure 8) recursively. We refer in Figure 9 to the part above the horizontal dashed lines as *de-composition phase* and to the part below dashed lines as *re-composition phase*.

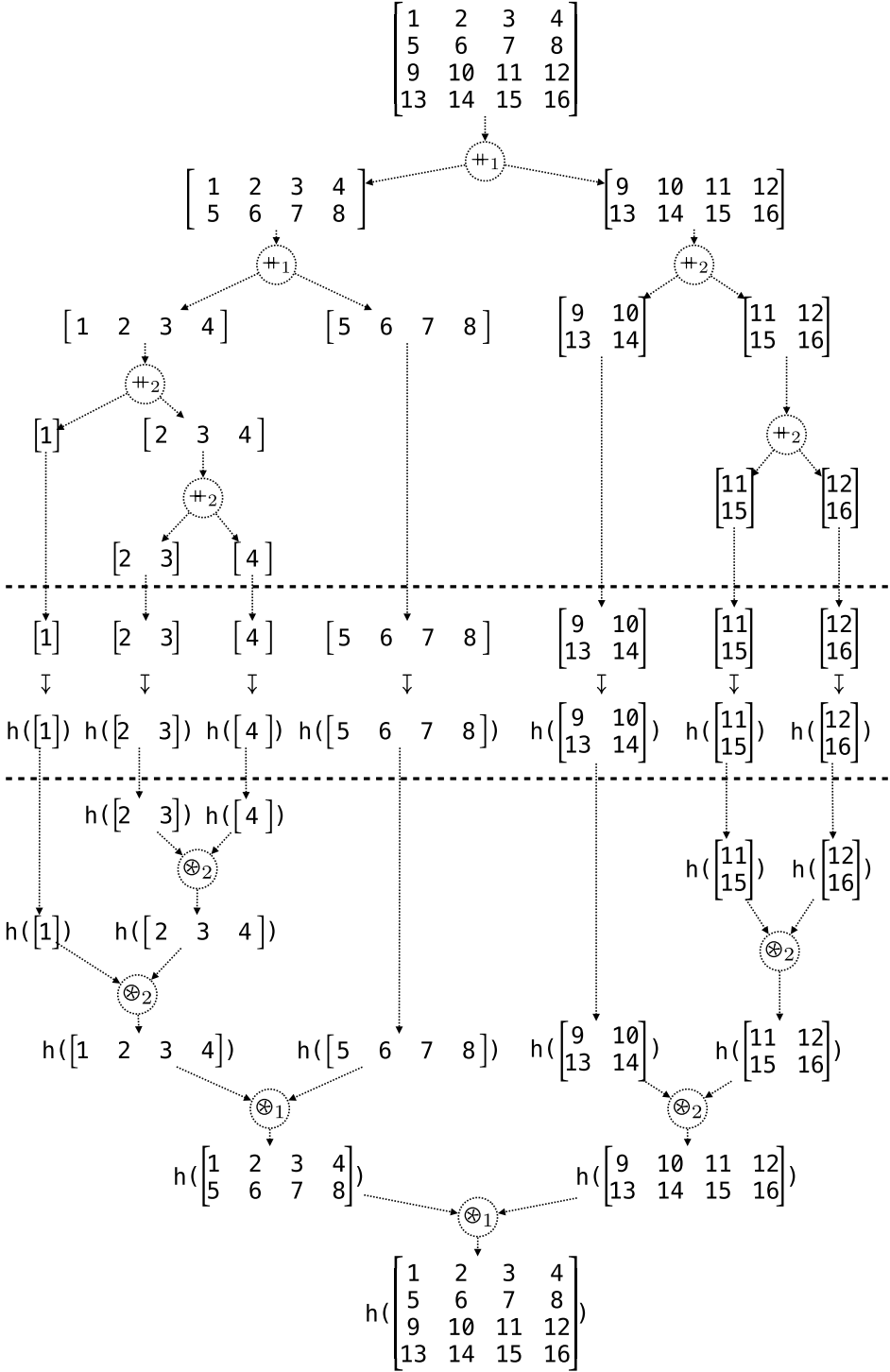


Fig. 9. MDH property recursively applied to a two-dimensional example computation.

*Definition 3 (MDH).* A function

$$h : T^{\text{INP}}[I_1, \dots, I_D] \rightarrow T^{\text{OUT}}[J_1, \dots, J_D]$$

is an MDH that has *input scalar type*  $T^{\text{INP}} \in \text{TYPE}$ , *output scalar type*  $T^{\text{OUT}} \in \text{TYPE}$ , and *dimensionality*  $D \in \mathbb{N}$ , iff for each  $d \in [1, D]_{\mathbb{N}}$ , there exists a combine operator  $\oplus_d$  (Definition 2), such that for any concatenated input MDA  $\mathbf{a}_1 \mathbin{+}_d \mathbf{a}_2$  in dimension  $d$ , the *homomorphic property* is satisfied:

$$h(\mathbf{a}_1 \mathbin{+}_d \mathbf{a}_2) = h(\mathbf{a}_1) \oplus_d h(\mathbf{a}_2)$$

We denote the type of MDHs concisely as MDH.

MDHs are defined such that applying them to a concatenated MDA in dimension  $d$  can be computed by applying the MDH  $h$  independently to the MDA's parts  $\mathbf{a}_1$  and  $\mathbf{a}_2$  and combining the intermediate results afterward by using its combine operator  $\oplus_d$ , as also informally discussed above.

*Example 3 (Function Mapping).* A simple example MDH is *function mapping* [González-Vélez and Leyton, 2010], computed by higher-order function  $\text{map}(f)(\mathbf{a})$ , which applies a user-defined scalar function  $f : T^{\text{INP}} \rightarrow T^{\text{OUT}}$  to each element within a  $D$ -dimensional MDA  $\mathbf{a}$ . Function  $\text{map}(f)$  is an MDH whose combine operators are concatenation  $\mathbin{+}$  in all of its  $D$  dimensions (Example 1).

*Example 4 (Reduction).* A further MDH function is *reduction* [González-Vélez and Leyton, 2010], implemented as higher-order function  $\text{red}(\oplus)(\mathbf{a})$ , which combines all elements within a  $D$ -dimensional MDA  $\mathbf{a}$  using a user-defined binary function  $\oplus : T \times T \rightarrow T$ . Reduction's combine operators are point-wise combination  $\vec{\oplus}(\oplus)$  in all dimensions (Example 2).

We show how Examples 3 and 4 (and particularly also more advanced examples) are expressed in our high-level representation in Section 2.4, based on higher-order functions `md_hom`, `inp_view`, and `out_view` (Figure 5) which we introduce in the following.

### Higher-Order Function `md_hom`

We define higher-order function `md_hom` which conveniently expresses MDH functions in a uniform and structured manner. For this, we exploit that any MDH function is uniquely determined by its combine operators and its behavior on singleton MDAs, as informally illustrated in the following figure:

$$h\left(\begin{bmatrix} 1 & 2 & 3 & 4 \\ 5 & 6 & 7 & 8 \\ 9 & 10 & 11 & 12 \\ 13 & 14 & 15 & 16 \end{bmatrix}\right) = \begin{array}{c} \xrightarrow{\oplus_2} \\ \begin{array}{l} h([1]) \ h([2]) \ h([3]) \ h([4]) \\ h([5]) \ h([6]) \ h([7]) \ h([8]) \\ h([9]) \ h([10]) \ h([11]) \ h([12]) \\ h([13]) \ h([14]) \ h([15]) \ h([16]) \end{array} \end{array} \xrightarrow{\oplus_1} \begin{array}{c} \xrightarrow{\oplus_2} \\ \begin{array}{l} f(1) \ f(2) \ f(3) \ f(4) \\ f(5) \ f(6) \ f(7) \ f(8) \\ f(9) \ f(10) \ f(11) \ f(12) \\ f(13) \ f(14) \ f(15) \ f(16) \end{array} \end{array} \xrightarrow{\oplus_1}$$

Here,  $f$  is the function on scalar values that behaves the same as  $h$  when restricted to singleton MDAs:  $f(\mathbf{a}[i_1, \dots, i_D]) := h(\mathbf{a})$ , for any MDA  $\mathbf{a} \in T[\{i_1\}, \dots, \{i_D\}]$  consisting of only one element that is accessed by (arbitrary) indices  $i_1, \dots, i_D \in \mathbb{N}_0$ . For singleton MDAs, we usually use  $f$  instead of  $h$ , because  $f$  can be defined more conveniently by the user as  $h$  (which needs to handle MDAs of arbitrary sizes, and not only singleton MDAs as  $f$ ). Also, since  $f$  takes as input a scalar value (rather than a singleton MDA, as  $h$ ), the type of  $f$  also becomes simpler, which further contributes to simplicity.

We now formally introduce function `md_hom` which uniformly expresses any MDH function, by using only the MDH's behavior  $f$  on scalar values and the MDH's combine operators.

*Definition 4 (Higher-Order Function `md_hom`).* The higher-order function `md_hom` is of type

$$\text{md\_hom} : \underbrace{\text{SF}}_f \times \underbrace{(\text{CO} \times \dots \times \text{CO})}_{\otimes_1 \dots, \otimes_D} \rightarrow_p \underbrace{\text{MDH}}_{\text{md\_hom}(f, (\otimes_1, \dots, \otimes_D))}$$

where SF denotes the set of scalar functions of type  $T^{\text{INP}} \rightarrow T^{\text{OUT}}$ . Function `md_hom` is partial (indicated by  $\rightarrow_p$  instead of  $\rightarrow$ ), which we motivate after this definition. The function takes as input a scalar function  $f$  and a tuple of  $D$ -many combine operators  $(\otimes_1, \dots, \otimes_D)$ , and it yields a function `md_hom`( $f, (\otimes_1, \dots, \otimes_D)$ ) which is defined as

$$\text{md\_hom}(f, (\otimes_1, \dots, \otimes_D))(\alpha) := \prod_{i_1 \in I_1}^{\otimes_1} \dots \prod_{i_D \in I_D}^{\otimes_D} f(\alpha[i_1, \dots, i_D]).$$

The combine operators' underset notation denotes straightforward iteration.<sup>9</sup> For `md_hom`, we require by definition the homomorphic property (Definition 3), i.e., for each  $d \in [1, D]_{\mathbb{N}}$ , it must hold:

$$\begin{aligned} \text{md\_hom}(f, (\otimes_1, \dots, \otimes_D))(\alpha_1 \oplus_d \alpha_2) = \\ \text{md\_hom}(f, (\otimes_1, \dots, \otimes_D))(\alpha_1) \otimes_d \text{md\_hom}(f, (\otimes_1, \dots, \otimes_D))(\alpha_2). \end{aligned}$$

Using Definition 4, we express any MDH function uniformly via higher-order function `md_hom` using only the MDH's behavior  $f$  on scalar values and its combine operators  $\otimes_1, \dots, \otimes_D$ . The other direction also holds: each function expressed via `md_hom` is an MDH function, because we require the homomorphic property for `md_hom`.

Note that function `md_hom` is defined as partial function, because the homomorphic property is not met for all potential combinations of combine operators, e.g.,  $\otimes_1 = +$  (point-wise addition) and  $\otimes_2 = *$  (point-wise multiplication). However, in many real-world examples, an MDH's combine operators are a mix of concatenations and point-wise combinations according to the same binary function. The following lemma proves that any instance of the `md_hom` higher-order function for such a mix of combine operators is a well-defined MDH function.

**LEMMA 1.** *Let  $\oplus : T \rightarrow T$  be an arbitrary but fixed associative and commutative binary function on scalar type  $T \in \text{TYPE}$ . Let further  $\otimes_1, \dots, \otimes_D$  be combine operators of which any is either concatenation (Example 1) or point-wise combination according to binary function  $\oplus$  (Example 2). It holds that `md_hom`( $f, (\otimes_1, \dots, \otimes_D)$ ) is well defined.*

**PROOF.** Proved by Rasch [2024], Section B.5. □

MDH functions are defined (Definition 3) such that they uniformly operate on MDAs (Figure 5). We introduce higher-order function `inp_view` to transform domain-specific inputs (e.g., a matrix and a vector in the case of matrix-vector multiplication) to an MDA, and we use function `out_view` to transform the output MDA back to the domain-specific data requirements (like storing it as a transposed matrix in the case of matrix multiplication, or splitting it into multiple outputs as we will see later with examples). We introduce both higher-order functions in the following.

<sup>9</sup> We implicitly interpret the output scalar of function  $f$  as a singleton MDA, as combine operators operate on MDAs and not on scalars (formal details provided by Rasch [2024], Definition 4).

### 2.3 View Functions

In the following, after introducing **Buffers (BUF)** which represent domain-specific input and output data in our approach (scalars, vectors, matrices, etc.), we define in Sections 2.3.1 and 2.3.2 the concepts of *input views* and *output views*—both are central building blocks in our approach. We define *input views* as arbitrary functions that map a collection of user-defined BUFs to our internal MDA data representation (Figure 5); higher-order function `inp_view` is then introduced to conveniently compute an important class of input view functions that are relevant for expressing real-world computations. Correspondingly, Section 2.3.2 defines *output views* as functions that transform an MDA to a collection of BUFs, and higher-order function `out_view` is introduced to conveniently compute important output views. Finally, we discuss in Section 2.3.3 the relationship between higher-order function `inp_view` and `out_view`: we prove that both functions are inversely related to each other, allowing arbitrarily switching between our internal MDA representation and our domain-specific BUF representation (as required for our code generation process discussed later).

*Definition 5 (Buffer).* A Buffer (BUF)  $\mathbf{b}$  that has dimensionality  $D \in \mathbb{N}_0$ ,<sup>10</sup> size  $N := \{N_1, \dots, N_D\} \in \mathbb{N}^D$ , and scalar type  $T \in \text{TYPE}$  is a function with the following signature:

$$\mathbf{b} : [0, N_1)_{\mathbb{N}_0} \times \dots \times [0, N_D)_{\mathbb{N}_0} \rightarrow T \cup \{\perp\}.$$

Here, we use  $\perp$  to denote the *undefined value*. We refer to  $[0, N_1)_{\mathbb{N}_0} \times \dots \times [0, N_D)_{\mathbb{N}_0} \rightarrow T \cup \{\perp\}$  as the *type* of BUF  $\mathbf{b}$ , which we also denote as  $T^{N_1 \times \dots \times N_D}$ . Analogously to Notation 1, we write  $\mathbf{b}[i_1, \dots, i_D]$  instead of  $\mathbf{b}(i_1, \dots, i_D)$  to avoid a too heavy usage of parentheses.

In contrast to MDAs, a BUF always operates on a contiguous range of natural numbers starting from 0, and a BUF may contain undefined values. These two differences allow straightforwardly transforming BUFs to data structures provided by low-level programming languages (e.g., *C arrays*, as used in OpenMP, CUDA, and OpenCL).

Note that in our generated program code (discussed later in Section 3), we implement MDAs on top of BUFs, as straightforward aliases that access BUFs, so that we do not need to transform MDAs to low-level data structures and/or store them otherwise physically in memory.

**2.3.1 Input Views.** We define *input views* as any function that compute an MDA from a collection of (user-defined) BUFs. For example, in the case of `MatVec`, its input view takes as input two BUFs—a matrix and a vector—and it yields a two-dimensional MDA containing pairs of matrix and vector elements (illustrated in Figure 1). In contrast, the input view of `Jacobi1D` takes as input a single BUF (representing a vector) only, and it computes an MDA containing triples of BUF elements (Figure 2).

*Definition 6 (Input View).* An *input view* from  $B$ -many BUFs,  $B \in \mathbb{N}$ , of arbitrary but fixed types  $T_b^{N_1^b \times \dots \times N_{D_b}^b}$ ,  $b \in [1, B]_{\mathbb{N}}$ , to an MDA of arbitrary but fixed type  $T[I_1, \dots, I_D]$  is any function `iv` of type:

$$\mathbf{iv} : \underbrace{\prod_{b=1}^B T_b^{N_1^b \times \dots \times N_{D_b}^b}}_{\text{BUFs}} \rightarrow_p \underbrace{T[I_1, \dots, I_D]}_{\text{MDA}}$$

We denote the type of `iv` as *IV*.

<sup>10</sup>We use the case  $D = 0$  to represent scalar values (details provided in Rasch [2024], Section B.7).

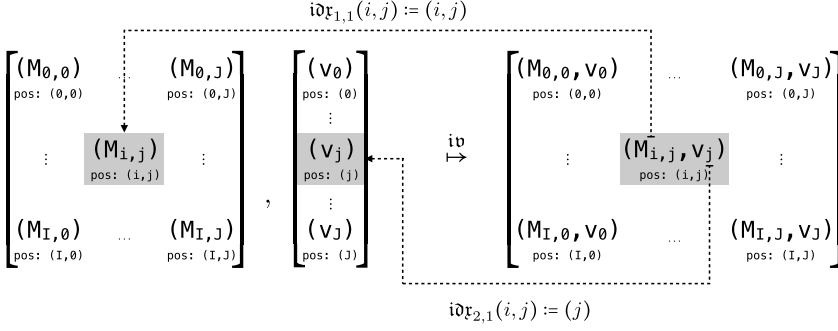


Fig. 10. Input view illustrated using the example MatVec.

*Example 5 (Input View—MatVec).* The input view of MatVec on a  $1024 \times 512$  matrix and 512-sized vector (sizes chosen arbitrarily) is defined as

$$\underbrace{[M(i, k)]_{i \in [0, 1024]_{\mathbb{N}_0}, k \in [0, 512]_{\mathbb{N}_0}}}_{\text{BUF (Matrix)}} \cdot \underbrace{[v(k)]_{k \in [0, 512]_{\mathbb{N}_0}}}_{\text{BUF (Vector)}} \mapsto \underbrace{[M(i, k), v(k)]_{i \in [0, 1024]_{\mathbb{N}_0}, k \in [0, 512]_{\mathbb{N}_0}}}_{\text{MDA}}$$

*Example 6 (Input View—Jacobi1D).* The input view of Jacobi1D on a 512-sized vector is defined as

$$\underbrace{[v(i)]_{i \in [0, 512]_{\mathbb{N}_0}}}_{\text{BUF (Vector)}} \mapsto \underbrace{[v(i+0), v(i+1), v(i+2)]_{i \in [0, 512-2]_{\mathbb{N}_0}}}_{\text{MDA}}.$$

In the following, we introduce higher-order function `inp_view` which conveniently computes important input views from user-defined index functions  $\text{id}\mathbf{x}_{b,a} : \{0, 1, \dots\} \rightarrow \{0, 1, \dots\}$ ,  $b \in [1, B]_{\mathbb{N}}$ ,  $a \in [1, A_b]_{\mathbb{N}}$ , in a uniform, structured manner. Here,  $B \in \mathbb{N}$  represents the number of BUFs that the computed input view will take as input, and  $A_b$  represents the number of accesses to the  $b$ -th BUF required for computing an individual MDA element.

In the case of MatVec (Figure 1), we use  $B := 2$  because MatVec has two input BUFs: a matrix  $M$  (the first input of MatVec and thus identified by  $b = 1$ ) and a vector  $v$  (identified by  $b = 2$ ). For the number of accesses, we use for the matrix  $A_1 := 1$ , as one element is accessed within matrix  $M$  to compute an individual MDA element—matrix element  $M[i, k]$  for computing MDA element at position  $(i, k)$ . For the vector, we use  $A_2 := 1$ , as the single element  $v[k]$  is accessed within the vector. The index functions of MatVec are  $\text{id}\mathbf{x}_{1,1}(i, k) := (i, k)$  (used to access the matrix) and  $\text{id}\mathbf{x}_{2,1}(i, k) := (k)$  (used for the vector).

In contrast, for Jacobi1D (Figure 2), we use  $B := 1$  because Jacobi1D has vector  $v$  as its only input, and we use  $A_1 := 3$  because the vector is accessed three times to compute an individual MDA element at arbitrary position  $i$ : first access  $v[i+0]$ , second access  $v[i+1]$ , and third access  $v[i+2]$ . The index functions of Jacobi1D are  $\text{id}\mathbf{x}_{1,1}(i) := (i+0)$ ,  $\text{id}\mathbf{x}_{1,2}(i) := (i+1)$ , and  $\text{id}\mathbf{x}_{1,3}(i) := (i+2)$ .

Figures 10 and 11 use the examples MatVec and Jacobi1D to informally illustrate how function `inp_view` uses index functions to compute input views. In the two figures, we use domain-specific identifiers for better clarity: in the case of MatVec, we use for its two input BUFs the identifiers  $M$  and  $v$  instead of  $\mathbf{b}_1$  and  $\mathbf{b}_2$ , as well as identifiers  $i$  and  $j$  instead of  $i_1$  and  $i_2$  for index variables; for Jacobi1D, we use identifier  $v$  instead of  $\mathbf{b}_1$  and  $i$  instead of  $i_1$ .



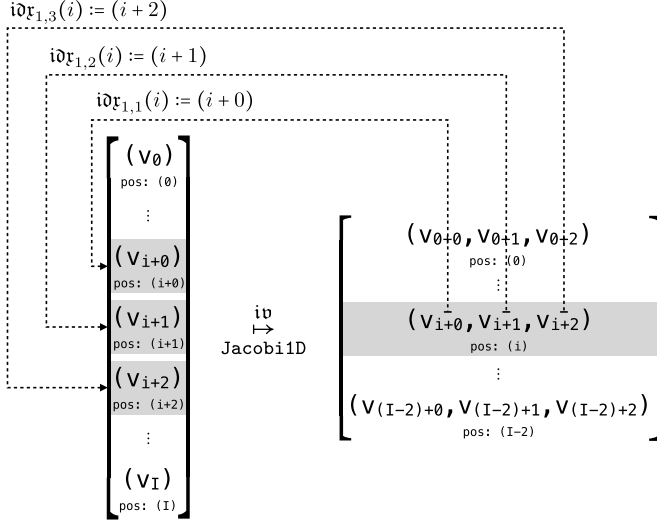


Fig. 11. Input view illustrated using the example Jacobi1D.

*Definition 7 (Higher-Order Function inp\_view).* Function  $\text{inp\_view}$  is of type

$$\text{inp\_view} : \left( \underbrace{\left( \prod_{b=1}^B \times \prod_{a=1}^{A_b} \right)}_{\text{Buffer Access}} \underbrace{\text{IDX-FCT}}_{\text{Index Function: } \text{idf}_{b,a}} \right) \rightarrow \underbrace{\text{IV}}_{\text{Input View: iv}}$$

Index Functions:  $\text{idf}_{1,1}, \dots, \text{idf}_{B,A_B}$

and it is defined as

$$\underbrace{(\text{idf}_{b,a})_{b \in [1,B]_{\mathbb{N}}, a \in [1,A_b]_{\mathbb{N}}}}_{\text{Index Functions}} \mapsto \underbrace{(\mathbf{b}_1, \dots, \mathbf{b}_B)}_{\text{BUFs}} \xrightarrow{\text{iv}} \underbrace{\mathbf{a}}_{\text{MDA}}$$

Input View

for

$$\mathbf{a}[i_1, \dots, i_D] := (\mathbf{a}_{b,a}[i_1, \dots, i_D])_{b \in [1,B]_{\mathbb{N}}, a \in [1,A_b]_{\mathbb{N}}}$$

and

$$\mathbf{a}_{b,a}[i_1, \dots, i_D] := \mathbf{b}_b[\text{idf}_{b,a}(i_1, \dots, i_D)]$$

Higher-order function  $\text{inp\_view}$  takes as input a collection of index functions of types  $\text{IDX-FCT}$ , and it computes an input view of type  $\text{IV}$  (Definition 6) based on the index functions, as illustrated in Figures 10 and 11.

Note that function  $\text{inp\_view}$  is not capable of computing every kind of input view function (Definition 6). For example,  $\text{inp\_view}$  cannot be used for computing MDAs that are required for expressing computations on sparse data formats [Hall, 2020], because such MDAs need dynamically accessing BUFs. This limitation of  $\text{inp\_view}$  can be relaxed by generalizing our index functions toward taking additional, dynamic input arguments, which we consider as future work (as outlined in Section 8).

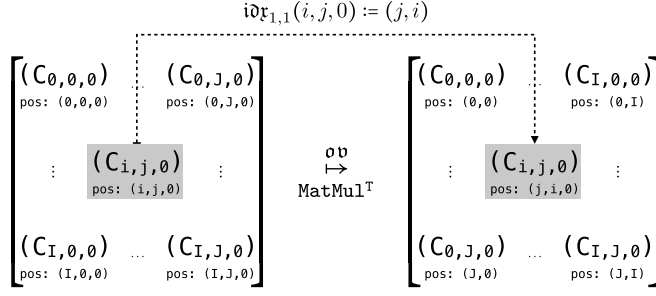


Fig. 12. Output view illustrated using the example *transposed matrix multiplication*.

*Notation 2 (Input Views).* For better readability, we use the following notation for the two-dimensional structure of index functions taken as input by function `inp_view`, inspired by Lattner et al. [2021]:

$$\text{inp\_view}(\text{ID}_1 : \text{id}\mathbf{x}_{1,1}, \dots, \text{id}\mathbf{x}_{1,A_1}, \dots, \text{ID}_B : \text{id}\mathbf{x}_{B,1}, \dots, \text{id}\mathbf{x}_{B,A_B})$$

Here,  $\text{ID}_1, \dots, \text{ID}_B$  denote arbitrary, user-defined identifiers (e.g.,  $\text{ID}_1 = \text{"M"}$  and  $\text{ID}_2 = \text{"v"}$  for `MatVec`).

*Example 7.* Function `inp_view` is used for `MatVec` and `Jacobi1D` (in Notation 2) as follows:

$$\begin{array}{ll} \text{MatVec:} & \text{inp\_view}(\underbrace{\text{M: } (i, k) \mapsto (i, k)}_{a=1}, \underbrace{\text{v: } (i, k) \mapsto (k)}_{a=1}) \\ & \underbrace{\hspace{10em}}_{b=1} \\ \text{Jacobi1D:} & \text{inp\_view}(\underbrace{\text{v: } (i) \mapsto (i+0)}_{a=1}, \underbrace{\text{v: } (i) \mapsto (i+1)}_{a=2}, \underbrace{\text{v: } (i) \mapsto (i+2)}_{a=3}) \\ & \underbrace{\hspace{10em}}_{b=1} \end{array}$$

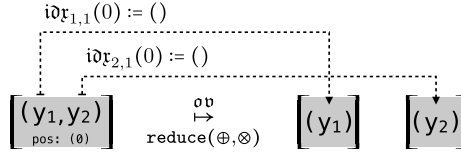
**2.3.2 Output Views.** An *output view* is the counterpart of an input view: in contrast to an input view which maps BUFs to an MDA, an output view maps an MDA to a collection of BUFs. In the following, we define output views, and we introduce higher-order function `out_view` which computes output views in a structured manner (analogously to function `inp_view` for input views).

Figures 12 and 13 illustrate output views informally using the examples *transposed Matrix Multiplication* and *Double Reduction*.

In the case of transposed matrix multiplication (Figure 12), the computed output MDA (the computation of matrix multiplication is presented later and not relevant for our following considerations) is stored via an output view as a matrix in a transposed fashion, using index function  $(i, j, 0) \mapsto (j, i)$ . Here, the MDA’s third dimension (accessed via index 0) represents the so-called reduction dimension of matrix multiplication, and it contains only one element after the computation, as all elements in this dimension are combined via addition.

For double reduction (Figures 13), we combine the elements within the vector twice—once using operator  $\oplus$  (e.g.,  $\oplus = +$  addition) and once using operator  $\otimes$  (e.g.,  $\otimes = *$  multiplication). The final outcome of double reduction is a singleton MDA containing a pair of two elements that represent the combined vector elements (e.g., the elements’ sum and product). We store this MDA via an output view as two individual scalar values, using index functions  $(0) \mapsto ()$ <sup>11</sup> for both pair elements.

<sup>11</sup>The empty braces denote accessing a scalar value (details provided by Rasch [2024], Section B.7).

Fig. 13. Output view illustrated using the example *double reduction*.

**Definition 8 (Output View).** An output view from an MDA of arbitrary but fixed type  $T[I_1, \dots, I_D]$  to  $B$ -many BUFs,  $B \in \mathbb{N}$ , of arbitrary but fixed types  $T_b^{N_1^b \times \dots \times N_{D_b}^b}$ ,  $b \in [1, B]_{\mathbb{N}}$ , is any function  $\mathbf{ov}$  of type:

$$\mathbf{ov} : \underbrace{T[I_1, \dots, I_D]}_{\text{MDA}} \rightarrow_p \underbrace{\prod_{b=1}^B T_b^{N_1^b \times \dots \times N_{D_b}^b}}_{\text{BUFs}}$$

We denote the type of  $\mathbf{ov}$  as OV.

**Example 8 (Output View—MatVec).** The output view of MatVec computing a 1024-sized vector (size is chosen arbitrarily), of integers  $\mathbb{Z}$ , is defined as

$$\underbrace{[w(i)]_{i \in [0, 1024)_{\mathbb{N}_0}, k \in \{0\}}}_{\text{MDA}} \mapsto \underbrace{[w(i)]_{i \in [0, 1024)_{\mathbb{N}_0}}}_{\text{BUF (Vector)}}$$

**Example 9 (Output View—Jacobi 1D).** The output view of Jacobi 1D computing a  $(512 - 2)$ -sized vector is defined as

$$\underbrace{[w(i)]_{i \in [0, 512-2)_{\mathbb{N}_0}, k \in \{0\}}}_{\text{MDA}} \mapsto \underbrace{[w(i)]_{i \in [0, 512-2)_{\mathbb{N}_0}}}_{\text{BUF (Vector)}}$$

We define higher-order function `out_view` formally as follows.

**Definition 9 (Higher-Order Function `out_view`).** Function `out_view` is of type

$$\underbrace{\underbrace{\prod_{b=1}^B \times}_{\text{Buffer Access}} \underbrace{\prod_{a=1}^{A_b} \times}_{\text{Index Function: } \mathbf{id}\mathbf{x}_{b,a}}}_{\text{Index Functions: } \mathbf{id}\mathbf{x}_{1,1}, \dots, \mathbf{id}\mathbf{x}_{B,A_B}} \rightarrow \underbrace{\text{OV}}_{\text{Output View: } \mathbf{ov}}$$

which differs from `inp_view`'s type only in mapping index functions to OV (Definition 8), rather than IV (Definition 6). Function `out_view` is defined as

$$\underbrace{(\mathbf{id}\mathbf{x}_{b,a})_{b \in [1, B]_{\mathbb{N}}, a \in [1, A_b]_{\mathbb{N}}}}_{\text{Index Functions}} \mapsto \underbrace{\underbrace{\mathbf{a}}_{\text{MDA}} \mapsto \underbrace{(\mathbf{b}_1, \dots, \mathbf{b}_B)}_{\text{BUFs}}}_{\text{Output View}}$$

for

$$\mathbf{b}_b[\mathbf{id}\mathbf{x}_{b,a}(i_1, \dots, i_D)] := \mathbf{a}_{b,a}[i_1, \dots, i_D]$$

and

$$(\mathbf{a}_{b,a}[i_1, \dots, i_D])_{b \in [1, B]_{\mathbb{N}}, a \in [1, A_b]_{\mathbb{N}}} := \mathbf{a}[i_1, \dots, i_D]$$

i.e.,  $\mathbf{a}_{b,a}[i_1, \dots, i_D]$  is the element at point  $i_1, \dots, i_D$  within MDA  $\mathbf{a}$  that belongs to the  $a$ -th access of the  $b$ -th BUF. We set  $\mathbf{b}_b[j_1, \dots, j_{D_b}] := \perp$  (symbol  $\perp$  denotes the undefined value) for all BUF indices which are not in the function range of the index functions.

Note that the computed output view  $\mathbf{ov}$  is partial (indicated by  $\rightarrow_p$  in Definition 8), because for non-injective index functions, it must hold  $\mathbf{id}\mathbf{x}_{b,a}(i_1, \dots, i_D) = \mathbf{id}\mathbf{x}_{b,a'}(i'_1, \dots, i'_D) \Rightarrow \mathbf{a}_{b,a}[i_1, \dots, i_D] = \mathbf{a}_{b,a'}[i'_1, \dots, i'_D]$  which may not be satisfied for each potential input MDA of the computed view.

*Notation 3 (Output Views).* Analogously to Notation 2, we denote `out_view` for a particular choice of index functions as

$$\text{out\_view}(ID_1 : \mathbf{id}\mathbf{x}_{1,1}, \dots, \mathbf{id}\mathbf{x}_{1,A_1} \quad \dots, \quad ID_B : \mathbf{id}\mathbf{x}_{B,1}, \dots, \mathbf{id}\mathbf{x}_{B,A_B})$$

*Example 10.* Function `out_view` is used for `MatVec` and `Jacobi1D` (in Notation 3) as follows:

$$\begin{array}{ccc} \text{MatVec:} & \text{out\_view}(w : \underbrace{(i, k) \mapsto (i)}_{\substack{a=1 \\ b=1}}) & \text{Jacobi1D:} & \text{out\_view}(w : \underbrace{(i) \mapsto (i)}_{a=1}) \end{array}$$

**2.3.3 Relation between View Functions.** We use view functions to transform data from their domain-specific representation (represented in our formalism as BUFs, Definition 5) to our internal, MDA-based representation (via input views) and back (via output views), as also illustrated in Figure 5. In our implementation presented later, we aim to access data uniformly in the form of MDAs, thereby being independent of domain-specific data representations. However, we aim to store the data physically in the domain-specific format, as such format is usually the more efficient representation. For example, we aim to store the input data of `MatVec` in the domain-specific matrix and vector format, rather than as an MDA, because the input MDA of `MatVec` contains many redundancies—each vector element once per row of the input matrix (as illustrated in Figure 10).

The following lemma proves that functions `inp_view` and `out_view` are invertible and that they are each others inverses. Consequently, the lemma shows how we can arbitrarily switch between the domain-specific and our MDA-based representation, and consequently also that we can implicitly identify MDAs with the domain-specific data representation. For example, for computing `MatVec`, we will specify the computations via pattern `md_hom` which operates on MDAs (see Figure 5), but we use the view functions in our implementation to implicitly forward the MDA accesses to the physically stored BUF representation.

LEMMA 2. *Let*

$$\text{inp\_view}(ID_1 : \mathbf{id}\mathbf{x}_{1,1}, \dots, \mathbf{id}\mathbf{x}_{1,A_1} \quad \dots, \quad ID_B : \mathbf{id}\mathbf{x}_{B,1}, \dots, \mathbf{id}\mathbf{x}_{B,A_B})$$

and

$$\text{out\_view}(ID_1 : \mathbf{id}\mathbf{x}_{1,1}, \dots, \mathbf{id}\mathbf{x}_{1,A_1} \quad \dots, \quad ID_B : \mathbf{id}\mathbf{x}_{B,1}, \dots, \mathbf{id}\mathbf{x}_{B,A_B})$$

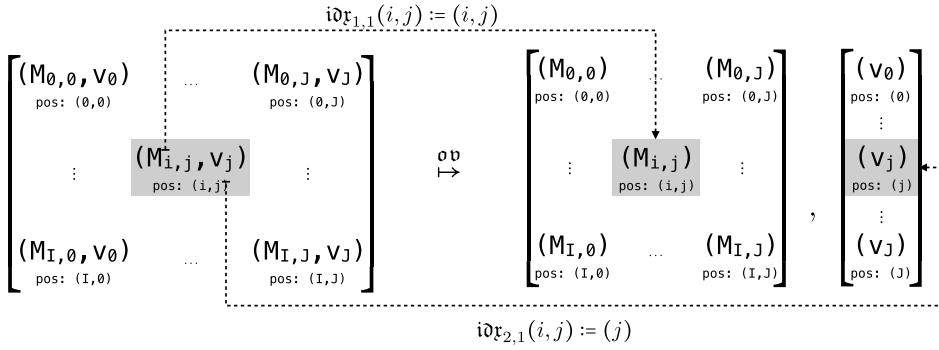
be two arbitrary instances of functions `inp_view` and `out_view` (in Notations 2 and 3), both using the same index functions  $\mathbf{id}\mathbf{x}_{1,1}, \dots, \mathbf{id}\mathbf{x}_{B,A_B}$ .

It holds (index functions omitted via ellipsis for brevity):

$$\text{inp\_view}(\dots) \circ \text{out\_view}(\dots) = \text{out\_view}(\dots) \circ \text{inp\_view}(\dots) = id$$

PROOF. Follows immediately from Definitions 7 and 9.  $\square$

The following figure illustrates the lemma using as example the inverse of `MatVec`'s input view (shown in Figure 10):



## 2.4 Examples

Figure 14 shows how our high-level representation is used for expressing different kinds of popular data-parallel computations. For brevity, we state only the index functions, scalar function, and combine operators of the higher-order functions; an expression as in Figure 6 is then obtained by straightforwardly inserting these building blocks into the higher-order functions.

*Subfigure 1.* We show how our high-level representation is used for expressing linear algebra routines: (1) Dot (*Dot Product*); (2) MatVec (*Matrix-Vector Multiplication*); (3) MatMul (*Matrix Multiplication*); (4) MatMul<sup>T</sup> (*Transposed Matrix Multiplication*) which computes matrix multiplication on transposed input and output matrices; (5) bMatMul (*batched Matrix Multiplication*) where multiple matrix multiplications are computed using matrices of the same sizes.

We can observe from the subfigure that our high-level expressions for the routines naturally evolve from each other. For example, the `md_hom` instance for MatVec differs from the `md_hom` instance for Dot by only containing a further concatenation dimension `+` for its  $i$  dimension. We consider this close relation between the high-level expressions of MatVec and Dot in our approach as natural and favorable, as MatVec can be considered as computing multiple times Dot—one computation of Dot for each value of MatVec's  $i$  dimension. Similarly, the `md_hom` instance for MatMul is very similar to the expression of MatVec, by containing the further concatenation dimension  $j$  for MatMul's  $j$  dimension. The same applies to bMatMul: its `md_hom` instance is the expression of MatMul augmented with one further concatenation dimension.

Regarding MatMul<sup>T</sup>, the basic computation part of MatMul<sup>T</sup> and MatMul are the same, which is exactly reflected in our formalisms: both MatMul<sup>T</sup> and MatMul are expressed using exactly the same `md_hom` instances. The differences between MatMul<sup>T</sup> and MatMul lies only in the data accesses—transposed accesses in the case of MatMul<sup>T</sup> and non-transposed accesses in the case of MatMul. Data accesses are expressed in our formalism, in a structured way, via view functions (as discussed in Section 2.3): for example, for MatMul<sup>T</sup>, we use for its first input matrix  $A$  the index function  $(i, j, k) \mapsto (k, i)$  for transposed access, instead of using index function  $(i, j, k) \mapsto (i, k)$  as for MatMul's non-transposed accesses.

Note that all `md_hom` instances in the subfigure are well defined according to Lemma 1.

*Subfigure 2.* We show how convolution-style stencil computations are expressed in our high-level representation: (1) Conv2D expresses a standard convolution that uses a two-dimensional sliding window [Podlozhnyuk, 2007]; (2) MCC expresses a so-called *Multi-Channel Convolution* [Dumoulin and Visin, 2018]—a generalization of Conv2D that is heavily used in the area of deep learning; (3) MCC\_Capsule is a recent generalization of MCC [Hinton et al., 2018] which attracted high attention due to its relevance for advanced deep learning neural networks [Barham and Isard, 2019].

While our `md_hom` instances for convolutions are quite similar to those of linear algebra routines (they all use multiplication `*` as scalar function and a mix of concatenations `+` and point-wise

md_hom	f	⊗ <sub>1</sub>	⊗ <sub>2</sub>	⊗ <sub>3</sub>	⊗ <sub>4</sub>	VIEWS	inp_view		out_view
							A	B	C
Dot	*	+				Dot	(k) ↦ (k)	(k) ↦ (k)	(k) ↦ (k)
MatVec	*	+	+			MatVec	(i,k) ↦ (i,k)	(i,k) ↦ (k)	(i,k) ↦ (i)
MatMul	*	+	+	+		MatMul	(i,j,k) ↦ (i,k)	(i,j,k) ↦ (k,j)	(i,j,k) ↦ (i,j)
MatMul <sup>T</sup>	*	+	+	+		MatMul <sup>T</sup>	(i,j,k) ↦ (k,i)	(i,j,k) ↦ (j,k)	(i,j,k) ↦ (j,i)
bMatMul	*	+	+	+	+	bMatMul	(b,i,j,k) ↦ (b,i,k)	(b,i,j,k) ↦ (b,k,j)	(b,i,j,k) ↦ (b,i,j)

## 1) Linear Algebra Routines

md_hom	f	⊗ <sub>1</sub>	⊗ <sub>2</sub>	⊗ <sub>3</sub>	⊗ <sub>4</sub>	⊗ <sub>5</sub>	⊗ <sub>6</sub>	⊗ <sub>7</sub>	⊗ <sub>8</sub>	⊗ <sub>9</sub>	⊗ <sub>10</sub>
Conv2D	*	+	+	+	+						
MCC	*	+	+	+	+	+	+	+			
MCC.Capsule	*	+	+	+	+	+	+	+	+	+	+

VIEWS	inp_view		out_view
	I	F	O
Conv2D	(p,q,r,s) ↦ (p+r,q+s)	(p,q,r,s) ↦ (r,s)	(p,q,r,s) ↦ (p,q)
MCC	(n,p,...) ↦ (n,p+r,q+s,c)	(n,p,...) ↦ (k,r,s,c)	(n,p,...) ↦ (n,p,q,k)
MCC.Capsule	(n,p,...) ↦ (n,p+r,q+s,c,mi,mk)	(n,p,...) ↦ (k,r,s,c,mk,mj)	(n,p,...) ↦ (n,p,q,k,mi,mj)

## 2) Convolution Stencils

md_hom	f	⊗ <sub>1</sub>	...	⊗ <sub>6</sub>	⊗ <sub>7</sub>	VIEWS	inp_view		out_view
							A	B	C
CCSD(T)	*	+	...	+	+	I1	(a,...,g) ↦ (g,d,a,b)	(a,...,g) ↦ (e,f,g,c)	(a,...,g) ↦ (a,...,f)
						I2	(a,...,g) ↦ (g,d,a,c)	(a,...,g) ↦ (e,f,g,b)	(a,...,g) ↦ (a,...,f)

## 3) Quantum Chemistry

md_hom	f	⊗ <sub>1</sub>	⊗ <sub>2</sub>	⊗ <sub>3</sub>	VIEWS	inp_view		out_view
						I	O	
Jacobi1D	J <sub>1D</sub>	+			Jacobi1D	(i1) ↦ (i1+0) , (i1) ↦ (i1+1) , ...	(i1) ↦ (i1)	
Jacobi2D	J <sub>2D</sub>	+	+		Jacobi2D	(i1,i2) ↦ (i1+0,i2+1) , ...	(i1,i2) ↦ (i1,i2)	
Jacobi3D	J <sub>3D</sub>	+	+	+	Jacobi3D	(i1,i2,i3) ↦ (i1+0,i2+1,i3+1) , ...	(i1,i2,i3) ↦ (i1,i2,i3)	

## 4) Jacobi Stencils

md_hom	f	⊗ <sub>1</sub>	⊗ <sub>2</sub>	VIEWS	inp_view		out_view
					N	E	M
PRL	wght	+	max <sub>PRL</sub>	PRL	(i,j) ↦ (i)	(i,j) ↦ (j)	(i,j) ↦ (i)

## 5) Probabilistic Record Linkage

md_hom	f	⊗ <sub>1</sub>	⊗ <sub>2</sub>	VIEWS	inp_view		out_view
					Elms	Bins	Out
Histo	f <sub>Histo</sub>	+	+	Histo	(e,b) ↦ (e)	(e,b) ↦ (b)	(e,b) ↦ (b)
GenHisto	f	⊗	+	GenHisto	(e,b) ↦ (e)	(e,b) ↦ (b)	(e,b) ↦ (b)

## 6) Histogram

md_hom	f	⊗ <sub>1</sub>	VIEWS	inp_view		out_view
				I	O <sub>1</sub>	O <sub>2</sub>
map(f)	f	+	map(f)	(i) ↦ (i)	(i) ↦ (i)	
reduce(⊕)	id	⊕	reduce(⊕)	(i) ↦ (i)	(i) ↦ (i)	
reduce(⊕, ⊗)	(x) ↦ (x,x)	(⊕, ⊗)	reduce(⊕, ⊗)	(i) ↦ (i)	(i) ↦ (i)	(i) ↦ (i)

## 7) Map/Reduce Patterns

md_hom	f	⊗ <sub>1</sub>	⊗ <sub>2</sub>	VIEWS	inp_view		out_view
					A	Out	
scan(⊕)	id	⊕	⊕	scan(⊕)	(i) ↦ (i)	(i) ↦ (i)	
MBBS	id	⊕	⊕	MBBS	(i,j) ↦ (i,j)	(i,j) ↦ (i)	

## 8) Prefix Sum Computations

Fig. 14. Data-parallel computations expressed in our high-level representation.



additions  $+$  as combine operators), the index functions used for the view functions of convolutions are notably different from those used for linear algebra routines: the index functions of convolutions contain arithmetic expressions (e.g.,  $p+r$  and  $q+s$ ) and thus access neighboring elements in their input—a typical access pattern in stencil computations that requires special optimizations [Hagedorn et al., 2018]. Moreover, convolution-style computations are often high-dimensional (e.g., 10 dimensions in the case of MCC\_Capsule), whereas linear algebra routines usually rely on less dimensions. Our experiments in Section 5 confirm that respecting the data access patterns and the high dimensionality of convolutions in the optimization process (as in our approach, which we discuss later) often achieves significantly higher performance than using optimizations chosen toward linear algebra routines, as in vendor libraries provided by NVIDIA and Intel for convolutions [Li et al., 2016].

*Subfigure 3.* We show how quantum chemistry computation *Coupled Cluster* (CCSD(T)) [Kim et al., 2019] is expressed in our high-level representation. The computation of CCSD(T) notably differs from those of linear algebra routines and convolution-style stencils, by accessing its high-dimensional input data in sophisticated transposed fashions: for example, the view function of CCSD(T)'s *instance one* (denoted as I1 in the subfigure) uses indices  $a$  and  $b$  to access the last two dimensions of its  $A$  input tensor (rather than the first two dimensions of the tensor, as would be the case for non-transposed accesses). For brevity, the subfigure presents only two CCSD(T) instances—in our experiments in Section 5, we present experimental results for nine different real-world CCSD(T) instances.

*Subfigures 4–6.* The subfigures present computations whose scalar functions and combine operators are different from those used in Subfigures 1–3 (which are in Subfigures 1–3 straightforward multiplications  $*$ , concatenation  $++$ , and point-wise additions  $+$  only). For example, Jacobi stencils (Subfigure 4) use as scalar function the Jacobi-specific computation  $J_{\text{nd}}$  [Cecilia et al., 2012], and *Probabilistic Record Linkage* (PRL) [Christen, 2012], which is heavily used in data mining to identify duplicate entries in a database, uses a PRL-specific both scalar function  $\text{wght}$  and combine operator  $\text{max}_{\text{PRL}}$  (point-wise combination via the PRL-specific binary operator  $\text{max}_{\text{PRL}}$ ) [Rasch et al., 2019b]. Histograms, in their generalized version [Henriksen et al., 2020] (denoted as GenHisto in Subfigure 6), use an arbitrary, user-defined scalar function  $f$  and a user-defined associative and commutative combine operator  $\oplus$ ; the standard histogram variant Histo is then a particular instance of GenHisto, for  $\oplus = +$  (point-wise addition) and  $f = f_{\text{Histo}}$ , where  $f_{\text{Histo}}(e, b) = 1$  iff  $e = b$  and  $f_{\text{Histo}}(e, b) = 0$  otherwise.

*Subfigure 7.* We show how typical map and reduce patterns [González-Vélez and Leyton, 2010] are implemented in our high-level representation. Examples  $\text{map}(f)$  and  $\text{reduce}(\oplus)$  (discussed in Examples 3 and 4) are simple and thus straightforwardly expressed in our representation. In contrast, example  $\text{reduce}(\oplus, \otimes)$  is more complex and shows how  $\text{reduce}(\oplus)$  is extended to combine the input vector simultaneously twice—once combining vector elements via operator  $\oplus$  and once using operator  $\otimes$ . The outcome of  $\text{reduce}(\oplus, \otimes)$  are two scalars—one representing the result of combination via  $\oplus$  and the other of combination via  $\otimes$ —which we map via the output view to output elements  $O_1$  (result of  $\oplus$ ) and  $O_2$  (result of  $\otimes$ ), correspondingly; this is also illustrated in Figure 13.

*Subfigure 8.* We present *prefix-sum* computations [Blelloch, 1990] which differ from the computations in Subfigures 1–7 in terms of their combine operators: the operator used for expressing computations in Subfigure 8 is different from concatenation (Example 1) and point-wise combinations (Example 2). Computation  $\text{scan}(\oplus)$  uses as combine operator  $++_{\text{prefix-sum}}(\oplus)$  which computes prefix-sum [Gorlatch and Lengauer, 1997] (formally defined by Rasch [2024], Section B.9) according to binary operator  $\oplus$ , and *Maximum Bottom Box Sum* (MBBS) [Farzan and Nicolet, 2019] uses a particular instance of prefix-sum for  $\oplus = +$  (addition).

### 3 Low-Level Representation for Data-Parallel Computations

We introduce our low-level representation for expressing data-parallel computations. In contrast to our high-level representation, our low-level representation explicitly expresses the de-composition and re-composition of computations (informally illustrated in Figure 3). Moreover, our low-level representation is designed such that it can be straightforwardly transformed to executable program code, because it explicitly captures and expresses the optimizations for the memory and core hierarchy of the target architecture.

In the following, after briefly discussing an introductory example in Section 3.1, we introduce in Section 3.2 our formal representation of computer systems, which we refer to as *Abstract System Model (ASM)*. Based on this model, we define *low-level MDAs*, *low-level BUFs*, and *low-level combine operators* in Section 3.3, which are basic building blocks of our low-level representation.

Note that all details and concepts discussed in this section are not exposed to the end users of our system and therefore transparent for them: expressions in our low-level representation are generated fully automatically for the user, from expressions in our high-level representation (Figure 4), according to the methodologies presented later in Section 4 and auto-tuning [Rasch et al., 2021].

#### 3.1 Introductory Example

Figure 15 illustrates our low-level representation by showing how MatVec (Matrix-Vector Multiplication) is expressed in our representation. In our example, we use an input matrix  $M \in T^{512 \times 4096}$  of size  $512 \times 4096$  (size chosen arbitrarily) that has an arbitrary but fixed scalar type  $T \in \text{TYPE}$ ; the input vector  $v \in T^{4096}$  is of size 4096, correspondingly.

For better illustration, we consider for this introductory example a straightforward, artificial target architecture that has only two memory layers—*Host Memory (HM)* and *Cache Memory (L1)*—and one *Core Layer (COR)* only; our examples presented and discussed later in this section target real-world architectures (e.g., CUDA-capable NVIDIA GPUs). The particular values of tuning parameters (discussed in detail later in this section), such as the number of threads and the order of combine operators, are chosen by hand for this example and as straightforward for simplicity.

Our low-level representations work in three phases: (1) *de-composition* (steps 1–7, in the right part of Figure 15), (2) *scalar* (step 8, bottom part of the figure), (3) *re-composition* (steps 9–15, left part). Steps are arranged from right to left, inspired by the application order of function composition.

(1) *De-Composition Phase*. The de-composition phase (steps 1–7 in Figure 15) partitions input MDA  $\downarrow \mathbf{a}$  (in the top right of Figure 15) to the structure  $\downarrow \mathbf{a}_f^{<\dots>}$  (bottom right) which we refer to as *low-level MDA* and define formally in the next subsection. The low-level MDA represents a partitioning of MDA  $\downarrow \mathbf{a}$  (a.k.a. *hierarchical, multi-dimensional tiling* in programming), where each particular choice of indices  $p_1^1 \in [0, 2)_{\mathbb{N}_0}$ ,  $p_2^1 \in [0, 4)_{\mathbb{N}_0}$ ,  $p_1^2 \in [0, 8)_{\mathbb{N}_0}$ ,  $p_2^2 \in [0, 16)_{\mathbb{N}_0}$ ,  $p_1^3 \in [0, 32)_{\mathbb{N}_0}$ ,  $p_2^3 \in [0, 64)_{\mathbb{N}_0}$  refers to an MDA that represents an individual part of MDA  $\downarrow \mathbf{a}$  (a.k.a. *tile* in programming—informally illustrated in Figure 7). The partitions are arranged on multiple layers (indicated by the  $p$ 's superscripts) and in multiple dimensions (indicated by subscripts)—as illustrated in Figure 16—according to the memory/COR of the target architecture and dimensions of the MDH computation: we partition for each of the target architecture's three layers (HM, L1, COR) and in each of the two dimensions of the MDH (dimensions 1 and 2, as we use example MatVec in Figure 15, which represents a two-dimensional MDH computation). Consequently, our partitioning approach allows efficiently exploiting each particular layer of the target architecture (both memory and core layers), and also optimizing for both dimensions of the target computation (in the case of MatVec, the  $i$ -dimension and also the  $k$ -dimension—see Figure 1), allowing fine-grained optimizations.

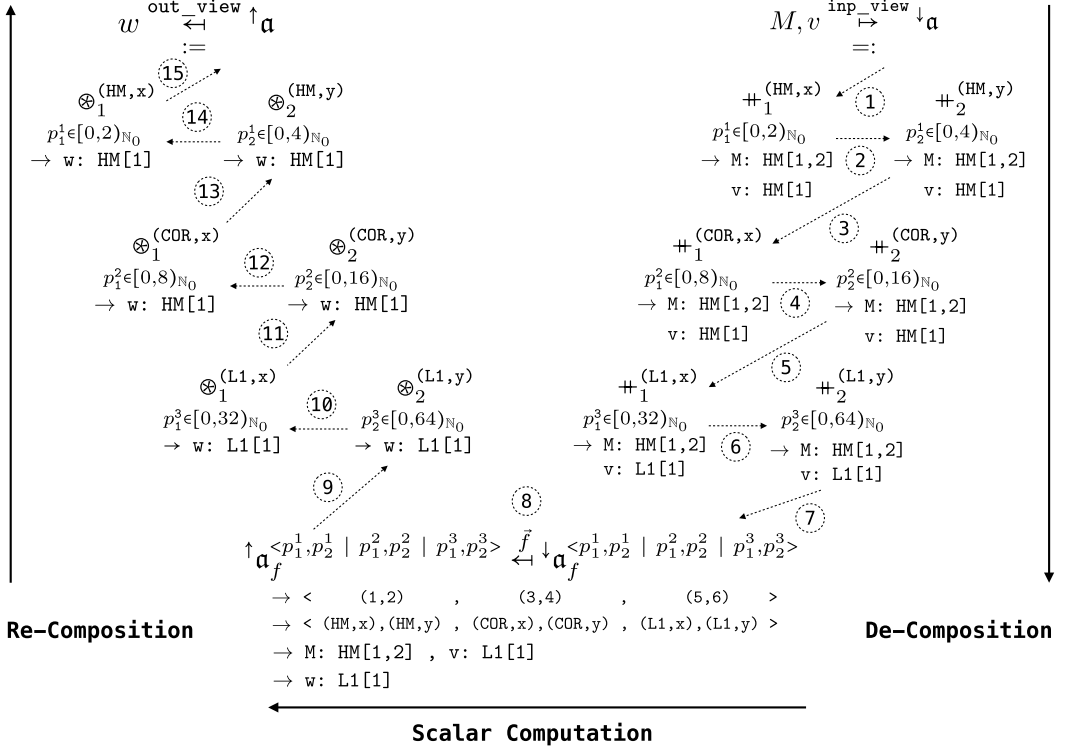


Fig. 15. Low-level expression for straightforwardly computing Matrix-Vector Multiplication (MatVec) on a simple, artificial architecture with two memory layers (HM L1) and one COR. Dotted lines indicate data flow.

We compute the partitionings of MDAs by applying the concatenation operator (Example 1) inversely (indicated by using  $\leftarrow$  instead of  $\leftarrow$  in the top right part of Figure 15). For example, we partition in Figure 15 MDA  $\downarrow a$  first via the inverse of  $\oplus_1^{(HM,x)}$  in dimension 1 (indicated by the subscript 1 of  $\oplus_1^{(HM,x)}$ ; the superscript (HM, x) is explained later) into two parts, as  $p_1^1$  iterates over interval  $[0, 2]_{N_0} = \{0, 1\}$  which consists of two elements (0 and 1)—the interval is chosen arbitrarily for this example. Afterward, each of the obtained parts is further partitioned, in the second dimension, via  $\oplus_2^{(HM,y)}$  into four parts ( $p_2^1$  iterates over  $[0, 4]_{N_0} = \{0, 1, 2, 3\}$  which consists of four elements). The  $(2 * 4)$ -many HM parts are then each further partitioned in both dimensions for the COR layer into  $(8 * 16)$  parts, and each individual COR part is again partitioned for the L1 layer into  $(32 * 64)$  parts, resulting in  $(2 * 8 * 32) * (4 * 16 * 64) = 512 * 4096$  parts in total.

We always use a *full partitioning* in our low-level expressions,<sup>12</sup> i.e., each particular choice of indices  $p_1^1, p_2^1, p_1^2, p_2^2, p_1^3, p_2^3$  points to an MDA that contains a single element only (in Figure 16, the individual elements are denoted via symbol  $\times$ , in the bottom part of the figure). By relying on a full partitioning, we can apply scalar function  $f$  to the fully partitioned MDAs later in the scalar phase (described in the next paragraph). This is because function  $f$  is defined on scalar values (Definition 4) to make defining scalar functions more convenient for the user (as discussed in Section 2.2).

<sup>12</sup>Our future work (outlined in Section 8) aims to additionally allow coarser-grained partitioning schemas, e.g., to target domain-specific hardware extensions (such as *NVIDIA Tensor Cores* [NVIDIA, 2017] which compute  $4 \times 4$  matrices immediately in hardware, rather than  $1 \times 1$  matrices as obtained in the case of a full partitioning).

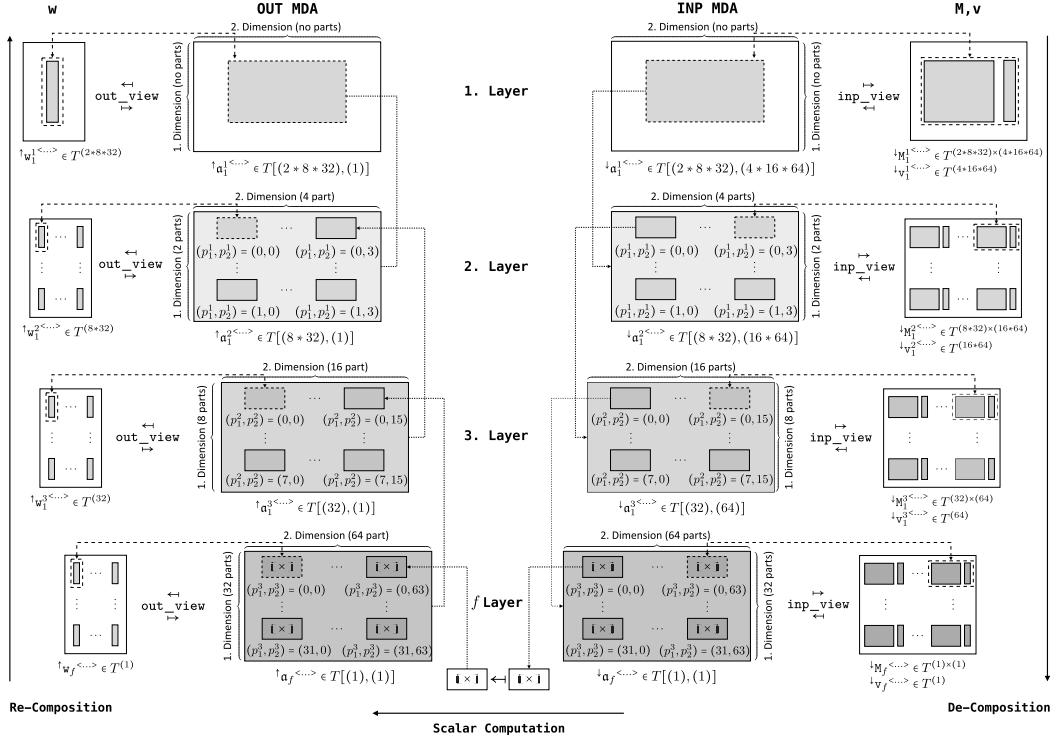


Fig. 16. Illustration of multi-layered, multi-dimensional MDA partitioning using the example MDA from Figure 15. In this example, we use three layers and two dimensions, according to Figure 15.

The superscript of combine operators, e.g.,  $(\text{COR}, x)$  of operator  $\oplus_1^{(\text{COR}, x)}$ , is a so-called *operator tag* (formal definition given in the next section). Such a tag indicates to our code generator whether its combine operator is assigned to a memory layer (and thus computed sequentially in our generated code) or to a COR (and thus computed in parallel). For example, tag  $(\text{COR}, x)$  indicates that parts processed by operator  $\oplus_1^{(\text{COR}, x)}$  should be computed by cores COR, and thus in parallel; the dimension tag  $x$  indicates that COR layer's  $x$  dimension should be used for computing the operator (we use dimension  $x$  for our example architecture as an analogous concept to CUDA's thread/block dimensions  $x, y, z$  for GPU architectures [NVIDIA, 2022g]), as we also discuss in the next section. In contrast, tag  $(\text{HM}, x)$  refers to a memory layer (HM) and thus, operator  $\oplus_1^{(\text{HM}, x)}$  is computed sequentially. Since the current state-of-practice programming approaches (OpenMP, CUDA, OpenCL, ...) have no explicit notion of memory tiles (e.g., by offering the potential variables `tileIdx.x/tileIdx.y/tileIdx.z`, as analogous concepts to CUDA variables `threadIdx.x/threadIdx.y/threadIdx.z`), the dimensions tag  $x$  in  $(\text{HM}, x)$  is currently ignored by our code generator, because HM refers to a memory layer.

Note that the number of parts (e.g., 2 parts on layer 1 in dimension 1, and 4 parts on layer 1 in dimension 2...), the combine operators' tags, and our partition order (e.g., first partitioning in MDA's dimension 1 and afterwards in dimension 2) are chosen arbitrarily for this example. These choices are critical for performance and should be optimized<sup>13</sup> for a particular target architecture

<sup>13</sup>We currently rely on auto-tuning [Rasch et al., 2021] for choosing optimized values of performance-critical parameters, as we discuss in Section 5.

and characteristics of the input and output data (size, memory layouts, etc.), as we discuss in detail later in this section.

(2) *Scalar Phase*. In the scalar phase (step 8 in Figure 15), we apply MDH's scalar function  $f$  to the individual MDA elements

$$\downarrow \mathbf{a}_f^{<p_1^1, p_2^1 \mid p_1^2, p_2^2 \mid p_1^3, p_2^3>}$$

for each particular choice of indices  $p_1^1, p_2^1, p_1^2, p_2^2, p_1^3, p_2^3$ , which results in

$$\uparrow \mathbf{a}_f^{<p_1^1, p_2^1 \mid p_1^2, p_2^2 \mid p_1^3, p_2^3>}$$

In the figure,  $\tilde{f}$  is the slight adaption of function  $f$  that operates on a singleton MDA, rather than a scalar (see Footnote 9).

Annotation  $\rightarrow <(1, 2), \dots>$  indicates the application order of applying scalar function (in this example, first iterating over  $p_1^1$ , then over  $p_2^1$ , etc.), and we use annotation  $\rightarrow <(\text{HM}, x), \dots>$  to indicate how the scalar computation is assigned to the target architecture (this is described in detail later in this section). Annotations  $\rightarrow \text{M}: \text{HM}$ ,  $v: \text{L1}$  and  $\rightarrow w: \text{L1}$  (in the bottom part of Figure 15) indicate the memory regions to be used for reading and writing the input scalar of function  $f$  (also described later in detail).

(3) *Re-Composition Phase*. Finally, the re-composition phase (steps 9–15 in Figure 15) combines the computed parts  $\uparrow \mathbf{a}_f^{<p_1^1, p_2^1 \mid p_1^2, p_2^2 \mid p_1^3, p_2^3>}$  (bottom left in the figure) to the final result  $\uparrow \mathbf{a}$  (top left) via MDH's combine operators, which are in the case of matrix-vector multiplication  $\oplus_1 := +$  (concatenation) and  $\oplus_2 := +$  (point-wise addition). In this example, we first combine the L1 parts in dimension 2 and then in dimension 1; afterward, we combine the COR parts in both dimensions, and finally the HM parts. Analogously to before, this order of combine operators and their tags are chosen arbitrarily for this example and should be auto-tuned for high performance.

In the de- and re-composition phases, the arrow notation below combine operators allow efficiently exploiting architecture's memory hierarchy, by indicating the memory region to read from (de-composition phase) or to write to (re-composition phase); the annotations also indicate the memory layouts to use. We exploit these memory and layout information in both (1) our code generation process to assign combine operators' input and output data to memory regions and to chose memory layouts for the data (row major, column major, etc.); (2) our formalism to specify constraints of programming models, e.g., that in CUDA, results of GPU cores can only be combined in designated memory regions [NVIDIA, 2022f]. For example, annotation  $\rightarrow \text{M}: \text{HM}[1, 2]$ ,  $v: \text{L1}[1]$  below an operator in the de-composition phase indicates to our code generator that the parts (a.k.a tiles) of matrix  $M$  used for this computation step should be read from the HM memory region and that parts of vector  $v$  should be copied to and accessed from fast L1 memory. The annotation also indicates that M should be stored using a row-major memory layout (as we use  $[1, 2]$  and not  $[2, 1]$ ). The memory regions and layouts are chosen arbitrarily for this example and should be chosen as optimized (auto-tuned) for the particular target architecture and characteristics of the input and output data. Formally, the arrow notation of combination operators is a concise notation to hide MDAs and BUFs for intermediate results (discussed by Rasch [2024], Section C.3, for the interested reader).

### Excursion: Code Generation<sup>14</sup>

Our low-level expressions can be straightforwardly transformed to executable program code in imperative-style programming languages (such as OpenMP, CUDA, and OpenCL). As code generation is not the focus of this work, we outline our code generation process briefly using the example of Figure 15. Details about our code generation are provided by Rasch [2024], Section E and will be presented and illustrated in detail in our future work.

We implement combine operators as sequential or parallel loops. For example, the operator  $+_1^{(HM, x)}$  is assigned to memory layer HM and thus implemented as a sequential loop (loop range indicated by  $[0, 2)_{\mathbb{N}_0}$ ), and operator  $+_1^{(COR, x)}$  is assigned to COR and thus implemented as a parallel loop (e.g., a loop annotated with `#pragma omp parallel` for in OpenMP [OpenMP, 2022], or variable `threadIdx.x` in CUDA [NVIDIA, 2022g]). Correspondingly, our three phases (de-composition, scalar, and re-composition) each correspond to an individual loop nest; we generate the nests as fused when the tags of combine operators have the same order in phases, as in Figure 15. Note that our currently targeted programming models (OpenMP, CUDA, and OpenCL) have no explicit notion of *tiles*, e.g., by offering the potential variable `tileIdx.x` for managing tiles automatically in the programming model (similarly as variable `threadIdx.x` automatically manages threads in CUDA). Consequently, when the operator tag refers to a memory layer, the dimension information within tags are currently ignored by our code generator (such as dimension  $x$  in tag  $(HM, x)$  which refers to memory layer HM).

Operators' memory regions correspond to straightforward allocations (e.g., in CUDA's device, shared, or register memory [NVIDIA, 2022g], according to the arrow annotations in our low-level expression). Memory layouts are implemented as aliases, e.g., *preprocessor directives* such as `#define M(i,k) M[k][i]` for storing MatVec's input matrix  $M$  as transposed.

We implement MDAs also as aliases (according to Definition 7), e.g., `#define inp_mda(i,k) M[i][k], v[k]` for MatVec's input MDA.

Code optimizations that are applied on a lower abstraction level than proposed by our representation in Example 15 are beyond the scope of this work and outlined by Rasch [2024], Section F, e.g., loop fusion and loop unrolling which are applied on the loop-based abstraction level.

We provide an open source *MDH compiler* for code generation [MDH Project, 2024]. Our compiler takes as input a high-level MDH expression (as in Figure 6), in the form of a Python program, and it fully automatically generates auto-tuned program code from it.

In the following, we introduce in Section 3.2 our formal representation of a computer system (which can be a single device, but also a multi-device or a multi-node system, as we discuss soon), and we illustrate our formal system representation using the example architectures targeted by programming models OpenMP, CUDA, and OpenCL. Afterward, in Section 3.3, we formally define the basic building blocks of our low-level representation—*low-level MDAs*, *low-level BUFs*, and *low-level combine operators*—based on our formal system representation.

## 3.2 ASM

**Definition 10 (Abstract System Model).** An  $L$ -Layered Abstract System Model (ASM),  $L \in \mathbb{N}$ , is any pair of two positive natural numbers

$$(\text{NUM\_MEM\_LYRS}, \text{NUM\_COR\_LYRS}) \in \mathbb{N} \times \mathbb{N}$$

for which  $\text{NUM\_MEM\_LYRS} + \text{NUM\_COR\_LYRS} = L$ .

<sup>14</sup>Our implementation of MDH is open source: <https://mdh-lang.org>



Our ASM representation is capable of modeling architectures with arbitrarily deep memory and core hierarchies<sup>15</sup>:  $\text{NUM\_MEM\_LYRS}$  denotes the target architecture's number of memory layers and  $\text{NUM\_COR\_LYRS}$  the architecture's number of COR, correspondingly. For example, the artificial architecture we use in Figure 15 is represented as an ASM instance as follows (bar symbols denote set cardinality):

$$\text{ASM}_{\text{artif.}} := ( |\{ \text{HM}, \text{L1} \}| , |\{ \text{COR} \}| ) = (2, 1)$$

The instance is a pair consisting of the numbers 2 and 1 which represent the artificial architecture's two memory layers (HM and L1) and its single COR.

*Example 11.* We show particular ASM instances that represent the device models of the state-of-practice approaches OpenMP, CUDA, and OpenCL:

$$\begin{aligned} \text{ASM}_{\text{OpenMP}} &:= ( |\{ \text{MM}, \text{L2}, \text{L1} \}| , |\{ \text{COR} \}| ) = (3, 1) \\ \text{ASM}_{\text{OpenMP+L3}} &:= ( |\{ \text{MM}, \text{L3}, \text{L2}, \text{L1} \}| , |\{ \text{COR} \}| ) = (4, 1) \\ \text{ASM}_{\text{OpenMP+L3+SIMD}} &:= ( |\{ \text{MM}, \text{L3}, \text{L2}, \text{L1} \}| , |\{ \text{COR}, \text{SIMD} \}| ) = (4, 2) \\ \text{ASM}_{\text{CUDA}} &:= ( |\{ \text{DM}, \text{SM}, \text{RM} \}| , |\{ \text{SMX}, \text{CC} \}| ) = (3, 2) \\ \text{ASM}_{\text{CUDA+WRP}} &:= ( |\{ \text{DM}, \text{SM}, \text{RM} \}| , |\{ \text{SMX}, \text{WRP}, \text{CC} \}| ) = (3, 3) \\ \text{ASM}_{\text{OpenCL}} &:= ( |\{ \text{GM}, \text{LM}, \text{PM} \}| , |\{ \text{CU}, \text{PE} \}| ) = (3, 2) \end{aligned}$$

OpenMP is often used to target  $(3 + 1)$ -layered architectures which rely on three memory regions (main memory MM and caches L2 and L1) and one COR. OpenMP-compatible architectures sometimes also contain the L3 memory region, and they may allow exploiting Single-Instruction-Multiple-Data parallelization (a.k.a. *vectorization* [Klemm et al., 2012]), which are expressed in our ASM representation as a further memory or COR, respectively.

CUDA's target architectures are  $(3 + 2)$ -layered: they consist of *Device Memory* (DM), *Shared Memory* (SM), and *Register Memory* (RM), and they offer as cores so-called *Streaming Multiprocessors* (SMX) which themselves consist of *Cuda Cores* (CC). CUDA also has an implicit notion of so-called *Warps* (WRP) which are not explicitly represented in the CUDA programming model [NVIDIA, 2022g], but often exploited by programmers—via special intrinsics (e.g., *shuffle* and *tensor core intrinsics* [NVIDIA, 2017, 2018])—to achieve highest performance.

OpenCL-compatible architectures are designed analogously to those targeted by CUDA; consequently, both OpenCL- and CUDA-compatible architectures are represented by the same ASM instance in our formalism. Apart from straightforward syntactical differences between OpenCL and CUDA [StreamHPC, 2016], we see as the main differences between the two programming models (from our ASM-based abstraction level) that OpenCL has no notion of warps, and it uses a different terminology—*Global/Local/Private Memory* (GM/LM/PM) instead of device/shared/register memory, and *Compute Unit* (CU) and *Processing Element* (PE), rather than SMX and CC.

In the following, we consider memory regions and cores of ASM-represented architectures as arrangeable in an arbitrary number of dimensions. Programming models for such architectures often have native support for such arrangements. For example, in the CUDA model, memory is accessed via arrays which can be arbitrary-dimensional (a.k.a. *multi-dimensional C arrays*), and cores are programmed in CUDA via threads which are arranged in CUDA's so-called dimensions  $x, y, z$ ; further thread dimensions can be explicitly programmed in CUDA, e.g., by embedding them in the last dimension  $z$ .

<sup>15</sup>We deliberately do not model into our ASM representation an architecture's particular number of cores and/or sizes of memory regions, because our optimization process is designed to be generic in these numbers and sizes, for high flexibility.

We express constraints of programming models—for example, that in CUDA, SMX can combine their results in DM only [NVIDIA, 2022f]—via so-called *tuning parameter constraints*, which we discuss later in this section.

Note that we call our abstraction *Abstract System Model* (rather than *Abstract Architecture Model*, or the like), because it can also represent systems consisting of multiple devices and/or nodes, and so on. For example, our ASM representation of a multi-GPU system is

$$\text{ASM}_{\text{Multi-GPU}} := ( |\{ \text{HM}, \text{DM}, \text{SM}, \text{RM} \}|, |\{ \text{GPU}, \text{SMX}, \text{CC} \}| ) = (4, 3)$$

It extends our ASM-based representation of CUDA devices (Example 11) by HM which represents the memory region of the system containing the GPUs (and in which the intermediate results of different GPUs are combined), and it introduces the further COR GPU representing the system's GPUs. Analogously, our ASM representation of a multi-node, multi-GPU system is

$$\text{ASM}_{\text{Multi-Node-Multi-GPU}} := ( |\{ \text{NM}, \text{HM}, \text{DM}, \text{SM}, \text{RM} \}|, |\{ \text{NOD}, \text{GPU}, \text{SMX}, \text{CC} \}| ) = (5, 4)$$

It adds to  $\text{ASM}_{\text{Multi-GPU}}$  the memory layer *Node Memory* (NM) which represents the memory region of the host node, and it adds COR *Node* (NOD) which represents the compute nodes. Our approach is currently designed for *homogeneous systems*, i.e., all devices/nodes/... are assumed to be identical. We aim to extend our approach to *heterogeneous systems* (which may consist of different devices/nodes/...) as future work, inspired by dynamic load balancing approaches [Chen et al., 2010].

### 3.3 Basic Building Blocks

We introduce the three main basic building blocks of our low-level representation: (1) *low-level MDAs* which we use to partition MDAs and that represent multi-layered, multi-dimensionally arranged collection of ordinary MDAs (Definition 1)—one ordinary MDA per memory/COR of their target ASM and for each dimension of the MDH computation (as illustrated in Figure 16); (2) *low-level BUFs* which are a collection of ordinary BUFs (Definition 5) and that are augmented with a *memory region* and a *memory layout*; (3) *low-level combine operators* which represent combine operators (Definition 2) to which the layer and dimension of their target ASM is assigned to be used to compute the operator in our generated code (e.g., a COR to compute the operator in parallel).

**Definition 11 (Low-Level MDA).** An  $L$ -layered,  $D$ -dimensional,  $P$ -partitioned *low-level MDA* that has scalar type  $T$  and index sets  $I$  is any function  $\mathbf{a}_{ll}$  of type:

$$\mathbf{a}_{ll}^{< \overbrace{(p_1^1, \dots, p_D^1) \in P_1^1 \times \dots \times P_D^1}^{\text{Partitioning: Layer 1}} \mid \dots \mid \overbrace{(p_1^L, \dots, p_D^L) \in P_1^L \times \dots \times P_D^L}^{\text{Partitioning: Layer L}} > : \\ I_1^{< p_1^1, \dots, p_D^1 \mid \dots \mid p_1^L, \dots, p_D^L > \times \dots \times I_D^{< p_1^1, \dots, p_D^1 \mid \dots \mid p_1^L, \dots, p_D^L > \rightarrow T$$

Next, we introduce *low-level BUFs* which work similarly as BUFs (Definition 5), but are tagged with a memory region and a memory layout. While these tags have no effect on the operators' semantics, they indicate later to our code generator in which memory region the BUF should be stored and accessed, and which memory layout to chose for storing the BUF. Moreover, we use these tags to formally define constraints of programming models, e.g., that according to the CUDA specification [NVIDIA, 2022f], SMX cores can combine their results in memory region DM only.

**Definition 12 (Low-Level BUF).** An  $L$ -layered,  $D$ -dimensional,  $P$ -partitioned *low-level BUF* that has scalar type  $T$  and size  $N$  is any function  $\mathbf{b}_{ll}$  of type ( $\hookrightarrow$  denotes bijection):

$$\mathbf{b}_{ll}^{\text{MEM} \in [1, \text{NUM\_MEM\_LYRS}]_{\mathbb{N}} \mid \sigma: [1, D]_{\mathbb{N}} \hookrightarrow [1, D]_{\mathbb{N}} \times \langle (p_1^1, \dots, p_D^1) \in P_1^1 \times \dots \times P_D^1 \mid \dots \mid (p_1^L, \dots, p_D^L) \in P_1^L \times \dots \times P_D^L \rangle} : \\ [0, N_1^{\langle p_1^1, \dots, p_D^1 \mid \dots \mid p_1^L, \dots, p_D^L \rangle}_{\mathbb{N}_0}} \times \dots \times [0, N_D^{\langle p_1^1, \dots, p_D^1 \mid \dots \mid p_1^L, \dots, p_D^L \rangle}_{\mathbb{N}_0}} \rightarrow T$$

We refer to MEM as low-level BUF's *memory region* and to  $\sigma$  as its *memory layout*, and we refer to the function

$$\mathbf{b}_{ll}^{\text{trans MEM} \in [1, \text{NUM\_MEM\_LYRS}]_{\mathbb{N}} \mid \sigma: [1, D]_{\mathbb{N}} \hookrightarrow [1, D]_{\mathbb{N}} \times \langle (p_1^1, \dots, p_D^1) \in P_1^1 \times \dots \times P_D^1 \mid \dots \mid (p_1^L, \dots, p_D^L) \in P_1^L \times \dots \times P_D^L \rangle} : \\ [0, N_{\sigma(1)}^{\langle p_1^1, \dots, p_D^1 \mid \dots \mid p_1^L, \dots, p_D^L \rangle}_{\mathbb{N}_0}} \times \dots \times [0, N_{\sigma(D)}^{\langle p_1^1, \dots, p_D^1 \mid \dots \mid p_1^L, \dots, p_D^L \rangle}_{\mathbb{N}_0}} \rightarrow T$$

that is defined as

$$\mathbf{b}_{ll}^{\text{trans MEM} \mid \sigma \times \langle p_1^1, \dots, p_D^1 \mid \dots \mid p_1^L, \dots, p_D^L \rangle} (i_{\sigma(1)}, \dots, i_{\sigma(D)}) := \mathbf{b}_{ll}^{\text{MEM} \mid \sigma \times \langle p_1^1, \dots, p_D^1 \mid \dots \mid p_1^L, \dots, p_D^L \rangle} (i_1, \dots, i_D)$$

as  $\mathbf{b}_{ll}$ 's *transposed function representation* (which we use to store the buffer in our generated code).

Finally, we introduce *low-level combine operators*. We define such operators to behave the same as ordinary combine operators (Definition 2), but we additionally tag them with a layer of their target ASM. Similarly as for low-level BUFs, the tag has no effect on semantics, but it is used in our code generation process to assign the computation to the hardware (e.g., indicating that the operator is computed by either an SMX, WRP, or CC when targeting CUDA—see Example 11). Also, we use the tags to define model-specific constraints in our formalism (as also discussed for low-level BUFs). We also tag the combine operator with a dimension of the ASM layer, enabling later in our optimization process to express advanced data access patterns (a.k.a. *swizzles* [Phothilimthana et al., 2019]). For example, when targeting CUDA, flexibly mapping ASM dimensions on CC layer (in CUDA terminology, the dimensions are called `threadIdx.x`, `threadIdx.y`, and `threadIdx.z`) to array dimensions enables the well-performing *coalesced global memory accesses* [NVIDIA, 2022f] for both transposed and non-transposed data layouts, by only using different dimension tags.

**Definition 13 (ASM Level).** We refer to pairs  $(l_{\text{ASM}}, d_{\text{ASM}})$ —consisting of an ASM layer  $l_{\text{ASM}} \in [1, L]_{\mathbb{N}}$  and an ASM dimension  $d_{\text{ASM}} \in [1, D]_{\mathbb{N}}$ —as *ASM Levels* (ASM-LVL)<sup>16</sup>

$$\text{ASM-LVL} := \{ (l_{\text{ASM}}, d_{\text{ASM}}) \mid l_{\text{ASM}} \in [1, L]_{\mathbb{N}}, d_{\text{ASM}} \in [1, D]_{\mathbb{N}} \}$$

**Definition 14 (Low-Level Combine Operator).** Let be  $L \in \mathbb{N}$  (representing an ASM's number of layers) and  $D \in \mathbb{N}$  (representing an MDH's number of dimensions). A *low-level combine operator*

$$\otimes^{\langle (l_{\text{ASM}}, d_{\text{ASM}}) \in \text{ASM-LVL} = \{ (l, d) \mid l \in [1, L]_{\mathbb{N}}, d \in [1, D]_{\mathbb{N}} \} \rangle}$$

is a function for which  $\otimes^{\langle (l_{\text{ASM}}, d_{\text{ASM}}) \rangle}$  is an ordinary combine operator (Definition 2), for each  $(l_{\text{ASM}}, d_{\text{ASM}}) \in \text{ASM-LVL}$ .

Note that in Figure 15, for better readability, we use domain-specific identifiers for ASM layers: HM:=1 as an alias for the ASM layer that has id 1, L1:=2 for the layer with id 2, and COR:=3 for the layer with id 3. For dimensions, we use aliases  $x := 1$  for ASM dimension 1 and  $y := 2$  for ASM dimension 2, correspondingly.

<sup>16</sup>For simplicity, we refrain from annotating identifier ASM-LVL with values  $L$  and  $D$  (e.g., ASM-LVL  $\langle L, D \rangle$ ), because both values will usually be clear from the context.

#### 4 Lowering: From High Level to Low Level

We have designed our formalism such that an expression in our high-level representation (as in Figure 6) can be *systematically lowered* to an expression in our low-level representation (as in Figure 15). For this, we parameterize our high-level representation, step-by-step, in tuning parameters; thereby, we obtain for concrete tuning parameter values a particular expression in our low-level representation—this is formally discussed and demonstrated by Rasch [2024], Section 4, for the interested reader. We chose optimized values of tuning parameters fully automatically via auto-tuning [Rasch et al., 2021]; Section 8 outlines alternative approaches for parameter selection.

Table 1 lists the tuning parameters of our lowering process—different values of tuning parameters lead to semantically equal expressions in our low-level representation (which is proven formally by Rasch [2024], Section 4), but the expressions will be translated to differently optimized code variants.<sup>17</sup>

In the following, we explain the 15 tuning parameters in Table 1. We give our explanations in a general, formal setting that is independent of a particular computation and programming model. Dotted lines in Table 1 separate parameters for different phases: parameters D1–D4 customize the de-composition phase, parameters S1–S6 the scalar phase, and parameters R1–R4 the re-composition phase, correspondingly; the parameter  $\emptyset$  impacts all three phases (separated by a straight line in the table).

Our tuning parameters in Table 1 have constraints: (1) *algorithmic constraints* which have to be satisfied by all target programming models, and (2) *model constraints* which are specific for particular programming models only (CUDA-specific constraints, OpenCL-specific constraints, etc), e.g., that the results of CUDA’s thread blocks can be combined in designated memory regions only [NVIDIA, 2022f]. We discuss algorithmic constraints in the following, together with our tuning parameters; model constraints are discussed by Rasch [2024], Section C.1, for the interested reader.

Note that our parameters do not aim to introduce novel optimization techniques, but to unify, generalize, and combine together well-proven optimizations, based on a formal foundation, toward an efficient, overall optimization process that applies to various combinations of data-parallel computations, architectures, and characteristics of input and output data (e.g., their size and memory layout).

In Table 1, we point to combine operators in Figure 15 using pairs  $(l, d)$  to which we refer as *MDH Levels*. We use the pairs as enumeration for operators in the de-composition and re-composition phases.

**Definition 15 (MDH Level).** We refer to pairs  $(l_{\text{MDH}}, d_{\text{MDH}})$ —consisting of a layer  $l_{\text{MDH}} \in [1, L]_{\mathbb{N}}$  and dimension  $d_{\text{MDH}} \in [1, D]_{\mathbb{N}}$ —as *MDH Levels* (MDH-LVL):

$$\text{MDH-LVL} := \{ (l_{\text{MDH}}, d_{\text{MDH}}) \mid l_{\text{MDH}} \in [1, L]_{\mathbb{N}}, d_{\text{MDH}} \in [1, D]_{\mathbb{N}} \}^{18}$$

We use the pairs to say, for example, that the MDH computation is partitioned on level  $(1, 1)$  (i.e., layer  $l = 1$ , dimension  $d = 1$ ) into two parts, as in Figure 15.

<sup>17</sup>Rasch [2024] (Section 3.5) shows that by choosing particular tuning parameter values, we can express in our formalism the (de/re)-compositions of different, existing state-of-the-art approaches, including scheduling-based approach TVM [Chen et al., 2018a], polyhedral compilers PPCG [Verdoolaeghe et al., 2013], and Pluto [Bondhugula et al., 2008b].

<sup>18</sup>The same as for identifier ASM-LVL (Definition 13), we refrain from annotating identifier MDH-LVL with values  $L$  and  $D$ . Note that MDH-LVL and ASM-LVL both refer to the same set of pairs, but we use identifier MDH-LVL when referring to MDH levels and identifier ASM-LVL when referring to ASM levels, correspondingly, for better clarity.

Table 1. Tuning Parameters of Our Low-Level Expressions

No.	Name	Range	Description
$\emptyset$	#PRT	$\text{MDH-LVL} \rightarrow \mathbb{N}$	number of parts
D1	$\sigma_{\downarrow\text{-ord}}$	$\text{MDH-LVL} \leftrightarrow \text{MDH-LVL}$	de-composition order
D2	$\leftrightarrow_{\downarrow\text{-ass}}$	$\text{MDH-LVL} \leftrightarrow \text{ASM-LVL}$	ASM assignment (de-composition)
D3	$\downarrow\text{-mem}^{<\text{ib}>}$	$\text{MDH-LVL} \rightarrow \text{MR}$	memory regions of input BUFs (ib)
D4	$\sigma_{\downarrow\text{-mem}}^{<\text{ib}>}$	$\text{MDH-LVL} \rightarrow [1, \dots, D_{\text{ib}}^{\text{IB}}]_{\mathcal{S}}$	memory layouts of input BUFs (ib)
S1	$\sigma_{f\text{-ord}}$	$\text{MDH-LVL} \leftrightarrow \text{MDH-LVL}$	scalar function order
S2	$\leftrightarrow_{f\text{-ass}}$	$\text{MDH-LVL} \leftrightarrow \text{ASM-LVL}$	ASM assignment (scalar function)
S3	$f^{\downarrow}\text{-mem}^{<\text{ib}>}$	MR	memory region of input BUF (ib)
S4	$\sigma_{f^{\downarrow}\text{-mem}}^{<\text{ib}>}$	$[1, \dots, D_{\text{ib}}^{\text{IB}}]_{\mathcal{S}}$	memory layout of input BUF (ib)
S5	$f^{\uparrow}\text{-mem}^{<\text{ob}>}$	MR	memory region of output BUF (ob)
S6	$\sigma_{f^{\uparrow}\text{-mem}}^{<\text{ob}>}$	$[1, \dots, D_{\text{ob}}^{\text{OB}}]_{\mathcal{S}}$	memory layout of output BUF (ob)
R1	$\sigma_{\uparrow\text{-ord}}$	$\text{MDH-LVL} \leftrightarrow \text{MDH-LVL}$	re-composition order
R2	$\leftrightarrow_{\uparrow\text{-ass}}$	$\text{MDH-LVL} \leftrightarrow \text{ASM-LVL}$	ASM assignment (re-composition)
R3	$\uparrow\text{-mem}^{<\text{ob}>}$	$\text{MDH-LVL} \rightarrow \text{MR}$	memory regions of output BUFs (ob)
R4	$\sigma_{\uparrow\text{-mem}}^{<\text{ob}>}$	$\text{MDH-LVL} \rightarrow [1, \dots, D_{\text{ob}}^{\text{OB}}]_{\mathcal{S}}$	memory layouts of output BUFs (ob)

*Parameter  $\emptyset$ .* Parameter #PRT is a function that maps pairs in MDH-LVL to natural numbers; the parameter determines *how much* data are grouped together into parts in our low-level expression (and consequently also in our generated code later), by setting the particular number of parts (a.k.a. *tiles*) used in our expression. For example, in Figure 15, we use  $\#PRT(1, 1) := 2$  which causes combine operators  $\oplus_1^{(\text{HM}, \text{x})}$  and  $\otimes_1^{(\text{HM}, \text{x})}$  to iterate over interval  $[0, 2)_{\mathbb{N}_0}$  (and thus partitioning the MDH computation on level  $(1, 1)$  into two parts), and we use  $\#PRT(1, 2) := 4$  to let operators  $\oplus_2^{(\text{HM}, \text{y})}$  and  $\otimes_2^{(\text{HM}, \text{x})}$  iterate over interval  $[0, 4)_{\mathbb{N}_0}$  (partitioning on level  $(1, 2)$  into four parts), and so on.

To ensure a full partitioning (so that we obtain singleton MDAs to which scalar function  $f$  can be applied in the scalar phase, as discussed above), we require the following algorithmic constraint for the parameter ( $N_d$  denotes the input size in dimension  $d$ ):

$$\prod_{l \in [1, L]_{\mathbb{N}}} \#PRT(l, d) = N_d, \text{ for all } d \in [1, D]_{\mathbb{N}}.$$

In our generated code, the number of parts directly translates to the number of *tiles* which are computed either sequentially (a.k.a. *cache blocking* [Lam et al., 1991]) or in parallel, depending on

the combine operators tags (which are chosen via Parameters D2, S2, R2, as discussed soon). In our example from Figure 15, we process parts belonging to combine operators tagged with HM and L1 sequentially, via for-loops, because HM and L1 correspond to ASM's memory layers (note that Parameter 0 only chooses the number of tiles; the parameter has no effect on explicitly copying data into fast memory resources, which is the purpose of Parameters D3, R3, S1, S2). The COR parts are computed in parallel in our generated code, because COR corresponds to ASM's COR, and thus, the number of COR parts determines the number of threads used in our code.

An optimized number of tiles is essential for achieving high performance [Bacon et al., 1994], e.g., due to its impact for locality-aware data accesses (number of sequentially computed tiles) and efficiently exploiting parallelism (number of tiles computed in parallel, which corresponds to the number of threads in our generated code).

*Parameters D1, S1, R1.* These three parameters are permutations on MDH-LVL (indicated by symbol  $\leftrightarrow$  in Table 1), determining *when* data are accessed and combined. The parameters specify the order of combine operators in the de-composition and re-composition phases (parameters D1 and R1), and the order of applying scalar function  $f$  to parts (parameter S1). Thereby, the parameters specify when parts are processed during the computation.

In our generated code, combine operators are implemented as sequential/parallel loops such that the parameters enable optimizing loop orders (a.k.a. *loop permutation* [McKinley et al., 1996]). For combine operators assigned to ASM's COR (via parameter R2 discussed in the next paragraph) and thus computed in parallel, parameter R1 particularly determines when the computed results of threads are combined: if we used in the re-composition phase of Figure 15 combine operators tagged with (COR, x) and (COR, y) immediately after applying scalar function  $f$  (i.e., in steps ⑩ and ⑪, rather than steps ⑫ and ⑬), we would combine the computed intermediate results of threads multiple times, repeatedly after each individual computation step of threads, and using the two operators at the end of the re-composition phase (in steps ⑭ and ⑮) would combine the result of threads only once, at the end of the re-composition phase. Combining the results of threads early in the computation usually has the advantages of reduced memory footprint, because memory needs to be allocated for one thread only, but at the cost of more computations, because the results of threads need to be combined multiple times. In contrast, combining the results of threads late in the computation reduces the amount of computations, but at the cost of higher memory footprint. Our parameters make this tradeoff decision generic in our approach such that the decision can be left to an auto-tuning system, for example.

Note that each phase corresponds to an individual loop nest which we fuse together when parameters D1, S1, R1 (as well as parameters D2, S2, R2) coincide (as also outlined by Rasch [2024], Section F).

*Parameters D2, S2, R2.* These parameters (symbol  $\leftrightarrow$  in the table denotes bijection) assign MDH levels to ASM levels, by setting the tags of low-level combine operators (Definition 14). Thereby, the parameters determine *by whom* data are processed (e.g., threads or for-loops), similar to the concept of bind in scheduling languages [Apache TVM Documentation, 2022a]. Consequently, the parameters determine which parts should be computed sequentially in our generated code and which parts in parallel. For example, in Figure 15, we use  $\leftrightarrow_{\downarrow -\text{ass}}(2, 1) := (\text{COR}, x)$  and  $\leftrightarrow_{\downarrow -\text{ass}}(2, 2) := (\text{COR}, y)$ , thereby assigning the computation of MDA parts on layer 2 in both dimensions to ASM's COR layer in the de-composition phase, which causes processing the parts in parallel in our generated code. For multi-layered core architectures, the parameters particularly determine the thread layer to be used for the parallel computation (e.g., block or thread in CUDA).



Using these parameters, we are able to flexibly set data access patterns in our generated code. In Figure 15, we assign parts on layer 2 to COR layers, which results in a so-called *block access* pattern of cores: we start  $8 * 16$  threads, according to the  $8 * 16$  core parts, and each thread processes a part of the input MDA representing a block of  $32 * 64$  MDA elements within the input data. If we had assigned in the figure the first computation layer to ASM's COR layer (in the figure, this layer is assigned to ASM's HM layer), we would start  $2 * 4$  threads and each thread would process MDA parts of size  $(8 * 32) * (16 * 64)$ ; assigning the last MDH layer to CORs would result in  $(2 * 8 * 32) * (4 * 16 * 64)$  threads, each processing a singleton MDA (a.k.a. *strided access*).

The parameters also enable expressing so-called *swizzle* access patterns [Phothilimthana et al., 2019]. For example, in CUDA, processing consecutive data elements in data dimension 1 by threads that are consecutive in thread dimension 2 (a.k.a. `threadIdx.y` dimension in CUDA) can achieve higher performance due to the hardware design of fast memory resources in NVIDIA GPUs. Such swizzle patterns can be easily expressed and auto-tuned in our approach; for example, by interchanging in Figure 15 tags (COR, x) and (COR, y). For memory layers (such as HM and L1), the dimension tags x and y currently have no effect on our generated code, as the programming models we target at the moment (OpenMP, CUDA, and OpenCL) have no explicit notion of tiles. However, this might change in the future when targeting new kinds of programming models, e.g., for upcoming architectures.

*Parameters D3, R3 and S3, S5.* Parameters D3 and R3 set for each BUF the memory region to be used, thereby determining *where* data are read from or written to, respectively. In the table, we use  $ib \in \mathbb{N}$  to refer to a particular input BUF (e.g.,  $ib=1$  to refer to the input matrix of matrix-vector multiplication, and  $ib=2$  to refer to the input vector), and  $ob \in \mathbb{N}$  refers to an output BUF, correspondingly. Parameter D3 specifies the memory region to read from, and parameter R3 the region to write to. The set  $MR := [1, \text{NUM\_MEM\_LYRS}]_{\mathbb{N}}$  denotes the ASM's memory regions.

Similarly to parameters D3 and R3, parameters S3 and S5 set the memory regions for the input and output of scalar function  $f$ .

Exploiting fast memory resources of architectures is a fundamental optimization [Bondhugula, 2020; Hristea et al., 1997; Mei et al., 2014; Salvador Rohwedder et al., 2023], particularly due to the performance gap between processors' cores and their memory systems [Oliveira et al., 2021; Wilkes, 2001].

*Parameters D4, R4 and S4, S6.* These parameters set the memory layouts of BUFs, thereby determining *how* data are accessed in memory; for brevity in Table 1, we denote the set of all BUF permutations  $[1, D]_{\mathbb{N}} \mapsto [1, D]_{\mathbb{N}}$  (Definition 12) as  $[1, \dots, D]_{\mathcal{S}}$  (symbol  $\mathcal{S}$  is taken from the notation of *symmetric groups* [Sagan, 2001]). In the case of our matrix-vector multiplication example in Figure 15, we use a standard memory layout for all matrices, which we express via the parameters by setting them to the identity function, e.g.,  $\sigma_{\text{mem}}^{<\text{M}>}(1, 1) := id$  (Parameter D4) for the matrix read by operator  $\oplus_1^{(\text{HM}, x)}$ .

An optimized memory layout is important to access data in a locality-aware and thus efficient manner.

## 5 Experimental Results

We experimentally evaluate our approach by comparing it to popular representatives of four important classes:

- (1) *Scheduling Approach:* TVM [Chen et al., 2018a] which generates GPU and CPU code from programs expressed in TVM's own high-level program representation;

- (2) *Polyhedral Compilers*: PPCG [Verdoolaeye et al., 2013] for GPUs<sup>19</sup> and Pluto [Bondhugula et al., 2008b] for CPUs, which automatically generate executable program code in CUDA (PPCG) or OpenMP (Pluto) from straightforward, unoptimized C programs;
- (3) *Functional Approach*: Lift [Steuwer et al., 2015] which generates OpenCL code from a Lift-specific, functional program representation;
- (4) *Domain-Specific Libraries*: NVIDIA cuBLAS [NVIDIA, 2022b] and NVIDIA cuDNN [NVIDIA, 2022e], as well as Intel oneMKL [Intel, 2022c] and Intel oneDNN [Intel, 2022b], which offer the user easy-to-use, domain-specific building blocks for programming. The libraries internally rely on pre-implemented assembly code that is optimized by experts for their target application domains: linear algebra (cuBLAS and oneMKL) or convolutions (cuDNN and oneDNN), respectively. To make comparison against the libraries challenging for us, we compare to all routines provided by the libraries. For example, the cuBLAS library offers three, semantically equal but differently optimized routines for computing MatMul: cublasSgemm (the default MatMul implementation in cuBLAS), cublasGemmEx which is part of the cuBLASEx extension of cuBLAS [NVIDIA, 2022c], and the most recent cublasLtMatmul which is part of the cuBLASLt extension [NVIDIA, 2022d]; each of these three routines may perform differently on different problem sizes (NVIDIA usually recommends to naively test which routine performs best for the particular target problem). To make comparison further challenging for us, we exhaustively test for each routine all of its so-called cublasGemmAlgo\_t variants and report the routine's runtime for the best performing variant. In the case of oneMKL, we compare also to its *JIT engine* [Intel, 2019] which is specifically designed and optimized for small problem sizes. We also compare to library *EKR* [Hentschel et al., 2008] which computes data mining example PRL (Figure 14) on CPUs—the library is implemented in the Java programming language and parallelized via *Java Threads*, and the library is used in practice by the *Epidemiological Cancer Registry* in North Rhine-Westphalia (Germany) which is the currently largest cancer registry in Europe.

We compare to the approaches experimentally in terms of

- (1) *Performance*: via a runtime comparison of our generated code against code that is generated according to the related approaches;
- (2) *Portability*: based on the *Pennycook Metric* [Pennycook et al., 2019] which mathematically defines portability<sup>20</sup> as

$$\Phi(a, p, H) = \begin{cases} \frac{|H|}{\sum_{i \in H} \frac{1}{e_i(a, p)}} & \text{if } i \text{ is supported, } \forall i \in H \\ 0 & \text{otherwise} \end{cases}$$

In words: “for a given set of platforms  $H$ , the *performance portability* ( $PP$ )  $\Phi$  of an application  $a$  solving problem  $p$  is defined as  $\Phi(a, p, H)$ , where  $e_i(a, p)$  is the performance efficiency (i.e., a ratio of observed performance relative to some proven, achievable level of performance) of application  $a$  solving problem  $p$  on platform  $i$ ; value  $\Phi(a, p, H)$  is 0, if any platform in  $H$  is unsupported by  $a$  running  $p$ ” [Pennycook et al., 2019]. Consequently, Pennycook defines portability as a real value in the interval  $[0, 1]_{\mathbb{R}}$  such that a value close to 1 indicates *high* portability and a value close to 0 indicates *low* portability. Here, platforms  $H$  represents a

<sup>19</sup>We cannot compare to polyhedral compiler TC [Vasilache et al., 2019] which is optimized toward deep learning computations on GPUs, because TC is not under active development anymore and thus is not working for newer CUDA architectures [Facebook Research, 2022]. Rasch et al. [2019a] show that our approach—already in its proof-of-concept version—achieves higher performance than TC for popular computations on real-world datasets.

<sup>20</sup>Pennycook's metric is actually called *PP*. Since *PP* particularly includes functional portability, we refer to Pennycook's *PP* also more generally as *Portability* only.

set of devices (CPUs, GPUs, ...), an application  $a$  is in our context a framework (such as TVM, a polyhedral compiler, or our approach), problems  $p$  are our case studies, and  $e_i(a, p)$  is computed as the runtime  $a_{p,i}^{\text{best}}$  of the application that achieves the best observed runtime for problem  $p$  on platform  $i$ , divided by the runtime of application  $a$  for problem  $p$  running on platform  $i$ .

- (3) *Productivity*: by intuitively arguing that our approach achieves the same/lower/higher productivity as the related approaches, using the representative example computation *Matrix-Vector Multiplication* (MatVec) (Figure 6). Classical code metrics, such as *Lines of Code*, *Constructive Cost Model* [Boehm et al., 1995], McCabe’s *Cyclomatic Complexity* [McCabe, 1976], and *Halstead Development Effort* [Halstead, 1977], are not meaningful for comparing the short and concise programs in high-level languages as proposed by the related work as well as our approach.

In the following, after discussing our application case studies, experimental setup, auto-tuning system, and code generator, we compare our approach to each of the four abovementioned classes of approaches (1)–(4) in Sections 5.1–5.4.

### Application Case Studies

We use for experiments in this section popular example computations from Figure 14 that belong to different classes of computations:

- Linear Algebra Routines: *Matrix Multiplication* (MatMul) and *Matrix-Vector Multiplication* (MatVec);
- Stencil Computations: *Jacobi Computation* (Jacobi3D) and *Gaussian Convolution* (Conv2D) which differ from linear algebra routines by accessing neighboring elements in their input data;
- Quantum Chemistry: *Coupled Cluster* (CCSD(T)) computations which differ from linear algebra routines and stencil computations by accessing their high-dimensional input data in complex, transposed fashions;
- Data Mining: PRL which differs from the previous computations by relying on a PRL-specific combine operator and scalar function (instead of straightforward additions or multiplications as the previous computations);
- Deep Learning: the most time-intensive computations within the popular neural networks ResNet-50 [He et al., 2015], VGG-16 [Simonyan and Zisserman, 2014], and MobileNet [Howard et al., 2017], according to their TensorFlow implementations [TensorFlow, 2022a,b,c]. Deep learning computations rely on advanced variants of linear algebra routines and stencil computations, e.g., MCC and MCC\_Capsule for computing convolution-like stencils, instead of the classical Conv2D variant of convolution (Figure 14)—the deep learning variants are considered as significantly more challenging to optimize than their classical variants [Barham and Isard, 2019].

We use for experiments this subset of computations from Figure 14 to make experimenting challenging for us: the computations differ in major characteristics (as discussed in Section 2.4), e.g., accessing neighboring elements in their input data (as stencil computations) or not (as linear algebra routines), thus usually requiring fundamentally different kinds of optimizations. Consequently, we consider it challenging for our approach to achieve high performance for our studies, because our approach relies on a generalized optimization process (discussed in Section 4) that uniformly applies to any kind of data-parallel computation and also parallel architecture. In contrast, the optimization processes of the related approaches are often specially designed and tied to a particular

application class and often also architecture. For example, NVIDIA cuBLAS and Intel oneMKL are highly optimized specifically for linear algebra routines on either GPU or CPU, respectively, and TVM is specifically designed and optimized for deep learning computations.

To make experimenting further challenging for us, we consider data sizes and characteristics either taken from real-world computations (e.g., from the *TCCG* benchmark suite [Springer and Bientinesi, 2016] for quantum chemistry computations) or sizes that are preferable for our competitors, e.g., powers of two for which many competitors are highly optimized, e.g., vendor libraries. For the deep learning case studies, we use data characteristics (sizes, strides, padding strategy, image/filter formats, etc.) taken from the particular implementations of the neural networks when computing the popular *ImageNet* [Krizhevsky et al., 2012] dataset (the particular characteristics are listed by Rasch [2024], Section D.1, for the interested reader). For all experiments, we use single precision floating point numbers (a.k.a. float or fp32), as such precision is the default in TensorFlow and many other frameworks.

## Experimental Setup

We run our experiments on a cluster containing two different kinds of GPUs and CPUs:

- NVIDIA Ampere GPU A100-PCIE-40GB
- NVIDIA Volta GPU V100-SXM2-16GB
- Intel Xeon Broadwell CPU E5-2683 v4 @ 2.10GHz
- Intel Xeon Skylake CPU Gold-6140 @ 2.30GHz

We represent the two CUDA GPUs in our formalism using model  $\text{ASM}_{\text{CUDA+WRP}}$  (Example 11). We rely on model  $\text{ASM}_{\text{CUDA+WRP}}$ , rather than the CUDA's standard model  $\text{ASM}_{\text{CUDA}}$  (also in Example 11), to exploit CUDA's (implicit) warp level for a fair comparison to the related approaches: warp-level optimizations are exploited by the related approaches (such as TVM), e.g., for *shuffle operations* [NVIDIA, 2018] which combine the results of threads within a warp with high performance. To fairly compare our approach to TVM and PPCG, we avoid exploiting warps' *tensor core intrinsics* [NVIDIA, 2017], in all experiments, which compute the multiplication of small matrices with high performance [Feng et al., 2023], because these intrinsics are not used in the TVM- and PPCG-generated CUDA code. For the two CPUs, we rely on model  $\text{ASM}_{\text{OpenCL}}$  (Example 11) for generating OpenCL code. The same as our approach, TVM also generates OpenCL code for CPUs; Pluto relies on the OpenMP approach to target CPUs.

For all experiments, we use the currently newest versions of frameworks, libraries, and compilers, as follows. We compile our generated GPU code using library CUDA NVRTC [NVIDIA, 2022h] from CUDA Toolkit 11.4, and we use Intel's OpenCL runtime version 18.1.0.0920 for compiling CPU code. For both compilers, we do not set any flags so that they run in their default modes. For the related approaches, we use the following versions of frameworks, libraries, and compilers:

- TVM [Apache, 2022] version 0.8.0 which also uses our system's CUDA Toolkit version 11.4 for GPU computations and Intel's runtime version 18.1.0.0920 for computations on CPU;
- PPCG [Michael Kruse, 2022] version 0.08.04 using flag `--target=cuda` for generating CUDA code, rather than OpenCL, as CUDA is usually better performing than OpenCL on NVIDIA GPUs, and we use flag `--sizes` followed by auto-tuned tile sizes—we rely on the *Auto-Tuning Framework (ATF)* [Rasch et al., 2021] for choosing optimized tile size values (as we discuss in the next subsection);

- Pluto [Uday Bondhugula, 2022] commit 12e075a using flag `--parallel` for generating OpenMP-parallelized C code (rather than sequential C), as well as flag `--tile` to use ATF-tuned tile sizes for Pluto; the Pluto-generated OpenMP code is compiled via Intel's `icx` compiler version 2022.0.0 using the Pluto-recommended optimization flags `-O3 -qopenmp`;
- NVIDIA cuBLAS [NVIDIA, 2022b] from CUDA Toolkit 11.4, using the NVIDIA-recommended compiler flags `-fast -O3 -DNDEBUG`;
- NVIDIA cuDNN [NVIDIA, 2022e] from CUDA Toolkit 11.4, using the NVIDIA-recommended compiler flags `-fast -O3 -DNDEBUG`;
- Intel oneMKL [Intel, 2022c] compiled with Intel's `icpx` compiler version 2022.0.0, using flags `-DMKL_ILP64 -qmk1=parallel -L${MKLRROOT}/lib/intel64 -liomp5 -lpthread -lm -ldl`, as recommended for oneMKL by Intel's *Link Line Advisor* tool [Intel, 2022a], as well as standard flags `-O3 -DNDEBUG`;
- Intel oneDNN [Intel, 2022b] also compiled with Intel's `icpx` compiler version 2022.0.0, using flags `-I${DNNLROOT}/include -L${DNNLROOT}/lib -ldnnl`, according to oneDNN's documentation, as well as standard flags `-O3 -DNDEBUG`;
- EKR [Hentschel et al., 2008] executed via Java SE 1.8.0 Update 281.

We profile runtimes of CUDA and OpenCL programs using the corresponding, event-based profiling APIs provided by CUDA and OpenCL. For Pluto which generates OpenMP-annotated C code, we measure runtimes via system call `clock_gettime` [GNU/Linux, 2022]. In the case of C++ libraries Intel oneMKL and Intel oneDNN, we use the C++ `chrono` library [C++ reference, 2022] for profiling. Libraries NVIDIA cuBLAS and NVIDIA cuDNN are also based on the CUDA programming model; thus, we profile them also via CUDA events. To measure the runtimes of the EKR Java library, we use Java function `System.currentTimeMillis()`.

All measurements of CUDA and OpenCL programs contain the pure program runtime only (a.k.a. *kernel runtime*). The runtime of *host code*<sup>21</sup> is not included in the reported runtimes, as performance of host code is not relevant for this work and the same for all approaches.

In all experiments, we collect measurements until the 99% confidence interval was within 5% of our reported means, according to the guidelines for *scientific benchmarking of parallel computing systems* by Hoefler and Belli [2015].

## Auto-Tuning

The auto-tuning process of our approach relies on the generic ATF [Rasch et al., 2021]. The ATF framework has proven to be efficient for exploring large search spaces of constrained tuning parameters (as our space introduced in Section 4). We use ATF, out of the box, exactly as described by Rasch et al. [2021]: (1) we straightforwardly represent in ATF our search space (Table 1) via *tuning parameters* which express the parameters in the table and their constraints; (2) we use ATF's pre-implemented cost functions for CUDA and OpenCL to measure the cost of our generated OpenCL and CUDA codes (in this article, we consider as cost program's runtime, rather than its energy consumption or similar); (3) we start the tuning process using ATF's default search technique (*AUC bandit* [Ansel et al., 2014]). ATF then fully automatically determines a well-performing tuning parameter configuration for the particular combination of a case study, architecture, and input/output characteristics (size, memory layout, etc.).

For scheduling approach TVM, we use its *Ansor* [Zheng et al., 2020a] optimization engine which is specifically designed and optimized toward generating optimized TVM schedules. Polyhedral

<sup>21</sup>Host code is required in approaches CUDA and OpenCL for program execution: it compiles the CUDA and OpenCL programs, performs data transfers between host and device, and so on. We rely on the high-level library dOCAL [Rasch et al., 2018, 2020a] for host code programming in this work.



compilers PPCG and Pluto do not provide own auto-tuning systems; thus, we use for them also ATF for auto-tuning, the same as for our approach. For both compilers, we additionally also report their runtimes when relying on their internal heuristics, rather than on auto-tuning, to fairly compare to them.

To achieve the best possible performance results for TVM, PPCG, and Pluto, we auto-tune each of these frameworks individually, for each particular combination of case study, architecture, and input/output characteristics, the same as for our approach. For example, we start for TVM one tuning run when auto-tuning case study MatMul for the NVIDIA Ampere GPU on one input size, and another, new tuning run for a new input size.

Hand-optimized libraries NVIDIA cuBLAS/cuDNN and Intel oneMKL/oneDNN rely on heuristics provided by experts, rather than auto-tuning. By relying on heuristics, the libraries avoid the time-intensive process of auto-tuning. However, auto-tuning is well amortized in many application areas (e.g., deep learning), because the auto-tuned implementations are re-used in many program runs. Moreover, auto-tuning avoids the complex and costly process of hand optimization by experts, and it often achieves higher performance than hand-optimized code (as we confirm later in our experiments), because well-performing optimizations are often not intuitive.

For a fair comparison, we use for each tuning run uniformly the same tuning time of 12 h. Even though for many computations well-performing tuning results could often be found in less than 12 h, for our approach as well as for other frameworks, we use such generous tuning time for all frameworks to avoid auto-tuning issues in our reported results—analyzing, improving, and accelerating the auto-tuning process is beyond the scope of this work and intended for our future work (as also outlined in Section 8). In particular, TVM’s Ansor optimizer was often able to find well performing optimizations in 6h of tuning time or less. This is because Ansor explores a small search space that is designed and optimized for deep learning computations—Ansor’s space is a proper subset of our space, as our space aims to capture general optimizations that apply to arbitrary data-parallel computations. However, the focus on deep learning causes Ansor to have difficulties with optimizing computations not taken from the deep learning area, as we confirm in our experiments.

To improve the auto-tuning efficiency for our implementations, we rely on a straightforward cost model that shrinks our search space in Table 1 before starting our ATF-based auto-tuning process: (1) we always use the same values for Parameters D1, S1, R1 as well as for Parameters D2, S2, R2, thereby generating the same loop structure for all three phases (de-composition, scalar, and re-composition) such that the structures can be generated as a fused loop nest; (2) we restrict Parameters D2, S2, R2 to two values—one value that let threads process outer parts (a.k.a. *blocked access* or *outer parallelism*, respectively) and one to let threads process inner parts (*strided access* or *inner parallelism*); all other permutations are currently ignored for simplicity or because they have no effect on the generated code (e.g., permutations of Parameters D2, S2, R2 that only differ in dimension tags belonging to memory layers, as discussed in the previous section); (3) we restrict Parameters D3, S3, S5, R3 such that each parameter is invariant under different values of  $d$  of its input pairs  $(l, d) \in \text{MDH-LVL}$ , i.e., we always copy full tiles in memory regions (and not a full tile of one input buffer and a half tile of another input buffer, which sometimes might achieve higher performance when memory is a limited resource).

Our cost model is straightforward and might filter out configurations from our search space that achieve potentially higher performance than we report for our approach in Sections 5.1–5.4. We aim to substantially improve our naive cost model in future work, based on *operational semantics* for our low-level representation, to improve the auto-tuning quality and to reduce (or even avoid) tuning time.

## Code Generation

We provide an open source *MDH compiler* [MDH Project, 2024] for generating executable program code from expressions in our high-level representation (as illustrated in Figure 4). Our compiler takes as input the high-level representation of the target computation (Figure 14), in the form of a Python program, and it fully automatically generates auto-tuned program code, based on the concepts and methodologies introduced and discussed in this article and the ATF [Rasch et al., 2021].

In our future work, we aim to integrate our code generation approach into the *MLIR* compiler framework [Lattner et al., 2021], building on work-in-progress results [Google SIG MLIR Open Design Meeting, 2020], thereby making our work better accessible to the community. We consider approaches such as *AnyDSL* [Leißa et al., 2018] and *BuildIt* [Brahmakshatriya and Amarasinghe, 2021] as further, interesting frameworks in which our compiler could be implemented.

### 5.1 Scheduling Approaches

*Performance.* Figures 17–22 report the performance of the TVM-generated code, which is in CUDA for GPUs and in OpenCL for CPUs. We observe that we usually achieve with our approach the high performance of TVM and often perform even better. For example, in Figure 21, we achieve a speedup  $> 2\times$  over TVM on NVIDIA Ampere GPU for matrix multiplications as used in the inference phase of the ResNet-50 neural network—an actually favorable example for TVM which is designed and optimized toward deep learning computations executed on modern NVIDIA GPUs. Our performance advantage over TVM is because we parallelize and optimize more efficiently reduction-like computations—in the case of MatMul (Figure 14), its 3rd-dimension (a.k.a.  $k$ -dimension). The difficulties of TVM with reduction computations become particularly obvious when computing dot products (Dot) on GPUs (Figure 17): the Dot’s main computation part is a reduction computation (via point-wise addition, see Figure 14), thus requiring reduction-focused optimization, in particular when targeting the highly parallel architecture of GPUs: in the case of Dot (Figure 17), our generated CUDA code exploits parallelization over CUDA blocks, whereas the Anso-generated TVM code exploits parallelization over threads within a single block only, because TVM currently cannot use blocks for parallelizing reduction computations [Apache TVM Community, 2022a]. Furthermore, while TVM’s Anso rigidly parallelizes outer dimensions [Zheng et al., 2020a], our ATF-based tuning process has auto-tuned our tuning parameters D2, S2, R2 in Table 1 to exploit parallelism for inner dimensions, which achieves higher performance for this particular MatMul example used in ResNet-50. Also, for MatMul-like computations, Anso always caches parts of the input in GPU’s shared memory, and it computes these cached parts always in register memory. In contrast, our caching strategy is auto-tunable (via parameters D3, S3 S5, R3 in Table 1), and ATF has determined to not cache the input matrices into fast memory resources for the MatMul example in ResNet-50. Surprisingly, Anso does not exploit fast memory resources for Jacobi stencils (Figure 18), as required to achieve high performance for them: our generated and auto-tuned CUDA kernel for Jacobi uses register memory for both inputs (image buffer and filter) when targeting NVIDIA Ampere GPU (small input size), thereby achieving a speedup over TVM+Anso of  $1.93\times$  for Jacobi. Most likely, Anso fails to foresee the potential of exploiting fast memory resources for Jacobi stencils, because the Jacobi’s index functions used for memory accesses (Figure 14) are injective. For the MatMul example of ResNet-50’s training phase (Figure 21), we achieve a speedup over TVM on NVIDIA Ampere GPU of  $1.26\times$ , because auto-tuning determined to store parts of input matrix  $A$  as transposed into fast memory (via parameter D4 in Table 1). Storing parts of the input/output data as transposed is not considered by Anso as optimization, perhaps because such optimization must be expressed in TVM’s high-level language, rather than in its scheduling



Linear Algebra	NVIDIA Ampere GPU							
	Dot		MatVec		MatMul		MatMul <sup>T</sup>	bMatMul
	2 <sup>24</sup>	10 <sup>7</sup>	4096,4096	8192,8192	10,500,64	1024,1024,1024	10,500,64	16,10,500,64
TVM+Ansor	172.48	128.22	1.74	1.23	1.00	1.00	1.00	1.17
PPCG	–	–	5.44	2.95	2.20	2.73	3.40	162.92
PPCG+ATF	–	–	4.22	2.77	1.20	1.87	1.32	3.06
cuBLAS	1.10	1.11	1.14	1.01	1.40	0.92	1.60	1.50
cuBLASEx	–	–	–	–	1.20	0.91	1.60	1.33
cuBLASLt	–	–	–	–	1.20	0.88	1.60	–

Linear Algebra	NVIDIA Volta GPU							
	Dot		MatVec		MatMul		MatMul <sup>T</sup>	bMatMul
	2 <sup>24</sup>	10 <sup>7</sup>	4096,4096	8192,8192	10,500,64	1024,1024,1024	10,500,64	16,10,500,64
TVM+Ansor	82.28	67.97	1.06	1.04	1.00	1.08	0.80	1.00
PPCG	–	–	2.67	1.71	1.40	3.07	2.60	111.98
PPCG+ATF	–	–	2.44	2.24	1.00	2.16	1.20	2.83
cuBLAS	1.06	1.09	1.10	1.07	2.60	1.11	1.80	1.83
cuBLASEx	–	–	–	–	1.80	0.30	1.40	1.17
cuBLASLt	–	–	–	–	1.20	0.96	1.40	–

Linear Algebra	Intel Skylake CPU							
	Dot		MatVec		MatMul		MatMul <sup>T</sup>	bMatMul
	2 <sup>24</sup>	10 <sup>7</sup>	4096,4096	8192,8192	10,500,64	1024,1024,1024	10,500,64	16,10,500,64
TVM+Ansor	5.07	6.14	1.03	3.39	1.06	1.15	1.02	1.10
Pluto	5.40	6.48	2.49	6.24	3.21	12.25	5.45	14.30
Pluto+ATF	5.39	6.01	1.43	3.38	2.98	4.78	4.79	2.14
oneMKL	0.64	0.57	0.42	3.83	6.27	0.69	3.42	0.98
oneMKL (JIT)	–	–	–	–	0.65	–	1.13	–

Linear Algebra	Intel Broadwell CPU							
	Dot		MatVec		MatMul		MatMul <sup>T</sup>	bMatMul
	2 <sup>24</sup>	10 <sup>7</sup>	4096,4096	8192,8192	10,500,64	1024,1024,1024	10,500,64	16,10,500,64
TVM+Ansor	5.60	8.46	1.21	1.63	1.20	1.11	1.11	1.00
Pluto	4.78	6.73	3.01	1.28	4.89	5.26	6.74	11.97
Pluto+ATF	4.75	6.72	2.91	1.21	1.94	2.85	3.46	1.23
oneMKL	1.03	0.41	0.57	0.59	2.00	0.66	1.98	0.84
oneMKL (JIT)	–	–	–	–	1.03	–	1.30	–

Fig. 17. Speedup (higher is better) of our approach for linear algebra routines on GPUs and CPUs over (1) scheduling approach TVM, (2) polyhedral compilers PPCG (GPU) and Pluto (CPU), as well as (3) hand-optimized libraries provided by vendors. Dash symbol “–” means that this framework does not support this particular combination of architecture, computation, and data characteristic.

Stencils	NVIDIA Ampere GPU				
	Jacobi3D		Conv2D		MCC
	256,256,256	512,512,512	224,224,5,5	4096,4096,5,5	1,512,7,7,512,3,3
TVM+Ansor	1.93	2.04	1.00	2.32	1.63
PPCG	4.19	5.27	1.58	2.36	–
PPCG+ATF	1.08	1.02	1.22	1.38	9.37
cuDNN	–	–	2.20	5.29	2.44

Stencils	NVIDIA Volta GPU				
	Jacobi3D		Conv2D		MCC
	256,256,256	512,512,512	224,224,5,5	4096,4096,5,5	1,512,7,7,512,3,3
TVM+Ansor	2.05	1.86	1.00	2.00	1.50
PPCG	7.01	13.87	1.45	1.75	–
PPCG+ATF	1.03	1.00	1.23	1.34	8.28
cuDNN	–	–	2.60	3.58	4.42

Stencils	Intel Skylake CPU				
	Jacobi3D		Conv2D		MCC
	256,256,256	512,512,512	224,224,5,5	4096,4096,5,5	1,512,7,7,512,3,3
TVM+Ansor	2.30	1.64	1.59	2.46	2.76
Pluto	3.65	2.66	2.39	1.38	143.80
Pluto+ATF	1.81	1.38	2.09	1.06	61.47
oneDNN	3.92	2.60	6.47	2.83	3.91

Stencils	Intel Broadwell CPU				
	Jacobi3D		Conv2D		MCC
	256,256,256	512,512,512	224,224,5,5	4096,4096,5,5	1,512,7,7,512,3,3
TVM+Ansor	2.21	1.78	3.14	3.98	3.99
Pluto	2.10	1.67	2.29	2.17	74.48
Pluto+ATF	1.29	1.05	1.74	1.25	74.47
oneDNN	16.09	15.02	7.29	16.42	7.69

Fig. 18. Speedup (higher is better) of our approach for stencil computations on GPUs and CPUs over (1) scheduling approach TVM, (2) polyhedral compilers PPCG (GPU) and Pluto (CPU), as well as (3) hand-optimized libraries provided by vendors. Dash symbol “–” means that this framework does not support this particular combination of architecture, computation, and data characteristic.

language [Apache TVM Community, 2022c]. For MatVec on NVIDIA Ampere GPU (Figure 17), we achieve a speedup over TVM of 1.22 $\times$  for the small input size, by exploiting a so-called *swizzle pattern* [Phothilimthana et al., 2019]: our ATF tuner has determined to assign threads that are consecutive in CUDA’s x-dimension to the second MDA dimension (via parameters D2, S2, R2 in Table 1), thereby accessing the input matrix in a GPU-efficient manner (a.k.a *coalesced global memory accesses* [NVIDIA, 2022f]). In contrast, for MatVec computations, Ansor assigns threads with consecutive x-ids always to the first data dimension, in a non-tunable manner, causing lower performance.

Quantum Chemistry	NVIDIA Ampere GPU							
	abcdef-gdab-efgc	abcdef-gdac-efgb	abcdef-gdbc-efga	abcdef-geab-dfgc	abcdef-geac-dfgb	abcdef-gebc-dfga	abcdef-gfab-degc	abcdef-gfbc-dega
TVM+Ansor	1.15	1.07	1.25	1.00	1.36	1.05	1.00	1.15
PPCG	10585.85	10579.40	9819.81	11211.57	10181.14	10482.81	11693.21	10585.85
PPCG+ATF	11.19	15.60	14.06	11.45	11.81	12.06	11.72	11.19

Quantum Chemistry	NVIDIA Volta GPU							
	abcdef-gdab-efgc	abcdef-gdac-efgb	abcdef-gdbc-efga	abcdef-geab-dfgc	abcdef-geac-dfgb	abcdef-gebc-dfga	abcdef-gfab-degc	abcdef-gfbc-dega
TVM+Ansor	1.09	0.93	1.04	1.03	1.01	1.11	1.01	1.09
PPCG	6466.22	6019.64	6300.31	6468.40	6608.80	5256.49	6602.22	6466.22
PPCG+ATF	8.28	9.61	9.38	7.21	6.60	5.14	7.77	8.28

Quantum Chemistry	Intel Skylake CPU							
	abcdef-gdab-efgc	abcdef-gdac-efgb	abcdef-gdbc-efga	abcdef-geab-dfgc	abcdef-geac-dfgb	abcdef-gebc-dfga	abcdef-gfab-degc	abcdef-gfbc-dega
TVM+Ansor	1.60	1.50	2.06	1.70	1.20	2.12	1.56	1.60
Pluto	147.45	151.55	206.60	162.58	157.43	145.17	321.66	147.45
Pluto+ATF	1.89	2.01	1.89	1.80	1.82	1.92	1.84	1.89

Quantum Chemistry	Intel Broadwell CPU							
	abcdef-gdab-efgc	abcdef-gdac-efgb	abcdef-gdbc-efga	abcdef-geab-dfgc	abcdef-geac-dfgb	abcdef-gebc-dfga	abcdef-gfab-degc	abcdef-gfbc-dega
TVM+Ansor	1.06	1.28	1.16	1.15	1.29	1.13	2.07	1.06
Pluto	-	-	-	-	-	-	-	-
Pluto+ATF	-	-	-	-	-	-	-	-

Fig. 19. Speedup (higher is better) of our approach for quantum chemistry computation *Coupled Cluster* (CCSD(T)) on GPUs and CPUs over (1) scheduling approach TVM and (2) polyhedral compilers PPCG (GPU) and Pluto (CPU). Dash symbol “-” means that this framework does not support this particular combination of architecture, computation, and data characteristic.

Our positive speedups over TVM on CPU are for the same reasons as discussed above for GPU. For example, we achieve a speedup of  $> 3\times$  over TVM on Intel Skylake CPU for MCC (Figure 22) as used in the training phase of the MobileNet neural network, because we exploit fast memory resources more efficiently than TVM: our auto-tuning process has determined to use register memory for the MCC’s second input (the filter buffer F, see Fig. 14) and using no fast memory for the first input (image buffer I), whereas Ansor uses shared memory rigidly for both inputs of MCC. Moreover, our auto-tuning process has determined to parallelize the inner dimensions of MCC, while Ansor always parallelizes outer dimensions. We achieve the best speedup over TVM for MCC on an input size taken from TVM’s own tutorials [Apache TVM Documentation, 2022b] (Figure 18), rather than from neural networks (as in Figures 21 and 22). This is because TVM’s MCC size includes large reduction computations, which are not efficiently optimized by TVM (as discussed above).

Data Mining	NVIDIA Ampere GPU					
	2 <sup>15</sup>	2 <sup>16</sup>	2 <sup>17</sup>	2 <sup>18</sup>	2 <sup>19</sup>	2 <sup>20</sup>
TVM+Ansor	–	–	–	–	–	–
PPCG	1.49	1.05	1.12	1.22	1.37	1.56
PPCG+ATF	1.40	1.22	1.50	1.63	1.83	2.12

Data Mining	NVIDIA Volta GPU					
	2 <sup>15</sup>	2 <sup>16</sup>	2 <sup>17</sup>	2 <sup>18</sup>	2 <sup>19</sup>	2 <sup>20</sup>
TVM+Ansor	–	–	–	–	–	–
PPCG	1.11	1.15	1.10	1.30	1.51	1.82
PPCG+ATF	1.26	1.37	1.47	1.77	2.07	2.48

Data Mining	Intel Skylake CPU					
	2 <sup>15</sup>	2 <sup>16</sup>	2 <sup>17</sup>	2 <sup>18</sup>	2 <sup>19</sup>	2 <sup>20</sup>
TVM+Ansor	–	–	–	–	–	–
Pluto	–	–	–	–	–	–
Pluto+ATF	–	–	–	–	–	–
EKR	6.18	5.39	9.62	19.87	26.42	24.78

Data Mining	Intel Broadwell CPU					
	2 <sup>15</sup>	2 <sup>16</sup>	2 <sup>17</sup>	2 <sup>18</sup>	2 <sup>19</sup>	2 <sup>20</sup>
TVM+Ansor	–	–	–	–	–	–
Pluto	–	–	–	–	–	–
Pluto+ATF	–	–	–	–	–	–
EKR	8.01	9.17	23.58	66.90	119.33	167.19

Fig. 20. Speedup (higher is better) of our approach for data mining algorithm Probabilistic Record Linkage (PRL) on GPUs and CPUs over (1) scheduling approach TVM and (2) polyhedral compilers PPCG (GPU) and Pluto (CPU), as well as the (3) hand-implemented Java CPU implementation used by *EKR*—the largest cancer registry in Europa. Dash symbol “–” means that this framework does not support this particular combination of architecture, computation, and data characteristic.

The TVM compiler achieves higher performance than our approach for some examples in Figures 17–22. However, in most cases, this is for a technical reason only: TVM uses the NVCC compiler for compiling CUDA code, whereas our proof-of-concept code generator currently relies on NVIDIA’s NVRTC library which surprisingly generates less-efficient CUDA assembly than NVCC. In three cases, the higher performance of TVM over our approach is because our ATF was not able to find a better performing tuning configuration than TVM’s Ansor optimization engine during our 12h tuning time; the three cases are: (1) MCC from VGG-16’s inference phase on NVIDIA Ampere GPU (Figure 21), (2) MCC (capsule variant) from VGG-16’s training phase on NVIDIA Ampere GPU (Figure 21), and (3) MCC (capsule variant) from ResNet-50’s training phase on Intel Skylake CPU (Figure 22). However, when we manually set the Ansor-found tuning configurations also for our approach, instead of using the ATF-found configurations, we achieve for these three cases exactly the same high performance as TVM+Ansor, i.e., the well-performing configurations are contained in our search space (Table 1). Most likely, Ansor was able to find this well-performing

Deep Learning	NVIDIA Ampere GPU									
	ResNet-50				VGG-16				MobileNet	
	Training		Inference		Training		Inference		Training	Inference
	MCC	MatMul	MCC	MatMul	MCC	MatMul	MCC	MatMul	MCC	MCC
TVM+Ansor	1.00	1.26	1.05	2.22	0.93	1.42	0.88	1.14	0.94	1.00
PPCG	3456.16	8.26	-	7.89	1661.14	7.06	5.77	5.08	2254.67	7.55
PPCG+ATF	3.28	2.58	13.76	5.44	4.26	3.92	9.46	3.73	3.31	10.71
cuDNN	0.92	-	1.85	-	1.22	-	1.94	-	1.81	2.14
cuBLAS	-	1.58	-	2.67	-	0.93	-	1.04	-	-
cuBLASEx	-	1.47	-	2.56	-	0.92	-	1.02	-	-
cuBLASLt	-	1.26	-	1.22	-	0.91	-	1.01	-	-

Deep Learning	NVIDIA Volta GPU									
	ResNet-50				VGG-16				MobileNet	
	Training		Inference		Training		Inference		Training	Inference
	MCC	MatMul	MCC	MatMul	MCC	MatMul	MCC	MatMul	MCC	MCC
TVM+Ansor	0.75	1.21	0.72	1.79	1.00	1.11	1.06	1.00	1.00	1.00
PPCG	1976.38	5.88	-	5.64	994.16	3.41	8.21	2.51	1411.92	7.26
PPCG+ATF	3.43	3.54	3.42	4.93	3.85	3.15	8.13	2.05	3.49	3.56
cuDNN	1.21	-	1.29	-	2.80	-	3.50	-	2.32	3.14
cuBLAS	-	1.33	-	1.14	-	1.09	-	1.04	-	-
cuBLASEx	-	1.21	-	1.07	-	1.04	-	1.03	-	-
cuBLASLt	-	1.00	-	1.07	-	1.04	-	1.02	-	-

Deep Learning (Capsule)	NVIDIA Ampere GPU					
	ResNet-50		VGG-16		MobileNet	
	Training	Inference	Training	Inference	Training	Inference
	MCC_Capsule	MCC_Capsule	MCC_Capsule	MCC_Capsule	MCC_Capsule	MCC_Capsule
TVM+Ansor	0.96	1.00	0.79	1.02	0.88	0.99
PPCG	4642.24	-	1013.55	-	4017.74	-
PPCG+ATF	25.98	85.33	4.41	13.64	8.89	22.12
cuDNN	-	-	-	-	-	-

Deep Learning (Capsule)	NVIDIA Volta GPU					
	ResNet-50		VGG-16		MobileNet	
	Training	Inference	Training	Inference	Training	Inference
	MCC_Capsule	MCC_Capsule	MCC_Capsule	MCC_Capsule	MCC_Capsule	MCC_Capsule
TVM+Ansor	0.95	1.01	1.05	0.97	1.04	0.87
PPCG	2935.40	-	945.16	-	2885.90	-
PPCG+ATF	19.24	19.68	8.28	12.29	8.84	6.41
cuDNN	-	-	-	-	-	-

Fig. 21. Speedup (higher is better) of our approach for the most time-intensive computations used in deep learning neural networks ResNet-50, VGG-16, and MobileNet on GPUs over (1) scheduling approach TVM, (2) polyhedral compilers PPCG (GPU), as well as (3) hand-optimized libraries provided by vendors. Dash symbol “-” means that this framework does not support this particular combination of architecture, computation, and data characteristic.

Deep Learning	Intel Skylake CPU									
	ResNet-50				VGG-16				MobileNet	
	Training		Inference		Training		Inference		Training	Inference
	MCC	MatMul	MCC	MatMul	MCC	MatMul	MCC	MatMul	MCC	MCC
TVM+Ansor	1.53	1.05	1.14	1.20	1.97	1.14	2.38	1.27	3.01	1.40
Pluto	355.81	49.57	364.43	13.93	130.80	93.21	186.25	36.30	152.14	75.37
Pluto+ATF	13.08	19.70	170.69	6.57	3.11	6.29	53.61	8.29	3.50	25.41
oneDNN	0.39	-	5.07	-	1.22	-	9.01	-	1.05	4.20
oneMKL	-	0.44	-	1.09	-	0.88	-	0.53	-	-
oneMKL (JIT)	-	6.43	-	8.33	-	27.09	-	9.78	-	-

Deep Learning	Intel Broadwell CPU									
	ResNet-50				VGG-16				MobileNet	
	Training		Inference		Training		Inference		Training	Inference
	MCC	MatMul	MCC	MatMul	MCC	MatMul	MCC	MatMul	MCC	MCC
TVM+Ansor	1.53	1.60	1.29	1.53	1.32	1.00	1.27	1.02	2.42	1.92
Pluto	4349.20	40.41	137.21	15.96	1865.07	53.57	113.40	24.10	2255.00	53.85
Pluto+ATF	6.43	8.93	61.60	6.91	5.07	4.38	42.63	4.45	6.43	29.18
oneDNN	1.30	-	1.81	-	2.94	-	2.85	-	1.83	4.47
oneMKL	-	1.45	-	1.36	-	1.35	-	0.50	-	-
oneMKL (JIT)	-	19.78	-	9.77	-	50.58	-	10.70	-	-

Deep Learning (Capsule)	Intel Skylake CPU					
	ResNet-50		VGG-16		MobileNet	
	Training	Inference	Training	Inference	Training	Inference
	MCC_Capsule	MCC_Capsule	MCC_Capsule	MCC_Capsule	MCC_Capsule	MCC_Capsule
TVM+Ansor	0.94	1.14	3.50	1.18	2.94	1.59
Pluto	209.36	265.77	-	166.45	160.49	159.34
Pluto+ATF	14.33	265.77	3.33	60.66	4.40	57.21
oneDNN	-	-	-	-	-	-

Deep Learning (Capsule)	Intel Broadwell CPU					
	ResNet-50		VGG-16		MobileNet	
	Training	Inference	Training	Inference	Training	Inference
	MCC_Capsule	MCC_Capsule	MCC_Capsule	MCC_Capsule	MCC_Capsule	MCC_Capsule
TVM+Ansor	2.61	1.30	3.55	1.00	1.32	2.24
Pluto	-	-	-	-	-	-
Pluto+ATF	4418.82	56.17	75.77	2173.72	202.34	158.52
oneDNN	-	-	-	-	-	-

Fig. 22. Speedup (higher is better) of our approach for the most time-intensive computations used in deep learning neural networks ResNet-50, VGG-16, and MobileNet on CPUs over (1) scheduling approach TVM, (2) polyhedral compilers Pluto (CPU), as well as (3) hand-optimized libraries provided by vendors. Dash symbol “-” means that this framework does not support this particular combination of architecture, computation, and data characteristic.

Listing 1. TVM Program Expressing Matrix-Vector Multiplication (MatVec)

---

```

1 def MatVec(I, K):
2     M = te.placeholder((I, K), name='M', dtype='float32')
3     v = te.placeholder((K,), name='v', dtype='float32')
4
5     k = te.reduce_axis((0, K), name='k')
6     w = te.compute(
7         (I,),
8         lambda i: te.sum(M[i, k] * v[k], axis=k)
9     )
10    return [M, v, w]

```

---

configuration within the 12 h tuning time, because it explores a significantly smaller search space that is particularly designed for deep learning computations. To avoid such tuning issues in our approach, we aim to substantially improve our auto-tuning process in future work: we plan to introduce an analytical cost model that assists (or even replaces) our auto-tuner, as we also outline in Section 8.

Note that the TVM compiler crashes for our data mining example PRL, because TVM has difficulties with computations relying on user-defined combine operators [Apache TVM Community, 2022d].

*Portability.* Figure 23 reports the portability of the TVM compiler. Our portability measurements are based on the Pennycook metric where a value close to 1 indicates high portability and a value close to 0 indicates low portability, correspondingly. We observe that except for the example of transposed matrix multiplication  $\text{GEMM}^T$ , we always achieve higher portability than TVM. The higher portability of TVM for  $\text{GEMM}^T$  is because TVM achieves for this example higher performance than our approach on NVIDIA Volta GPU. However, the higher performance of TVM is only due to the fact that TVM uses NVIDIA’s NVCC compiler for compiling CUDA code, while we currently rely on NVIDIA’s NVRTC library which surprisingly generates less-efficient CUDA assembly, as discussed above.

*Productivity.* Listing 1 shows how matrix-vector multiplication (MatVec) is implemented in TVM’s high-level program representation which is embedded into the Python programming language. In line 1, the input size  $(I, K) \in \mathbb{N} \times \mathbb{N}$  of matrix  $M \in T^{I \times K}$  (line 2) and vector  $v \in T^K$  (line 3) are declared, in the form of function parameters; the matrix and vector are named  $M$  and  $v$  and both are assumed to contain elements of scalar type  $T = \text{float32}$  (floating point numbers). Line 5 defines a so-called *reduction axis* in TVM, in which all values are combined in line 8 via `te.sum` (addition). The basic computation part of MatVec—multiplying matrix element  $M[i, k]$  with vector element  $v[k]$ —is also specified in line 8.

While we consider the MatVec implementations of TVM (Listing 1) and our approach (Figure 6) basically on the same level of abstraction, we consider our approach as more expressive in general. This is because our approach supports multiple reduction dimensions that may rely on different combine operators, e.g., as required for expressing the MBBS example in Figure 14. In contrast, TVM is struggling with different combine operators—adding support for multiple, different reduction dimensions is considered in the TVM community as a non-trivial extension of TVM [Apache TVM Community, 2020, 2022b]. Also, we consider our approach as slightly less error-prone: we automatically compute the expected sizes of matrix  $M$  (as  $I \times K$ ) and vector  $v$  (as  $K$ ), based on the user-defined input size  $(I, K)$  in line 1 and index functions  $(i, k) \mapsto (i, k)$  for the matrix and  $(i, k) \mapsto (k)$  for the vector in line 8 (the formula for computing the sizes is described by Rasch



Linear Algebra	Pennycook Metric							
	Dot		MatVec		MatMul		MatMul <sup>T</sup>	bMatMul
	2 <sup>24</sup>	10 <sup>7</sup>	4096,4096	8192,8192	10,500,64	1024,1024,1024	10,500,64	16,10,500,64
MDH+ATF	0.88	0.64	0.65	0.85	0.88	0.54	0.94	0.95
TVM+Ansor	0.01	0.02	0.54	0.47	0.83	0.50	0.97	0.89

Stencils	Pennycook Metric				
	Jacobi3D		Conv2D		MCC
	256,256,256	512,512,512	224,224,5,5	4096,4096,5,5	1,512,7,7,512,3,3
MDH+ATF	1.00	1.00	1.00	1.00	1.00
TVM+Ansor	0.47	0.55	0.59	0.37	0.41

Quantum Chemistry	Pennycook Metric							
	abcdefg-gdab-efgc	abcdefg-gdac-efgb	abcdefg-gdbc-efga	abcdefg-geab-dfgc	abcdefg-geac-dfgb	abcdefg-gebc-dfga	abcdefg-gfab-degc	abcdefg-gfbc-dega
	1.00	0.98	1.00	1.00	1.00	1.00	1.00	1.00
TVM+Ansor	0.82	0.82	0.73	0.82	0.82	0.74	0.71	0.84

Data Mining	Pennycook Metric					
	2 <sup>15</sup>	2 <sup>16</sup>	2 <sup>17</sup>	2 <sup>18</sup>	2 <sup>19</sup>	2 <sup>20</sup>
	1.00	1.00	1.00	1.00	1.00	1.00
TVM+Ansor	0.00	0.00	0.00	0.00	0.00	0.00

Deep Learning	Pennycook Metric									
	ResNet-50				VGG-16				MobileNet	
	Training		Inference		Training		Inference		Training	Inference
	MCC	MatMul	MCC	MatMul	MCC	MatMul	MCC	MatMul	MCC	MCC
MDH+ATF	0.67	0.76	0.91	1.00	0.98	0.95	0.97	0.68	0.98	1.00
TVM+Ansor	0.53	0.62	0.89	0.59	0.76	0.81	0.70	0.61	0.54	0.75

Deep Learning (Capsule)	Pennycook Metric					
	ResNet-50		VGG-16		MobileNet	
	Training	Inference	Training	Inference	Training	Inference
	MCC_Capsule	MCC_Capsule	MCC_Capsule	MCC_Capsule	MCC_Capsule	MCC_Capsule
MDH+ATF	0.96	1.00	0.94	0.99	0.97	0.96
TVM+Ansor	0.71	0.90	0.44	0.95	0.63	0.69

Fig. 23. Portability (higher is better), according to Pennycook metric, of our MDH-based approach and TVM over GPUs and CPUs for case studies. Polyhedral compilers PPCG/Pluto and vendor libraries by NVIDIA and Intel are not listed: due to their limitation to certain architectures, all of them achieve the lowest portability of 0 only.

[2024], Definition 8, for the interested reader). In contrast, TVM redundantly requests these matrix and vector sizes from the user: once in lines 2 and 3 of Listing 1, and again in lines 5 and 7. TVM uses these sizes for generating the function specification of its generated MatVec code, which lets TVM generate incorrect low-level code—without issuing an error message—when the user sets non-matching sizes in lines 2/3 and lines 5/7.

## 5.2 Polyhedral Compilers

*Performance.* Figures 17–22 report the performance achieved by the PPCG-generated CUDA code for GPUs and of the OpenMP-annotated C code generated by polyhedral compiler Pluto for CPUs. For a fair comparison, we report for both polyhedral compilers their performance achieved for ATF-tuned tile sizes (denoted as PPCG+ATF/Pluto+ATF in the figures), as well as the performance of the two compilers when relying on their internal heuristics instead of auto-tuning (denoted as PPCG and Pluto). In some cases, PPCG’s heuristic crashed with error “too many resources requested for launch,” because the heuristic seems to not take into account device-specific constraints, e.g., limited availability of GPUs’ fast memory resources.

We observe from Figures 17–22 that in all cases, our approach achieves better performance than PPCG and Pluto—sometimes by multiple orders of magnitude, in particular for deep learning computations (Figures 21 and 22). This is caused by the rigid optimization goals of PPCG and Pluto, e.g., always parallelizing outer dimensions, which causes severe performance losses. For example, we achieve a speedup over PPCG of  $> 13\times$  on NVIDIA Ampere GPU and of  $> 60\times$  over Pluto on Intel Skylake CPU for MCC as used in the inference phase of the real-world ResNet-50 neural network. Compared to PPCG, our better performance for this MCC example is because PPCG has difficulties with efficiently parallelizing computations relying on more than three dimensions. Most likely, this is because CUDA offers per default three dimensions for parallelization (called x, y, z dimension in CUDA). However, MCC relies on seven parallelizable dimensions (as shown in Figure 14), and exploiting the parallelization opportunities of the four further dimensions (as done in our generated CUDA code) is essential to achieve high performance for this MCC example from ResNet-50. Our performance advantage over Pluto for the MCC example is because Pluto parallelizes the outer dimensions of MCC only (whereas our approach has the potential to parallelize all dimensions); however, the dimension has a size of only 1 for this real-world example, resulting in starting only 1 thread in the Pluto-generated OpenMP code.

For dot products Dot (Figure 17), we can observe that PPCG fails to generate parallel CUDA code, because PPCG cannot parallelize and optimize computations which rely solely on combine operators different from concatenation, as we also discuss in Section 6.2. In Section 6.2, we particularly discuss that we do not consider the performance issues of PPCG and Pluto as weaknesses of the polyhedral approach in general, but of the particular polyhedral transformations chosen for PPCG and Pluto.

Note that Pluto crashes for our data mining example (Figure 20), with “Error extracting polyhedra from source file,” because the scalar function of this example is too complex for Pluto (it contains if-statements). Moreover, Intel’s icx compiler struggles with compiling the Pluto-generated OpenMP code for quantum chemistry computations (Figure 19): we aborted icx’s compilation process after 24 h compilation time. The icx’s issue with the Pluto-generated code is most likely because of too aggressive loop unrolling of Pluto—the Pluto-generated OpenMP code has often a size  $> 50$  MB for our real-world quantum chemistry examples.

*Portability.* Since PPCG and Pluto are each designed for particular architectures only, they achieve the lowest portability of 0 for all our studies in Figure 23, according to the Pennycook metric. To simplify for PPCG and Pluto the portability comparison with our approach, we compute the Pennycook metric additionally also for two restricted sets of devices: only GPUs to make comparison against our approach easier for PPCG, and only CPUs to make comparison easier for Pluto.

Figures 24–28 report the portability of PPCG when considering only GPUs, as well as the portability of Pluto for only CPUs. We observe that we achieve higher portability for all our studies, as we constantly achieve higher performance than the two polyhedral compilers for the studies.

Listing 2. PPCG/Pluto Program Expressing Matrix-Vector Multiplication (MatVec)

---

```

1  for( int i = 0 ; i < I ; ++i )
2    for( int k = 0 ; k < K ; ++k )
3      w[i] += M[i][k] * v[k];

```

---

Note that even when restricting our set of devices to only GPUs for PPCG or only CPUs for Pluto, the two polyhedral compilers still achieve a portability of 0 for some examples, because they fail to generate code for them (as discussed above).

*Productivity.* Listing 2 shows the input program of polyhedral compilers PPCG and Pluto for MatVec. Both take as input easy-to-implement, straightforward, sequential C code. We consider these two polyhedral compilers as more productive than our approach (as well as scheduling and functional approaches, and also polyhedral compilers that take DSL programs as input, such as TC [Vasilache et al., 2019]), because both compilers fully automatically generate optimized parallel code from unoptimized, sequential program code.

Rasch et al. [2020b,c] show that our approach can achieve the same high user productivity as polyhedral compilers, by using a polyhedral frontend for our approach: we can alternatively take as input the same sequential program code as PPCG and Pluto, instead of programs implemented in our high-level program representation (as in Figure 6). The sequential input program is then transformed via polyhedral tool *pet* [Verdoolaege and Grosser, 2012] to its polyhedral representation which is then automatically transformed to our high-level program representation, according to the methodology presented by Rasch et al. [2020b,c].

### 5.3 Functional Approaches

Our previous work [Rasch et al., 2019a] already shows that while functional approaches provide a solid formal foundation for computations, they typically suffer from performance and portability issues. For this, our previous work compares our approach (in its original, proof-of-concept implementation [Rasch et al., 2019a]) to the state-of-the-art *Lift* [Steuer et al., 2015] framework which, to the best of our knowledge, has so far not been improved toward higher performance and/or better portability. Consequently, we refrain from a further performance and portability evaluation of *Lift* and focus in the following on analyzing and discussing the productivity potentials of functional approaches, using again the state-of-the-art *Lift* approach as running example. In Section 6.3, we discuss the performance and portability issues of functional approaches from a general perspective.

*Performance/Portability.* Already experimentally evaluated in previous work [Rasch et al., 2019a] and discussed in general terms in Section 6.3.

*Productivity.* Listing 3 shows how MatVec is implemented in *Lift*. In line 1, type parameters  $n$  and  $m$  are declared, via the *Lift* building block *nFun*. Line 2 declares a function *fun* that takes as input a matrix of size  $m \times n$  and a vector of size  $n$ , both consisting of floating point numbers (*float*). The computation of MatVec is specified in lines 3 and 4. In line 3, *Lift*'s *map* pattern iterates over all rows of the matrix, and the *zip* pattern in line 4 combines each row pair-wise with the input vector. Afterward, multiplication  $*$  is applied to each pair, using *Lift*'s *map* pattern again, and the obtained products are finally combined via addition  $+$  using *Lift*'s *reduce* pattern.

Already for expressing MatVec, we can observe that *Lift* relies on a vast set of small, functional building blocks (five building blocks for MatVec: *nFun*, *fun*, *map*, *zip*, and *reduce*), and the blocks have to be composed and nested in complex ways for expressing computations. Consequently, we consider programming in *Lift* and *Lift*-like approaches as complex and their productivity

Listing 3. Lift Program Expressing Matrix-Vector Multiplication (MatVec)

---

```

1 nFun(n => nFun(m =>
2   fun(matrix: [[float]n]m => fun(xs: [float]n =>
3     matrix :>> map(fun(row =>
4       zip(xs, row) :>> map(*) :>> reduce(+, 0)
5     )) )) )

```

---

for the user as limited. Moreover, the approaches often need fundamental extension for targeting new kinds of computations, e.g., so-called *macro-rules* which had to be added to Lift to efficiently target matrix multiplications [Rommelg et al., 2016] and primitives *slide* and *pad* together with optimization *overlapped tiling* for expressing stencil computations [Hagedorn et al., 2018]. This need for extensions limits the expressivity of the Lift language and thus further hinders productivity.

In contrast to Lift, our approach relies on exactly three higher-order functions (Figure 5) to express various kinds of data-parallel computations (Figure 14): (1) *inp\_view* (Definition 7) which prepares the input data; our *inp\_view* function is designed as general enough to subsume, in a structured way, the subset of all Lift patterns intended to change the view on input data, including patterns *zip*, *pad*, and *slide*; (2) *md\_hom* (Definition 3) expresses the actual computation part, and it subsumes the Lift patterns performing actual computations (*fun*, *map*, *reduce*, ...); (3) *out\_view* (Definition 9) expresses the view on output data and is designed to work similarly as function *inp\_view* (Lemma 2). Our three functions are always composed straightforwardly, in the same, fixed order (Figure 5), and they do not rely on complex function nesting for expressing computations.

Note that even though our language is designed as minimalistic, it should cover the expressivity of the Lift language<sup>22</sup> and beyond: for example, we are currently not aware of any Lift program being able to express the prefix-sum examples in Figure 14. For the above reasons, we consider programming in our high-level language as more productive for the user than programming in Lift-like, functional-style languages. Furthermore, as discussed in Section 5.2, our approach can take as input also straightforward, sequential program code, which further contributes to the productivity of our approach.

## 5.4 Domain-Specific Approaches

*Performance.* Figures 17–22 report for completeness and also performance results achieved by domain-specific approaches. Since domain-specific approaches are specifically designed and optimized for particular application domains and often also architectures (e.g., only linear algebra routines on only GPU), we consider comparing to them as most challenging for us: our approach is designed and optimized for data-parallel computations in general, from arbitrary application domains (the same as also polyhedral compilers and many functional approaches), and our approach is also designed as generic in the target parallel architecture.

We observe in Figures 17–22 that the domain-specific libraries NVIDIA cuBLAS/cuDNN (for linear algebra routines and convolutions on GPUs) and Intel oneMKL/oneDNN (for linear algebra routines and convolutions on CPUs) sometimes perform better and sometimes worse than our approach.

<sup>22</sup>This work is focused on dense computations. Lift supports sparse computations [Pizzuti et al., 2020] which we consider as future work for our approach (as also outlined in Section 8). We consider Lift’s approach, based on their so-called *position dependent arrays*, as a great inspiration for our future goal.

The better performance of libraries over our approach is most likely<sup>23</sup> because the libraries internally rely on assembly-level optimizations, while we currently focus on the higher CUDA/OpenCL level of abstraction which offers less optimization opportunities [Goto and Geijn, 2008; Lai and Seznec, 2013]. The cuBLASEx extension of cuBLAS achieves in one case—MatMul on NVIDIA Volta GPU for square  $1024 \times 1024$  input matrices—significantly higher performance than our approach. The high performance is achieved by cuBLASEx when using its CUBLAS\_GEMM\_ALGO1\_TENSOR\_OP algorithm variant, which casts the float-typed inputs implicitly to the half precision type (a.k.a. half or fp16), allowing cuBLASEx to exploit the GPU’s tensor core extension [NVIDIA, 2017]. Thereby, cuBLASEx achieves significantly higher performance than our approach, because tensor cores compute small matrix multiplication immediately in hardware; however, at the cost of a significant precision loss: the half scalar type achieves only half the accuracy achieved by scalar type float. When using cuBLASEx’s default algorithm CUBLAS\_GEMM\_DEFAULT (rather than algorithm CUBLAS\_GEMM\_ALGO1\_TENSOR\_OP), which retains the float type and thus meets the accuracy expected from the computation, we achieve a speedup of  $1.11\times$  over cuBLASEx.<sup>24</sup>

The reason for the better performance of our approach over NVIDIA and Intel libraries is most likely because our approach allows generating code that is also optimized (auto-tuned) for data characteristics, which is important for high performance [Tillet and Cox, 2017]. In contrast, the vendor libraries usually rely on pre-implemented code that is optimized toward only average high performance for a range of data characteristics (size, memory layout, etc.). By relying on these fixed, pre-implemented code, the libraries avoid the auto-tuning overhead. However, auto-tuning is often amortized, particularly for deep learning computations—the main target of libraries NVIDIA cuDNN und Intel oneDNN—because the auto-tuned implementations are re-used in many program runs. Moreover, we achieve better performance for convolutions (Figure 18), because the libraries re-use optimizations for these computations originally intended for linear algebra routines [Li et al., 2016], whereas our optimization space (Table 1) is designed for data-parallel computations in general and not as specifically oriented toward linear algebra.

Compared to the EKR library (Figure 20), we achieve higher performance, because the EKR’s Java implementation inefficiently handles memory: the library is implemented using Java’s ArrayList data structure which is convenient to use for the Java programmer, but inefficient in terms of performance, because the structure internally performs costly memory re-allocations.

*Portability.* Similar to polyhedral compilers PPCG and Pluto, the domain-specific approaches work for certain architectures only and thus achieve the lowest portability of 0 only in Figure 23 for our studies. The domain-specific approaches are also restricted to a narrow set of studies, e.g., only linear algebra routines as NVIDIA cuBLAS and Intel oneMKL or only data mining example PRL as EKR. Consequently, the approaches achieve for these unsupported studies also a portability of only 0 in Figures 24–28 in which our portability evaluation is limited to only GPUs or CPUs, respectively, to make comparison against our approach easier for the vendor libraries.

For their target studies, domain-specific approaches achieve high portability. This is because the approaches are specifically designed and optimized toward these studies, e.g., via assembly-level optimizations which are currently beyond the scope of our work and considered as future work for our approach (see Section 8).

<sup>23</sup>Since the Intel and NVIDIA libraries are not open source, we cannot explain their performance behavior with certainty.

<sup>24</sup>For the interested reader, Rasch [2024] (Section D.2) reports the runtime of cuBLASEx for all its algorithm variants, including reports for the accuracy achieved by the different variants.

Linear Algebra	Pennycook Metric (GPUs only)							
	Dot		MatVec		MatMul		MatMul <sup>T</sup>	bMatMul
	2 <sup>24</sup>	10 <sup>7</sup>	4096,4096	8192,8192	10,500,64	1024,1024,1024	10,500,64	16,10,500,64
MDH+ATF	1.00	1.00	1.00	1.00	1.00	0.45	0.89	1.00
TVM+Ansor	0.01	0.01	0.71	0.88	1.00	0.42	1.00	0.92
PPCG	0.00	0.00	0.25	0.43	0.56	0.15	0.30	0.01
PPCG+ATF	0.00	0.00	0.30	0.40	0.91	0.21	0.71	0.34
cuBLAS	0.93	0.91	0.89	0.96	0.50	0.42	0.52	0.60
cuBLASEx	0.00	0.00	0.00	0.00	0.67	0.98	0.60	0.00
cuBLASLt	0.00	0.00	0.00	0.00	0.83	0.48	0.60	0.00

Linear Algebra	Pennycook Metric (CPUs only)							
	Dot		MatVec		MatMul		MatMul <sup>T</sup>	bMatMul
	2 <sup>24</sup>	10 <sup>7</sup>	4096,4096	8192,8192	10,500,64	1024,1024,1024	10,500,64	16,10,500,64
MDH+ATF	0.78	0.48	0.48	0.74	0.79	0.67	1.00	0.90
TVM+Ansor	0.15	0.06	0.44	0.32	0.71	0.60	0.94	0.86
Pluto	0.15	0.07	0.18	0.24	0.20	0.08	0.16	0.07
Pluto+ATF	0.15	0.07	0.23	0.37	0.31	0.18	0.24	0.55
oneMKL	0.99	1.00	1.00	0.41	0.17	1.00	0.37	1.00
oneMKL (JIT)	0.00	0.00	0.00	0.00	0.98	0.00	0.83	0.00

Fig. 24. Portability (higher is better), according to Pennycook metric, for linear algebra routines computed on only GPUs or CPUs, respectively. The restriction simplifies for frameworks with limited architectural support (such as polyhedral compilers and vendor libraries) the portability comparisons against our approach.

Stencils	Pennycook Metric (GPUs only)				
	Jacobi3D		Conv2D		MCC
	256,256,256	512,512,512	224,224,5,5	4096,4096	1,512,7,7,512,3,3
MDH+ATF	1.00	1.00	1.00	1.00	1.00
TVM+Ansor	0.50	0.51	1.00	0.46	0.64
PPCG	0.18	0.10	0.66	0.49	0.00
PPCG+ATF	0.95	0.99	0.82	0.74	0.11
cuDNN	0.00	0.00	0.42	0.23	0.29

Stencils	Pennycook Metric (CPUs only)				
	Jacobi3D		Conv2D		MCC
	256,256,256	512,512,512	224,224,5,5	4096,4096	1,512,7,7,512,3,3
MDH+ATF	1.00	1.00	1.00	1.00	1.00
TVM+Ansor	0.44	0.58	0.42	0.31	0.30
Pluto	0.35	0.46	0.43	0.56	0.01
Pluto+ATF	0.65	0.83	0.52	0.86	0.01
oneDNN	0.10	0.11	0.15	0.10	0.17

Fig. 25. Portability (higher is better), according to Pennycook metric, for stencil computations computed on only GPUs or CPUs, respectively. The restriction simplifies for frameworks with limited architectural support (such as polyhedral compilers and vendor libraries) the portability comparisons against our approach.

Quantum Chemistry	Pennycook Metric (GPUs only)							
	abcdefg-gdab-efgc	abcdefg-gdac-efgb	abcdefg-gdbc-efga	abcdefg-geab-dfgc	abcdefg-geac-dfgb	abcdefg-gebc-dfga	abcdefg-gfab-degc	abcdefg-gfbc-dega
MDH+ATF	1.00	0.96	1.00	1.00	1.00	1.00	1.00	1.00
TVM+Ansor	0.90	0.96	0.87	0.99	0.84	0.93	0.99	1.00
PPCG	0.00	0.00	0.00	0.00	0.00	0.00	0.00	0.00
PPCG+ATF	0.10	0.08	0.09	0.11	0.11	0.12	0.10	0.15

Quantum Chemistry	Pennycook Metric (CPUs only)							
	abcdefg-gdab-efgc	abcdefg-gdac-efgb	abcdefg-gdbc-efga	abcdefg-geab-dfgc	abcdefg-geac-dfgb	abcdefg-gebc-dfga	abcdefg-gfab-degc	abcdefg-gfbc-dega
MDH+ATF	1.00	1.00	1.00	1.00	1.00	1.00	1.00	1.00
TVM+Ansor	0.75	0.72	0.62	0.70	0.80	0.62	0.55	0.72
Pluto	0.00	0.00	0.00	0.00	0.00	0.00	0.00	0.00
Pluto+ATF	0.00	0.00	0.00	0.00	0.00	0.00	0.00	0.00

Fig. 26. Portability (higher is better), according to Pennycook metric, for quantum chemistry computation *Coupled Cluster* (CCSD(T)) computed on only GPUs or CPUs, respectively. The restriction simplifies for frameworks with limited architectural support (such as polyhedral compilers and vendor libraries) the portability comparisons against our approach.

Data Mining	Pennycook Metric (GPUs only)					
	2 <sup>15</sup>	2 <sup>16</sup>	2 <sup>17</sup>	2 <sup>18</sup>	2 <sup>19</sup>	2 <sup>20</sup>
MDH+ATF	1.00	1.00	1.00	1.00	1.00	1.00
TVM+Ansor	0.00	0.00	0.00	0.00	0.00	0.00
PPCG	0.77	0.91	0.90	0.80	0.69	0.59
PPCG+ATF	0.75	0.77	0.67	0.59	0.51	0.43

Data Mining	Pennycook Metric (CPUs only)					
	2 <sup>15</sup>	2 <sup>16</sup>	2 <sup>17</sup>	2 <sup>18</sup>	2 <sup>19</sup>	2 <sup>20</sup>
MDH+ATF	1.00	1.00	1.00	1.00	1.00	1.00
TVM+Ansor	0.00	0.00	0.00	0.00	0.00	0.00
Pluto	0.00	0.00	0.00	0.00	0.00	0.00
Pluto+ATF	0.00	0.00	0.00	0.00	0.00	0.00
EKR	0.14	0.14	0.06	0.02	0.01	0.01

Fig. 27. Portability (higher is better), according to Pennycook metric, for data mining algorithm *Probabilistic Record Linkage* (PRL) computed on only GPUs or CPUs, respectively. The restriction simplifies for frameworks with limited architectural support (such as polyhedral compilers and vendor libraries) the portability comparisons against our approach.

**Productivity.** Listing 4 shows the implementation of MatVec in domain-specific approach NVIDIA cuBLAS; the implementation of MatVec in other domain-specific approaches, e.g., Intel oneMKL, is analogous to the implementation in Listing 4.

We consider domain-specific approaches as most productive for their target domain: in the case of MatVec, the user simply calls the high-level function `cublasSgemv` and passes to it the input matrices (omitted via ellipsis in the listing) together with some meta information (memory layout of matrices, etc); cuBLAS then automatically starts the GPU computation for MatVec.



Deep Learning	Pennycook Metric (GPUs only)									
	ResNet-50					VGG-16				MobileNet
	Training		Inference		MCC	Training		Inference		MCC
	MCC	MatMul	MCC	MatMul		MCC	MatMul	MCC	MatMul	
MDH+ATF	0.82	1.00	0.84	1.00	0.96	0.95	0.94	1.00	0.97	1.00
TVM+Ansor	0.96	0.81	0.98	0.50	1.00	0.75	0.97	0.93	1.00	1.00
PPCG	0.00	0.14	0.00	0.15	0.00	0.18	0.14	0.26	0.00	0.13
PPCG+ATF	0.24	0.33	0.11	0.19	0.24	0.27	0.11	0.35	0.28	0.14
cuBLAS	0.76	0.00	0.55	0.00	0.48	0.00	0.35	0.00	0.47	0.38
cuBLASEx	0.00	0.69	0.00	0.53	0.00	0.95	0.00	0.96	0.00	0.00
cuBLASLt	0.00	0.75	0.00	0.55	0.00	0.97	0.00	0.97	0.00	0.00
cuDNN	0.00	0.88	0.00	0.87	0.00	0.98	0.00	0.98	0.00	0.00

Deep Learning	Pennycook Metric (CPUs only)									
	ResNet-50					VGG-16				MobileNet
	Training		Inference		MCC	Training		Inference		MCC
	MCC	MatMul	MCC	MatMul		MCC	MatMul	MCC	MatMul	
MDH+ATF	0.56	0.61	1.00	1.00	1.00	0.94	1.00	0.51	1.00	1.00
TVM+Ansor	0.37	0.50	0.82	0.73	0.61	0.87	0.55	0.45	0.37	0.60
Pluto	0.00	0.01	0.00	0.07	0.00	0.01	0.01	0.02	0.00	0.02
Pluto+ATF	0.05	0.04	0.01	0.15	0.24	0.17	0.02	0.08	0.20	0.04
oneMKL	0.87	0.00	0.29	0.00	0.48	0.00	0.17	0.00	0.69	0.23
oneMKL (JIT)	0.00	0.82	0.00	0.82	0.00	0.85	0.00	1.00	0.00	0.00
oneDNN	0.00	0.06	0.00	0.11	0.00	0.02	0.00	0.05	0.00	0.00

Deep Learning (Capsule)	Pennycook Metric (GPUs only)					
	ResNet-50		VGG-16		MobileNet	
	Training	Inference	Training	Inference	Training	Inference
	MCC_Capsule	MCC_Capsule	MCC_Capsule	MCC_Capsule	MCC_Capsule	MCC_Capsule
MDH+ATF	0.95	1.00	0.88	0.98	0.94	0.93
TVM+Ansor	1.00	0.99	0.98	0.99	0.98	1.00
PPCG	0.00	0.00	0.00	0.00	0.00	0.00
PPCG+ATF	0.04	0.02	0.14	0.08	0.11	0.07
cuDNN	0.00	0.00	0.00	0.00	0.00	0.00

Deep Learning (Capsule)	Pennycook Metric (CPUs only)					
	ResNet-50		VGG-16		MobileNet	
	Training	Inference	Training	Inference	Training	Inference
	MCC_Capsule	MCC_Capsule	MCC_Capsule	MCC_Capsule	MCC_Capsule	MCC_Capsule
MDH+ATF	0.97	1.00	1.00	1.00	1.00	1.00
TVM+Ansor	0.55	0.82	0.28	0.92	0.47	0.52
Pluto	0.00	0.00	0.00	0.00	0.00	0.00
Pluto+ATF	0.00	0.01	0.03	0.00	0.01	0.01
oneDNN	0.00	0.00	0.00	0.00	0.00	0.00

Fig. 28. Portability (higher is better), according to Pennycook metric, for deep learning computations computed on only GPUs or CPUs, respectively. The restriction simplifies for frameworks with limited architectural support (such as polyhedral compilers and vendor libraries) the portability comparisons against our approach.

Listing 4. cuBLAS Program Expressing Matrix-Vector Multiplication (MatVec)

---

```
1 cublasSgemv( /* ... */ );
```

---

Besides the fact that domain-specific approaches typically target only particular target architectures, a further fundamental productivity issue of domain-specific approaches is that they can only be used for a narrow class of computations only, e.g., only linear algebra routines as NVIDIA cuBLAS and Intel oneMKL. Moreover, in the case of domain-specific libraries from NVIDIA and Intel, it is often up to the user to manually choose among different, semantically equal but differently performing implementations for high performance. For example, the cuBLAS library offers three different routines for computing matrix multiplications: (1) `cublasSgemm` (part of standard cuBLAS), (2) `cublasGemmEx` (part of the cuBLASEx extension of cuBLAS), and (3) routine `cublasLtMatmul` (part of the cuBLASLt extension). These routines often also offer different, so-called *algorithms* (e.g., 42 algorithm variants in the case cuBLASEx) which impact the internal optimization process. When striving for the highest performance potentials of libraries, the user is in charge of naively testing each possible combination of routine and algorithm variant (as we have done in Figures 17–22 to make experimenting challenging for us). In addition, the user must be aware that different combinations of routines and algorithms can produce results of reduced accuracy (as discussed above), which can be critical for accuracy-sensitive use cases.

## 6 Related Work

Three major classes of approaches currently focus on code generation and optimization for data-parallel computations: (1) scheduling, (2) polyhedral, and (3) functional. In the following, we compare in Sections 6.1–6.3 our approach to each of these three classes—in terms of *performance*, *portability*, and *productivity*. In contrast to Section 5, which has compared our approach against these classes experimentally, this section is focused on discussions in a more general, non-experimental context. Afterward, we outline domain-specific approaches in Section 6.4, which are specifically designed and optimized toward their target application domains. In Section 6.5, we outline approaches focusing on optimizations that operate at the algorithmic level of abstraction (and thus at a higher abstraction level than our approach); we consider these higher-level approaches as greatly combinable with our work. Finally, we discuss in Section 6.6 the differences between our approach introduced in this article and the already existing work on MDHs.

### 6.1 Scheduling Approaches

Popular examples of scheduling approaches include *UTF* [Kelly and Pugh, 1998], *URUK* [Girbal et al., 2006], *CHill* [Chen et al., 2008, Khan et al., 2013], *Halide* [Ragan-Kelley et al., 2013], *Clay* [Baghères et al., 2016], *TVM* [Chen et al., 2018a], *TeML* [Susungi et al., 2020], *Tiramisu* [Baghdadi et al., 2019], *DaCe* [Ben-Nun et al., 2019], *Fireiron* [Hagedorn et al., 2020a], *Elevate* [Hagedorn et al., 2020b], *DISTAL* [Yadav et al., 2022], and *LoopStack* [Wasti et al., 2022]. While scheduling approaches usually achieve high performance, they often have difficulties with achieving portability and productivity, as we discuss in the following.<sup>25</sup>

<sup>25</sup>Rasch et al. [2023] introduce (optionally) a scheduling language for MDH to incorporate expert knowledge into MDH’s optimization process, e.g., to achieve (1) better optimization, as an auto-tuning system might not always make the same high-quality optimization decisions as a human expert, and/or (2) faster auto-tuning, as some (or even all) optimization decisions might be made by the expert user and thus are not left to the costly auto-tuner.

*Performance.* Scheduling approaches usually achieve high performance. For this, the approaches incorporate human expert knowledge into their optimization process which is based on two major steps: (1) a human expert implements an optimization program (a.k.a *schedule*) in a so-called *scheduling language*—the program specifies the basic optimizations to perform, such as tiling and parallelization; (2) an auto-tuning system (or a human hardware expert) chooses values of performance-critical parameter of the optimizations implemented in the schedule, e.g., particular values of tile sizes and concrete numbers of threads.

Our experiments in Section 5 show that compared to the state-of-the-art scheduling approach TVM (using its recent Ansor optimizer [Zheng et al., 2020a] for schedule generation), our approach achieves competitive and sometimes even better performance, e.g., speedups up to  $2.22\times$  on GPU and  $3.55\times$  on CPU over TVM+Ansor for computations taken from TVM’s favorable application domain (deep learning). Section 5 discusses that our better performance is due to the design and structure of our general optimization space (Table 1) which can be efficiently explored — fully automatically — using state-of-the-art auto tuning techniques [Rasch et al., 2021]. We focus on TVM in our experiments (rather than, e.g. Halide) to make experimenting challenging for us: TVM+Ansor has proved to achieve higher performance on GPUs and CPUs than popular state-of-practice approaches [Zheng et al., 2020a], including Halide, pyTorch [Paszke et al., 2019], and the recent FlexTensor optimizer [Zheng et al., 2020b].

Recent approach TensorIR [Feng et al., 2023] is a compiler for deep learning computations that achieves higher performance than TVM on NVIDIA GPUs. However, this performance gain over TVM is mainly achieved by exploiting the domain-specific *tensor core* [NVIDIA, 2017] extensions of NVIDIA GPUs, which compute in hardware the multiplications of small, low-precision  $4 \times 4$  matrices. For this, TensorIR introduces the concept of *blocks* which represent sub-computations, e.g., multiplying  $4 \times 4$  matrices. These blocks are then mapped by TensorIR to domain-specific hardware extensions, which often leads to high performance.

While domain-specific hardware extensions are not targeted in this article, we can naturally exploit them in our approach, similar to TensorIR, as we plan for our future work: the sub-computations targeted by the current hardware extensions, such as matrix multiplication on  $4 \times 4$  matrices, can be straightforwardly expressed in our approach (Figure 14). Thus, we can match these sub-expressions in our low-level representation and map them to hardware extensions in our generated code. For this, instead of relying on a full partitioning in our low-level representation (as in Figure 15) such that we can apply scalar function  $f$  to the fully de-composed data (consisting of a single scalar value only in the case of a full partitioning), we plan to rely on a coarser-grained partitioning schema, e.g., down to only  $4 \times 4$  matrices (rather than  $1 \times 1$  matrices, as in the case of a full partitioning). This allows us replacing scalar function  $f$  (which in the case of matrix multiplication is a simple scalar multiplication  $*$ ) with the operation supported by the hardware extension, such as matrix multiplication on  $4 \times 4$  matrices. We expect for our future work to achieve the same advantages over TensorIR as over TVM, because apart from supporting domain-specific hardware extensions, TensorIR is very similar to TVM.

*Portability.* While scheduling approaches achieve high performance, they tend to struggle with achieving portability. This is because even though the approaches often offer different, pre-implemented backends (e.g., a CUDA backend to target NVIDIA GPUs and an OpenCL backend for CPUs), they do not propose any structured methodology about how new backends can be added, e.g., for potentially upcoming architectures, with potentially deeper memory and core hierarchies than GPUs and CPUs. This might be particularly critical (or requiring significant development effort) for the application area of deep learning which is the main target of many scheduling approaches, e.g., TVM and TensorIR, and for which new architectures are arising continuously [Hennessy and Patterson, 2019].

In contrast, we introduce in this article a formally precise recipe for correct-by-construction code generation in different backends (including OpenMP, CUDA, and OpenCL), generically in the target architecture: we introduce an architecture-agnostic low-level representation (Section 3) as target for our high-level programs (Section 2), and we describe formally how our high-level programs are automatically lowered to our low-level representation (Section 4), based on the architecture-agnostic optimization space in Table 1. Rasch [2024] (Section E) outlines how executable, imperative-style program code is straightforwardly generated from low-level expressions, which we plan to discuss and illustrate in detail in our future work.

*Productivity.* Scheduling approaches rely on a two-step optimization process, as discussed above: implementing a schedule (first step) and choosing optimized values of performance-critical parameters within that schedule (second step). While the second step often can be easily automatized, e.g., via auto-tuning [Chen et al., 2018b], the first step—implementing a schedule—usually has to be conducted manually by the user to achieve high performance, which requires expert knowledge and thus hinders productivity. The lack of formal foundation of many scheduling approaches further complicates implementing schedules for the user, as implementation becomes error prone and hardly predictable. For example, Fireiron’s schedules can achieve high performance, close to GPUs’ peak, but schedules in Fireiron can easily generate incorrect low-level code: Fireiron cannot guarantee that optimizations expressed in its scheduling language are semantics preserving, e.g., based on a formal foundation as done in this work, making programming Fireiron’s schedules error prone and complex for the user. Similarly, TVM is sometimes unable to detect user errors in both its high-level language (as discussed in Section 5.1) as well as scheduling language [Apache TVM Community, 2022e]. Safety in parallel programming is an ongoing major demand, in particular from industry [Khronos, 2022a].

Auto schedulers, such as Halide’s optimization engine [Mullapudi et al., 2016] and TVM’s recent Anzor [Zheng et al., 2020a], aim to automatically generate well-performing, correct schedules for the user. However, a major flaw of the current auto schedulers is that even though they work well for some computations (e.g., from deep learning, as TVM’s Anzor), they may perform worse for others. For example, our approach achieves a speedup over TVM+Anzor of  $> 100\times$  already for straightforward dot products (Figure 17). This is because Anzor does not exploit multiple thread blocks and uses only a small number of threads for reduction computations. While such optimization decisions are often beneficial for reductions as used in deep learning (e.g., within the computations of convolutions and matrix multiplications on deep learning workloads, because parallelization can be better exploited for outer loops of these computations), these rigid optimization decisions of Anzor may perform worse in other contexts (e.g., for computing dot product).

To avoid the productivity issues of scheduling approaches, we have designed our optimization process as fully auto-tunable, thereby freeing the user from the burden and complexity of making complex optimization decisions. Our optimization space (Table 1) is designed as generic in the target application area and hardware architecture, thereby achieving high performance for various combinations of data-parallel computations and architectures (Section 5). Correctness of optimizations is ensured in our approach by introducing a formal foundation that enables mathematical reasoning about correctness. Particularly, our optimization process is designed as *correct-by-construction*, meaning that any valid optimization decisions (i.e., a particular choice of tuning parameters in Table 1 that satisfy the constraints) leads to a correct expression in our low-level expression (as in Figure 15). In contrast, approaches such as introduced by Clément and Cohen [2022] formally validate optimization decisions of scheduling approaches in already generated low-level code. Thereby, such approaches work potentially for arbitrary scheduling approaches (Halide, TVM, ...), but the approaches cannot save the user at the high abstraction level from implementing incorrect

optimizations (e.g., via easy-to-understand, high-level error messages indicating that an invalid optimization decisions is made) or restricting the optimization space otherwise to valid decisions only, e.g., for an efficient auto-tuning process, because the approaches check already generated program code.

Scheduling approaches often also suffer from expressivity issues. For example, Fireiron is limited to computing only matrix multiplications on only NVIDIA GPUs, and TVM does not support computations that rely on multiple combine operators different from concatenation [Apache TVM Community, 2020, 2022b], e.g., as required for expressing the MBBS example in Figure 14. Also, TVM has difficulties with user-defined combine operators [Apache TVM Community, 2022d] and thus crashes for example PRL in Figure 14. In contrast to TVM, we introduce a formal methodology about how to manage different kinds of arbitrary, user-defined combine operators (Section 3), which is considered challenging [Apache TVM Community, 2020].

## 6.2 Polyhedral Approaches

Polyhedral approaches, as introduced by Feautrier [1992], as well as *Pluto* [Bondhugula et al., 2008b], *Polly* [Grosser et al., 2012], *PPCG* [Verdoolaage et al., 2013], *Polyhedral Tensor Schedulers* [Meister et al., 2019], *TC* [Vasilache et al., 2019], and *AKG* [Bastoul et al., 2022] rely on a formal, geometrically inspired representation, called *polyhedral model*. Polyhedral approaches often achieve high user productivity, e.g., by automatically parallelizing and optimizing straightforward sequential code. However, the approaches tend to have difficulties with achieving high performance and portability when used for generating low-level program code, as we outline in the following. In Section 6.5, we revisit the polyhedral approach as a potential frontend for our approach, as polyhedral transformations have proven to be efficient when used for high-level code optimizations (e.g., *loop skewing* [Wolf and Lam, 1991]), rather than low-level code generation.

*Performance.* Polyhedral compilers tend to struggle with achieving their full performance potential. We argue that this performance issue of polyhedral compilers is mainly caused by the following two major reasons.

While we consider the set of polyhedral transformation (so-called *affine transformation*) as broad, expressive, and powerful, each polyhedral compiler implements a subset of expert-chosen transformations. This subset of transformations, as well as the application order of transformations, are usually fixed in a particular polyhedral compiler and chosen toward specific optimization goals only, e.g., coarse-grained parallelization and locality-aware data accesses (a.k.a. *Pluto algorithm* [Bondhugula et al., 2008a]), causing the search spaces of polyhedral compilers to be a proper subset of our space in Table 1. Consequently, computations that require for high performance other subsets of polyhedral transformations and/or application orders of transformations (e.g., transformations toward fine-grained parallelization) might not achieve their full performance potential when compiled with a particular polyhedral compiler [Consolaro et al., 2024].

In contrast to the currently existing polyhedral compilers, we have designed our optimization process as generic in goals: for example, our space is designed such that the degree of parallelization (coarse, fine, ...) is fully auto-tunable for the particular combination of target architecture and computation to optimize. We consider it as an interesting future work to investigate the strength and weaknesses of the polyhedral model for expressing our generic optimization space.

We see the second reason for potential performance issues in polyhedral compilers in their difficulties with reduction-like computations. This is mainly caused by the fact that the polyhedral model captures less semantic information than the high-level program representation introduced in Section 2 of this article: combine operators which are used to combine the intermediate results

of computations (e.g., operator + from Example 2 for combining the intermediate results of the dot products within matrix multiplication) are not explicitly represented in the polyhedral model; the polyhedral model is rather focused on modeling memory accesses and their relative order only. Most likely, these semantic information are missing in the polyhedral model, because polyhedral approaches were originally intended to fully automatically optimize loop-based, sequential code (such as Pluto and PPCG)—extracting combine operators automatically from sequential code is challenging and often even impossible (Rice’s theorem).

In contrast, our proposed high-level representation explicitly captures combine operators (Figure 14), by requesting these operators explicitly from the user. This is important, because the operators are often required for generating code that fully utilizes the highly parallel hardware of state-of-the-art architectures (GPUs, etc.), as discussed in Section 5. Similarly to our approach, polyhedral compiler TC also requests combine operators explicitly from the user. However, TC is restricted to operators + (addition), \* (multiplication), min (minimum), and max (maximum) only, thereby TC is not able to express important examples in Figure 14, e.g., PRL which is popular in data mining. Moreover, TC outsources the computation of its combine operators to the NVIDIA CUB library [NVIDIA, 2022a]; most likely as a workaround, because TC relies on the polyhedral model which is not designed to capture and exploit semantic information about combine operators for optimization. Thereby, TC is dependent on external approaches for computing combine operators, which might not always be available (e.g., for upcoming architectures).

Workarounds have been proposed by the polyhedral community to target reduction-like computations [Doerfert et al., 2015; Reddy et al., 2016]. However, these approaches are limited to a subset of computations, e.g., by not supporting user-defined scalar types [Doerfert et al., 2015] (as required for our PRL example in Figure 14), or by being limited to GPUs only [Reddy et al., 2016]. Comparing the semantic information captured in the polyhedral model vs. our MDH-based representation have been the focus of discussions between polyhedral experts and MDH developers [Google SIG MLIR Open Design Meeting, 2020].

*Portability.* The polyhedral approach, in its general form, is a framework offering transformation rules (affine transformations), and each individual polyhedral compiler implements a set of such transformations which are then instantiated (e.g., with particular tile sizes) and applied when compiling a particular application. However, individual polyhedral compilers (e.g., PPCG and Pluto) apply a fixed set of affine transformations, thereby rigidly optimizing for a particular target architecture only, e.g., only GPU (as PPCG) or only CPU (as Pluto), and it remains open which affine transformations have to be used and how for other architectures, e.g., upcoming accelerators for deep learning computations [Hennessy and Patterson, 2019] with potentially more complex memory and core hierarchies than GPUs and CPUs. Moreover, while we introduce an explicit low-level representation (Section 3), the polyhedral approach does not introduce representations on different abstraction levels: the model relies on one representation that is transformed via affine transformations. Apart from the ability of our low-level representation to handle combine operators (which we consider as complex and important), we see the advantages of our explicit low-level representation in, for example, explicitly representing memory regions, which allows formally defining important correctness constraints, e.g., that GPU architectures allow combining the results of threads in designated memory regions only. Furthermore, our low-level representation also allows straightforwardly generating executable code from it (shown by Rasch [2024], Section E, and planned to be discussed thoroughly in future work). In contrast, code generation from the polyhedral model has proven challenging [Bastoul et al., 2022; Vasilache et al., 2022; Grosser et al., 2015].



*Productivity.* Most polyhedral compilers achieve high user productivity, by fully automatically parallelizing and optimizing straightforward sequential code (as Pluto and PPCG). Our approach currently relies on a *Domain-Specific Language (DSL)* for expressing computations, as discussed in Section 2; thus, our approach can be considered as less productive than many polyhedral compilers. However, Rasch et al. [2020b, c] show that DSL programs in our approach can be automatically generated from sequential code (optionally annotated with simple, OpenMP-like directives for expressing combine operators, enabling advanced optimizations), by using polyhedral tool pet [Verdoolaage and Grosser, 2012] as a frontend for our approach. Thereby, we are able to achieve the same, high user productivity as polyhedral compilers. We consider this direction—combing the polyhedral model with our approach—as promising, as it enables benefitting from the advantages of both directions: optimizing sequential programs and making them parallelizable using polyhedral techniques (like *loop skewing*, as also outlined in Section 6.5), and mapping the optimized and parallelizable code eventually to parallel architectures based on the concepts and methodologies introduced in this article.

### 6.3 Functional Approaches

Functional approaches map data-parallel computations that are expressed via small, formally defined building blocks (a.k.a. patterns [Gorlatch and Cole, 2011], such as map and reduce) to the memory and core hierarchies of parallel architectures, based on a strong formal foundation. Notable functional approaches include Accelerate [Chakravarty et al., 2011], Obsidian [Svensson et al., 2011], so-called *skeleton libraries* [Steuwer et al., 2011, Aldinucci et al., 2017, Enmyren and Kessler, 2010, Ernstsson et al., 2018], and the modern Lift approach [Steuwer et al., 2015] (recently also known as RISE [Steuwer et al., 2022]).

In the following, as functional approaches usually follow the same basic concepts and methodologies, we focus on comparing to Lift, because Lift is more recent than, e.g., Accelerate and Obsidian.

*Performance.* Functional approaches tend to struggle with achieving their full performance potential, often caused by the design of their optimization spaces. For example, analogously to our approach, functional approach Lift relies on an internal low-level representation [Steuwer et al., 2017] that is used as target for Lift’s high-level programs. However, Lift’s transformation process, from high level to low level, turned out to be challenging: Lift’s lowering process relies on an infinitely large optimization space—identifying a well-performing configuration within that space is too complex to be done automatically in general, due to the space’s large and complex structure. As a workaround, Lift currently uses approach Elevate [Hagedorn et al., 2020b] to incorporate user knowledge into the optimization process; however, at the cost of productivity, as manually expressing optimization is challenging, particularly for non-expert users.

In contrast, our optimization process is designed as auto-tunable (Table 1), thereby achieving fully automatically high performance, as confirmed in our experiments (Section 5), without involving the user for optimization decisions. In particular, our previous work already showed that our approach—even in its original, proof-of-concept implementation [Rasch et al., 2019a]—can significantly outperform Lift on GPU and CPU [Rasch et al., 2019a]. Our performance advantage over Lift is mainly caused by the design of our optimization process: relying on formally defined tuning parameters (Table 1), rather than on formal transformation rules that span a too large and complex search space (as Lift), thereby contributing to a simpler, fully auto-tunable optimization process.

*Portability.* The current functional approaches usually are designed and optimized toward code generation in a particular programming model only. For example, Lift inherently relies on the



OpenCL programming model, because OpenCL works for multiple kinds of architectures: NVIDIA GPU, Intel CPU, and so on. However, we see two major disadvantages in addressing the portability issue via OpenCL only: (1) GPU-specific optimizations (such as *shuffle operations* [NVIDIA, 2018]) are available only in the CUDA programming model, but not in OpenCL; (2) the set of OpenCL-compatible devices is broad but still limited; in particular, in the *new golden age for computer architectures* [Hennessy and Patterson, 2019], upcoming architectures are arising continuously and may not support the OpenCL standard. We consider targeting new programming models as challenging for Lift, as its formal low-level representation is inherently designed for OpenCL [Steuwer et al., 2017]; targeting further programming models with Lift would require the design and implementation of new low-level representations, which we do not consider as straightforward.

To allow easily targeting new programming models with our approach, we have designed our formalism as generic in the target model: our low-level representation (Figure 15) and optimization space (Table 1) are designed and optimized toward an abstract system model (Definition 10) which is capable of representing the device models of important programming approaches, including OpenMP, CUDA, and OpenCL (Example 11). Furthermore, we have designed our high- and low-level representations as minimalistic (Figures 6 and 15), e.g., by relying on three higher-order functions only for expressing programs at the high abstraction level, which simplifies and reduces the development effort for implementing code generators for programming models.

In addition, we believe that compared to our approach, the following basic design decisions of Lift (and similar functional approaches) complicate the process of code generation for them and increase the development effort for implementing code generators: (1) relying on a vast set of small patterns for expressing computations, rather than aiming at a minimalistic design as we do (as also discussed in Section 5.3); (2) relying on complex function nestings and compositions for expressing computations, rather than avoiding nesting and relying on a fixed composition structure of functions, as in our approach (Figure 5); (3) requiring new patterns for targeting new classes of data-parallel computations (such as patterns `slide` and `pad` for stencils [Hagedorn et al., 2018]), which have to be non-trivially integrated into Lift’s type and optimization system (often via extensions of the systems [Hagedorn et al., 2018, Rummel et al., 2016]), instead of relying on a fixed set of expressive patterns (Figure 6) and generalized optimizations (Table 1) that work for various kinds of data-parallel computations (Figure 14); (4) expressing high-level and low-level concepts in the same language, instead of separating high-level and low-level concepts for a more structured and thus simpler code generation process (Figure 4). We consider these four design decisions as disadvantageous for code generation, because they require from a code generator handling various kinds of patterns (decision 1), and the patterns need to be translated to significantly different code variants, depending on their nesting level and composition order (decision 2). Moreover, each extension of patterns (decision 3) might affect code generation also for the already supported patterns, because the existing patterns need to be combined with the new ones via composition and nesting (decision 2). We consider mixing up high-level and low-level concepts in the same language (decision 4) as further complicating the code generation process, because code generators cannot be implemented in clear, distinct stages: *high-level language* → *low-level language* → *executable program code*.

*Productivity.* Functional approaches are expressive frameworks—to the best of our knowledge, the majority of these approaches should also be able to express (possibly after some extension) many of the high-level programs that can also be expressed via our high-level representation (e.g., those presented in Figure 14).

A main difference we see between the high-level representations of existing functional approaches and the representation introduced by our approach is that the existing approaches rely on a vast

set of higher-order functions for expressing computations; these functions have to be functionally composed and nested in complex ways for expressing computations. For example, expressing matrix multiplication in Lift requires also involving Lift’s pattern transpose (also when operating on non-transposed input matrices) [Rommelg et al., 2016], as per design in Lift, multi-dimensional data is considered as an array of arrays (rather than a MDA, as in our approach as well as polyhedral approaches). In contrast, we aim to keep our high-level language minimalistic, by expressing data-parallel computations using exactly three higher-order functions and which are always used in the same, fixed order (shown in Figure 5). Rasch et al. [2020b, c] confirm that due to the minimalistic and structured design of our high-level representation, programs in our representation can even be systematically generated from straightforward, sequential program code.

Functional approaches also tend to require extension when targeting new application areas, which hinders the expressivity of the frameworks and thus also their productivity. For example, functional approach Lift [Steuer et al., 2015] required notable extension for targeting, e.g., matrix multiplications (so-called *macro-rules* had to be added to Lift [Rommelg et al., 2016]) and stencil computations (primitives *slide* and *pad* were added, and Lift’s tiling optimization had to be extended toward *overlapped tiling* [Hagedorn et al., 2018]). In contrast, we have formally defined our class of targeted computations (as MDH functions, Definition 3), and the generality of our approach allows expressing matrix multiplications and stencils out of the box, without relying on domain-specific building blocks.

## 6.4 Domain-Specific Approaches

Many approaches focus on code generation and optimization for particular domains. A popular domain-specific approach is *ATLAS* [Whaley and Dongarra, 1998] for linear algebra routines on CPUs.<sup>26</sup> Similar to *ATLAS*, approach *FFTW* [Frigo and Johnson, 1998] targets *Fast Fourier Transform*, and *SPIRAL* [Puschel et al., 2005] works for *Digital Signal Processing*.

Nowadays, the best performing, state-of-practice domain-specific approaches are often provided by vendors and specifically designed and optimized toward their target application domain and also architecture. For example, the popular vendor library NVIDIA cuBLAS [NVIDIA, 2022b] is optimized by hand, on the assembly level, toward computing linear algebra routines on NVIDIA GPUs—cuBLAS is considered in the community as gold standard for computing linear algebra routines on GPUs. Similarly, Intel’s oneMKL library [Intel, 2022c] computes with high performance linear algebra routines on Intel CPUs, and libraries NVIDIA cuDNN [NVIDIA, 2022e] and Intel oneDNN [Intel, 2022b] work well for convolution computations on either NVIDIA GPU (cuDNN) or Intel CPU (oneDNN), respectively.

In the following, we discuss domain-specific approaches in terms of *performance*, *portability*, and *productivity*.

*Performance.* Domain-specific approaches, such as cuBLAS and cuDNN, usually achieve high performance. This is because the approaches are hand-optimized by performance experts—on the assembly level—to exploit the full performance potential of their target architecture. In our experiments (Section 5), we show that our approach often achieves competitive and sometimes even better performance than domain-specific approaches provided by NVIDIA and Intel, which is mainly caused by their portability issues across different data characteristics, as we discuss in the next paragraph.

<sup>26</sup>Previous work [Rasch et al., 2021] shows that MDH (already in its original, proof-of-concept implementation) achieves higher performance than *ATLAS*.

*Portability.* Domain-specific approaches usually struggle with achieving portability across different architectures. This is because the approaches are often implemented in architecture-specific assembly code to achieve high performance, but thereby also being limited to their target architecture. The domain-specific approaches often also struggle with achieving portability of performance across different data characteristics (e.g., their sizes): the approaches usually rely on a set of pre-implemented implementations that are each designed and optimized toward average high performance across a range of data characteristic. In contrast, our approach (as well as many scheduling and polyhedral approaches) allow automatically optimizing (auto-tuning) computations for particular data characteristics, which is important for achieving high performance [Tillet and Cox, 2017]. Thereby, our approach often outperforms domain-specific approaches (as confirmed in Section 5), particularly for advanced data characteristics (small, uneven, irregularly shaped, . . . ), e.g., as used in deep learning. The costly time for auto-tuning is well amortized in many application areas, because the auto-tuned implementations are re-used in many program runs. Furthermore, auto-tuning avoids the time-intensive and costly process of hand-optimization by human experts.

*Productivity.* Domain-specific approaches usually achieve highest productivity for their target domain (e.g., linear algebra), by providing easy to use high-level abstractions. However, the approaches suffer from significant expressivity issues, because—per design—they are inherently restricted to their target application domain only. Also, the approaches are often inherently bound to only particular architectures, e.g., only GPU (as NVIDIA cuBLAS and cuDNN) or only CPU (as Intel oneMKL and oneDNN). Domain-specific vendor libraries, such as NVIDIA cuBLAS and Intel oneMKL, also tend to offer the user differently performing variants of computations; the variants have to be naively tested by the user when striving for the full performance potentials of approaches (as discussed in Section 5.4), which is cumbersome for the user.

## 6.5 Higher-Level Approaches

There is a broad range of existing work that is focused on higher-level optimizations than proposed by this work. We consider such higher-level approaches as greatly combinable with our approach. For example, the polyhedral approach is capable of expressing algorithmic-level optimizations, like *loop skewing* [Wolf and Lam, 1991], to make programs parallelizable; such optimizations are beyond the scope of this work, but they can be combined with our approach as demonstrated by Rasch et al. [2020b,c]. Similarly, we consider the approaches introduced by Farzan and Nicolet [2019], Frigo et al. [1999], Gunnels et al. [2001], Yang et al. [2021], which also focus on algorithmic-level optimizations, as greatly combinable with our approach: algorithmically optimizing user code according to the approaches' techniques, and using our methodologies to eventually map the optimized code to executable program code for parallel architectures.

Futhark [Henriksen et al., 2017], Dex [Paszke et al., 2021], and ATL [Liu et al., 2022] are further approaches focused on high-level program transformations, like advanced *flattening* mechanisms [Henriksen et al., 2019], thereby optimizing programs at the algorithmic level of abstraction. We consider using our work as backend for these approaches as promising: the three approaches often struggle with mapping their algorithmically optimized program variants eventually to the multi-layered memory and core hierarchies of state-of-the-art parallel architectures, which is exactly the focus of this work.

## 6.6 Existing Work on MDH

Our work is inspired by the algebraic formalism of MDHs which is introduced in the work-in-progress paper [Rasch and Gorlatch, 2016]. The MDH approach, as presented in the previous work, relies on a semi-formal foundation and focuses on code generation for the OpenCL programming

model only [Rasch et al., 2019a]. This work makes major contributions over the existing work on MDHs and its OpenCL code generation approach.

We introduce a full formalization of MDH's high-level program representation. In our new formalism, we rely on expressive typing: for example, we encode MDHs' data sizes into our type system, e.g., by introducing *index sets* for MDAs (Definition 1), and we respect and maintain these sets thoroughly during MDH computations. Our expressive typing significantly contributes to correct and simplified code generation, as all relevant type and data size information are contained in our formal, low-level program representation (Figure 15) from which we eventually generate executable program code (Section 3). In contrast, the existing MDH work considers MDAs of arbitrary sizes and dimensionalities to be all of the same, straightforward type, which has greatly simplified the design of the proof-of-concept MDH formalism introduced by Rasch and Gorlatch [2016] (in particular, the definition and usage of combine operators), but at the cost of significantly harder and error-prone code generation: all the missing, type-relevant information need to be elaborated by the implementer of the code generator in the existing MDH work, e.g., allocation sizes of fast memory resources used for caching input data or for storing computed intermediate results. Furthermore, while the original MDH work [Rasch and Gorlatch, 2016] is focused on introducing higher-order function `md_hom` only, this work particularly also introduces higher order functions `inp_view` and `out_view` (Section 2.3) which express input and output views in a formally structured and concise manner, and which are central building blocks in our new approach for expressing computations (Figure 14). Also, by introducing and exploiting the index set concept for MDAs, we have improved the definition of the concatenation operator  $+$  (Example 1) toward commutativity, which is required for important optimizations. e.g., loop permutations (expressed via Parameters D1, S1, R1 in Table 1).

A further substantial improvement is the introduction of our low-level representation (Section 3). It relies on a novel combination of tuning parameters (Table 1) that enhance, generalize, and extend the existing, proof-of-concept MDH parameters which capture a subset of OpenCL-orientated features only [Rasch et al., 2019a]. Moreover, while the existing MDH work introduces formally only parameters for flexibly choosing numbers of threads [Rasch and Gorlatch, 2016] (which corresponds to a very limited variant of our tuning parameter  $\theta$  in Table 1, because our parameter  $\theta$  also chooses numbers of memory tiles and is not restricted to OpenCL), the other OpenCL parameters are introduced and discussed by Rasch et al. [2019a] only informally, from a technical perspective. With our novel parameter set, we are able to target various kinds of programming models (e.g., also CUDA, as in Section 5) and also to express important optimizations that are beyond the existing work on MDH, e.g., optimizing the memory access pattern of computations: for example, we achieve speedups  $> 2\times$  over existing MDH for the deep learning computations discussed in Section 5. Our new tuning parameters are expressive enough to represent state-of-the-art, data-parallel implementations, e.g., as generated by scheduling and polyhedral approaches (shown by Rasch [2024], Figures 20–23), and our experiments in Section 5 confirm that auto-tuning our parameters enables performance beyond the state of the art, including hand-optimized solutions provided by vendors, which is not possible when using the existing MDH approach. The expressivity of our parameters particularly also enables comparing significantly differently optimized implementations, based on the values of formally specified tuning parameters, which we consider as promising for structured performance analysis in future work. Moreover, our new low-level representation targets architectures that may have arbitrarily deep memory and core hierarchies, by having optimized our representation toward an abstract system model (Definition 10); in contrast, the existing MDH work is focused on OpenCL-compatible architectures only.

Our experimental evaluation extends the previous MDH experiments by comparing also to the popular state-of-practice approach TVM which is attracting increasing attention from both academia [Apache Software Foundation, 2021] and industry [OctoML, 2022]. Also, we compare to the popular polyhedral compilers PPCG and Pluto, as well as the currently newest versions of hand-optimized, high-performance libraries provided by vendors. Furthermore, we have included a real-world case study in our experiments, considering the most time-intensive computations within the three popular deep learning neural networks ResNet-50, VGG-16, and MobileNet; the study also includes Capsule-style convolution computations, which are considered challenging to optimize [Barham and Isard, 2019]. Moreover, Table 14 analyses MDH’s expressivity using new examples: it shows that MDH—based on the new contributions of this work (e.g., view functions)—is capable of expressing computations bMatMuL, MCC\_Capsule, Histo, scan, and MBBS, which have not been expressed via MDH in previous work. Our experiments confirm that we achieve high performance for bMatMuL and MCC\_Capsule on GPUs and CPUs, and our future work aims to thoroughly analyze our approach for computations Histo, scan, and MBBS in terms of performance, portability, and productivity.

## 7 Conclusion

We introduce a formal (de/re)-composition approach for data-parallel computations targeting state-of-the-art parallel architectures. Our approach aims to combine three major advantages over related approaches—performance, portability, and productivity—by introducing formal program representations on both (1) *high level*, for conveniently expressing—in one uniform formalism—various kinds of data-parallel computations (including linear algebra routines, stencil computations, data mining algorithms, and quantum chemistry computations), agnostic from hardware and optimization details, while still capturing all information relevant for generating high-performance program code; (2) *low level*, which allows uniformly reasoning—in the same formalism—about optimized (de/re)-compositions of data-parallel computations targeting different kinds of parallel architectures (GPUs, CPUs, etc.). We *lower* our high-level representation to our low-level representation, in a formally sound manner, by introducing a generic search space that is based on performance-critical parameters. The parameters of our lowering process enable fully automatically optimizing (auto-tuning) our low-level representations for a particular target architecture and characteristics of the input and output data, and our low-level representation is designed such that it can be straightforwardly transformed to executable program code in imperative-style programming languages (including OpenMP, CUDA, and OpenCL). Our experiments confirm that due to the design and structure of our generic search space in combination with auto-tuning, our approach achieves higher performance on GPUs and CPUs than popular state-of-practice approaches, including hand-optimized libraries provided by vendors.

## 8 Future Work

We consider this work as a promising starting point for future directions. A major future goal is to extend our approach toward expressing and optimizing simultaneously multiple data-parallel computations (e.g., matrix multiplication followed by convolution), rather than optimizing computations individually and thus independently from each other (e.g., only matrix multiplication or only convolution). Such extension enables optimizations, such as *kernel fusion*, which is important for the overall application performance and considered challenging [Fukuhara and Takimoto, 2022; Li et al., 2022; Wahib and Maruyama, 2014]. We see this work as a promising foundation for our future goal, because it enables expressing and reasoning about different computations in the same formal framework. Targeting computations on sparse input/output data formats, inspired by Ben-Nun et al. [2017], Hall [2020], Kjolstad et al. [2017], Pizzuti et al. [2020], is a further major goal, which



requires extending our approach toward irregularly-shaped input and output data, similarly as done by Pizzuti et al. [2020]. Regarding our optimization process, we aim to introduce an analytical cost model for computations expressed in our formalism—based on operational semantics—thereby accelerating (or even avoiding) the auto-tuning overhead, similarly as done by Li et al. [2021], Muller and Hoffmann [2021]. Moreover, we aim to incorporate methods from machine learning into our optimization process [Leather et al., 2014, Merouani et al., 2024], instead of relying on empirical auto-tuning methods only. To make our work better accessible for the community, we aim to implement our approach into *MLIR* [Lattner et al., 2021] which offers a reusable compiler infrastructure. The contributions of this work give a precise, formal recipe of how to implement our introduced methods into approaches such as *MLIR*. Moreover, relying on the *MLIR* framework will contribute to a structured code generation process in assembly-level programming models, such as *LLVM* [Lattner and Adve, 2004] and *NVIDIA PTX* [NVIDIA, 2022i]. We consider targeting assembly languages as important for our future work: assembly code offers further, low-level optimization opportunities [Goto and Geijn, 2008, Lai and Sezner, 2013], thereby enabling our approach to potentially achieve higher performance than reported in Section 5 for our generated *CUDA* and *OpenCL* code. Also, we aim to extend our approach toward distributed multi-device systems that are heterogeneous, inspired by dynamic load balancing approaches [Chen et al., 2010] and advanced data distributions techniques [Yadav et al., 2022]. Targeting domain-specific hardware extensions, such as *NVIDIA Tensor Cores* [NVIDIA, 2017] is also an important goal for our future work, as such extensions allow significantly accelerating computations for the target of the extensions (e.g., deep learning [Markidis et al., 2018]). Finally, we aim to support more target backends (additionally to *OpenMP*, *CUDA*, and *OpenCL*), e.g., *AMD's HIP* [AMD, 2024] which is efficient for programming *AMD GPUs*. Similarly, we consider *Triton* [Tillet et al., 2019], *AMOS* [Zheng et al., 2022], and *Graphene* [Hagedorn et al., 2023] as further, promising backends for our approach.

## Acknowledgments

The author would like to thank Richard Schulze for conducting the extensive set of experiments and the reviewers for their thorough reading of the paper and their comments and remarks that helped us to improve this work.

## References

- Marco Aldinucci, Marco Danelutto, Peter Kilpatrick, and Massimo Torquati. 2017. Fastflow: High-Level and Efficient Streaming on Multi-Core. In *Programming Multi-Core and Many-Core Computing Systems, Parallel and Distributed Computing*. John Wiley & Sons, Ltd. 261–280. DOI: <https://doi.org/10.1002/9781119332015.ch13>
- AMD. 2024. HIP: C++ Heterogeneous-Compute Interface for Portability. Retrieved from <https://github.com/ROCm/HIP>
- Jason Ansel, Shoaib Kamil, Kalyan Veeramachaneni, Jonathan Ragan-Kelley, Jeffrey Bosboom, Una-May O'Reilly, and Saman Amarasinghe. 2014. OpenTuner: An Extensible Framework for Program Autotuning. In *Proceedings of the 23rd International Conference on Parallel Architectures and Compilation (PACT '14)*. ACM, New York, NY, 303–316. DOI: <https://doi.org/10.1145/2628071.2628092>
- Apache. 2022. TVM: Open Deep Learning Compiler Stack. Retrieved from <https://github.com/apache/tvm>
- Apache Software Foundation. 2021. TVM and Open Source ML Acceleration Conference. Retrieved from <https://www.tvmcon.org>
- Apache TVM Community. 2020. Non Top-Level Reductions in Compute Statements. Retrieved from <https://discuss.tvm.apache.org/t/non-top-level-reductions-in-compute-statements/5693>
- Apache TVM Community. 2022a. Bind Reduce Axis to Blocks. Retrieved from <https://discuss.tvm.apache.org/t/bind-reduce-axis-to-blocks/2907>
- Apache TVM Community. 2022b. Expressing Nested Reduce Operations. Retrieved from <https://discuss.tvm.apache.org/t/expressing-nested-reduce-operations/8784>
- Apache TVM Community. 2022c. Implementing Array Packing via Cache\_Read. Retrieved from <https://discuss.tvm.apache.org/t/implementing-array-packing-via-cache-read/13360>

- Apache TVM Community. 2022d. Invalid comm\_reducer. Retrieved from <https://discuss.tvm.apache.org/t/invalid-comm-reducer/12788>
- Apache TVM Community. 2022e. Undetected Parallelization Issue. Retrieved from <https://discuss.tvm.apache.org/t/undetected-parallelization-issue/13224>
- Apache TVM Documentation. 2022a. Bind ivar to Thread Index thread\_ivar. Retrieved from <https://tvm.apache.org/docs/reference/api/python/te.html?highlight=bind#tvm.te.Stage.bind>
- Apache TVM Documentation. 2022b. Tuning High Performance Convolution on NVIDIA GPUs. Retrieved from [https://tvm.apache.org/docs/how\\_to/tune\\_with\\_autotvm/tune\\_conv2d\\_cuda.html](https://tvm.apache.org/docs/how_to/tune_with_autotvm/tune_conv2d_cuda.html)
- David F. Bacon, Susan L. Graham, and Oliver J. Sharp. 1994. Compiler Transformations for High-Performance Computing. *ACM Computing Surveys* 26, 4 (Dec. 1994), 345–420. DOI : <https://doi.org/10.1145/197405.197406>
- Riyadh Baghdadi, Jessica Ray, Malek Ben Romdhane, Emanuele Del Sozzo, Abdurrahman Akkas, Yunming Zhang, Patricia Suriana, Shoaib Kamil, and Saman Amarasinghe. 2019. Tiramisu: A Polyhedral Compiler for Expressing Fast and Portable Code. In *Proceedings of the IEEE/ACM International Symposium on Code Generation and Optimization (CGO '19)*. 193–205. DOI : <https://doi.org/10.1109/CGO.2019.8661197>
- Lénaïc Bagnères, Oleksandr Zinenko, Stéphane Huot, and Cédric Bastoul. 2016. Opening Polyhedral Compiler'S Black Box. In *Proceedings of the International Symposium on Code Generation and Optimization (CGO '16)*. ACM, New York, NY, 128–138. DOI : <https://doi.org/10.1145/2854038.2854048>
- Prasanna Balaprakash, Jack Dongarra, Todd Gamblin, Mary Hall, Jeffrey K. Hollingsworth, Boyana Norris, and Richard Vuduc. 2018. Autotuning in High-Performance Computing Applications. *Proceedings of the IEEE* 106, 11 (2018), 2068–2083. DOI : <https://doi.org/10.1109/JPROC.2018.2841200>
- Paul Barham and Michael Isard. 2019. Machine Learning Systems Are Stuck in a Rut. In *Proceedings of the Workshop on Hot Topics in Operating Systems (HotOS '19)*. ACM, New York, NY, 177–183. DOI : <https://doi.org/10.1145/3317550.\protect\penalty-\@M3321441>
- Cedric Bastoul, Zhen Zhang, Harenome Razanajato, Nelson Lossing, Adilla Susungi, Javier de Juan, Etienne Filhol, Baptiste Jarry, Gianpietro Consolaro, and Renwei Zhang. 2022. Optimizing GPU Deep Learning Operators with Polyhedral Scheduling Constraint Injection. In *Proceedings of the IEEE/ACM International Symposium on Code Generation and Optimization (CGO '22)*. 313–324. DOI : <https://doi.org/10.1109/CGO53902.2022.9741260>
- Tal Ben-Nun, Johannes de Fine Licht, Alexandros Nikolaos Ziogas, Timo Schneider, and Torsten Hoefer. 2019. Stateful Dataflow Multigraphs: A Data-Centric Model for Performance Portability on Heterogeneous Architectures. In *Proceedings of the International Conference for High Performance Computing, Networking, Storage and Analysis (SC '19)*.
- Tal Ben-Nun, Michael Sutton, Sreepathi Pai, and Keshav Pingali. 2017. Groute: An Asynchronous Multi-GPU Programming Model for Irregular Computations. *ACM SIGPLAN Notices* 52, 8 (Jan. 2017), 235–248. DOI : <https://doi.org/10.1145/3155284.3018756>
- Richard S. Bird. 1989. Lectures on Constructive Functional Programming. In *Constructive Methods in Computing Science*. Manfred Broy (Ed.), Springer, Berlin, 151–217.
- Guy E. Blelloch. 1990. *Prefix Sums and Their Applications*. Technical Report CMU-CS-90-190. School of Computer Science, Carnegie Mellon University.
- Barry Boehm, Bradford Clark, Ellis Horowitz, Chris Westland, Ray Madachy, and Richard Selby. 1995. Cost Models for Future Software Life Cycle Processes: COCOMO 2.0. *Annals of Software Engineering* 1, 1 (1995), 57–94. DOI : <https://doi.org/10.1007/BF02249046>
- Uday Bondhugula. 2020. High Performance Code Generation in MLIR: An Early Case Study with GEMM. arXiv:2003.00532. Retrieved from <https://doi.org/10.48550/arXiv.2003.00532>
- Uday Bondhugula, Muthu Baskaran, Sriram Krishnamoorthy, J. Ramanujam, Atanas Rountev, and P. Sadayappan. 2008a. Automatic Transformations for Communication-Minimized Parallelization and Locality Optimization in the Polyhedral Model. In *Compiler Construction*. Laurie Hendren (Ed.), Springer, Berlin, 132–146.
- Uday Bondhugula, Albert Hartono, J. Ramanujam, and P. Sadayappan. 2008b. Pluto: A Practical and Fully Automatic Polyhedral Program Optimization System. In *Proceedings of the ACM SIGPLAN 2008 Conference on Programming Language Design and Implementation (PLDI '08)* (June 2008). Citeseer.
- Ajay Brahmakshatriya and Saman Amarasinghe. 2021. BuildIt: A Type-Based Multi-stage Programming Framework for Code Generation in C++. In *Proceedings of the IEEE/ACM International Symposium on Code Generation and Optimization (CGO '21)*. 39–51. DOI : <https://doi.org/10.1109/CGO51591.2021.9370333>
- C++ Reference. 2022. Date and Time Utilities. Retrieved from <https://en.cppreference.com/w/cpp/chrono>
- José Maria Cecilia, José Manuel García, and Manuel Ujaldón. 2012. CUDA 2D Stencil Computations for the Jacobi Method. In *Applied Parallel and Scientific Computing*. Kristján Jónasson (Ed.), Springer, Berlin, 173–183.
- Manuel M. T. Chakravarty, Gabriele Keller, Sean Lee, Trevor L. McDonell, and Vinod Grover. 2011. Accelerating Haskell Array Codes with Multicore GPUs. In *Proceedings of the 6th Workshop on Declarative Aspects of Multicore Programming (DAMP '11)*. ACM, New York, NY, 3–14. DOI : <https://doi.org/10.1145/1926354.1926358>



- Chun Chen, Jacqueline Chame, and Mary Hall. 2008. *CHILL: A Framework for Composing High-Level Loop Transformations*. Technical Report 08-897, University of Southern California.
- Long Chen, Oreste Villa, Sriram Krishnamoorthy, and Guang R. Gao. 2010. Dynamic Load Balancing on Single- and Multi-GPU Systems. In *Proceedings of the 2010 IEEE International Symposium on Parallel Distributed Processing (IPDPS '10)*. 1–12. DOI: <https://doi.org/10.1109/IPDPS.2010.5470413>
- Tianqi Chen, Thierry Moreau, Ziheng Jiang, Lianmin Zheng, Eddie Yan, Haichen Shen, Meghan Cowan, Leyuan Wang, Yuwei Hu, Luis Ceze, Carlos Guestrin, and Arvind Krishnamurthy. 2018a. TVM: An Automated End-to-End Optimizing Compiler for Deep Learning. In *Proceedings of the 13th USENIX Symposium on Operating Systems Design and Implementation (OSDI '18)*. USENIX Association, Carlsbad, CA, 578–594. Retrieved from <https://www.usenix.org/conference/osdi18/presentation/chen>
- Tianqi Chen, Lianmin Zheng, Eddie Yan, Ziheng Jiang, Thierry Moreau, Luis Ceze, Carlos Guestrin, and Arvind Krishnamurthy. 2018b. Learning to Optimize Tensor Programs. In *Proceedings of the Advances in Neural Information Processing Systems*. Samy Bengio, Hanna Wallach, Hugo Larochelle, Kristen Grauman, Nicolò Cesa-Bianchi, and Roman Garnett (Eds.), Vol. 31. Curran Associates, Inc. Retrieved from <https://proceedings.neurips.cc/paper/2018/file/8b5700012be65c9da25f49408d959ca0-Paper.pdf>
- Peter Christen. 2012. *Data Matching: Concepts and Techniques for Record Linkage, Entity Resolution, and Duplicate Detection*. Springer Publishing Company, Incorporated.
- Basile Clément and Albert Cohen. 2022. End-to-End Translation Validation for the Halide Language. In *Proceedings of the Conference on Object-Oriented Programming Systems, Languages, and Applications (OOPSLA '22)* (Proceedings of the ACM on Programming Languages (PACMPL), Vol. 6). DOI: <https://doi.org/10.1145/3527328>
- Murray I. Cole. 1995. Parallel Programming with List Homomorphisms. *Parallel Processing Letters* 05, 02 (1995), 191–203. DOI: <https://doi.org/10.1142/S0129626495000175>
- Gianpietro Consolaro, Zhen Zhang, Harenome Razanajato, Nelson Lossing, Nassim Tchoulak, Adilla Susungi, Artur Cesar Araujo Alves, Renwei Zhang, Denis Barthou, Corinne Ancourt, and Cedric Bastoul. 2024. PolyTOPS: Reconfigurable and Flexible Polyhedral Scheduler. In *Proceedings of the IEEE/ACM International Symposium on Code Generation and Optimization (CGO '24)*. 28–40. DOI: <https://doi.org/10.1109/CGO57630.2024.10444791>
- Johannes Doerfert, Kevin Streit, Sebastian Hack, and Zino Benaissa. 2015. Polly's Polyhedral Scheduling in the Presence of Reductions. arXiv:1505.07716. Retrieved from <http://arxiv.org/abs/1505.07716>
- Vincent Dumoulin and Francesco Visin. 2018. A Guide to Convolution Arithmetic for Deep Learning. arXiv:1603.07285.
- Johan Enmyren and Christoph W. Kessler. 2010. SkePU: A Multi-Backend Skeleton Programming Library for Multi-GPU Systems. In *Proceedings of the 4th International Workshop on High-Level Parallel Programming and Applications (HLPP '10)*. ACM, New York, NY, 5–14. DOI: <https://doi.org/10.1145/1863482.1863487>
- August Ernstsson, Lu Li, and Christoph Kessler. 2018. SkePU 2: Flexible and Type-Safe Skeleton Programming for Heterogeneous Parallel Systems. *International Journal of Parallel Programming* 46, 1 (2018), 62–80. DOI: <https://doi.org/10.1007/s10766-017-0490-5>
- Facebook Research. 2022. Tensor Comprehensions. Retrieved from <https://github.com/facebookresearch/Tensor-Comprehensions>
- Azadeh Farzan and Victor Nicolet. 2019. Modular Divide-and-Conquer Parallelization of Nested Loops. In *Proceedings of the 40th ACM SIGPLAN Conference on Programming Language Design and Implementation (PLDI '19)*. ACM, New York, NY, 610–624. DOI: <https://doi.org/10.1145/3314221.3314612>
- Paul Feautrier. 1992. Some Efficient Solutions to the Affine Scheduling Problem. I. One-Dimensional Time. *International Journal of Parallel Programming* 21, 5 (1992), 313–347. DOI: <https://doi.org/10.1007/BF01407835>
- Siyuan Feng, Bohan Hou, Hongyi Jin, Wuwei Lin, Junru Shao, Ruihang Lai, Zihao Ye, Lianmin Zheng, Cody Hao Yu, and Tianqi Chen. 2023. TensorIR: An Abstraction for Automatic Tensorized Program Optimization. In *Proceedings of the 28th ACM International Conference on Architectural Support for Programming Languages and Operating Systems (ASPLOS '23)*, Vol. 2. ACM, New York, NY, 804–817. DOI: <https://doi.org/10.1145/3575693.3576933>
- Matteo Frigo and Steven G. Johnson. 1998. FFTW: An Adaptive Software Architecture for the FFT. In *Proceedings of the 1998 IEEE International Conference on Acoustics, Speech and Signal Processing (ICASSP '98)* (Cat. No.98CH36181), Vol. 3. 1381–1384. DOI: <https://doi.org/10.1109/ICASSP.1998.681704>
- Matteo Frigo, Charles E. Leiserson, Harald Prokop, and Sridhar Ramachandran. 1999. Cache-Oblivious Algorithms. In *Proceedings of the 40th Annual Symposium on Foundations of Computer Science (Cat. No.99CB37039)*. 285–297. DOI: <https://doi.org/10.1109/SFFCS.1999.814600>
- Junji Fukuhara and Munehiro Takimoto. 2022. Automated Kernel Fusion for GPU Based on Code Motion. In *Proceedings of the 23rd ACM SIGPLAN/SIGBED International Conference on Languages, Compilers, and Tools for Embedded Systems (LCTES '22)*. ACM, New York, NY, 151–161. DOI: <https://doi.org/10.1145/3519941.3535078>
- Sylvain Girbal, Nicolas Vasilache, Cédric Bastoul, Albert Cohen, David Parello, Marc Sigler, and Olivier Temam. 2006. Semi-Automatic Composition of Loop Transformations for Deep Parallelism and Memory Hierarchies. *International Journal of Parallel Programming* 34, 3 (2006), 261–317. DOI: <https://doi.org/10.1007/s10766-006-0012-3>

- GNU/Linux. 2022. `clock_gettime(3)` – Linux Man Page. Retrieved from [https://linux.die.net/man/3/clock\\_gettime](https://linux.die.net/man/3/clock_gettime)
- Horacio González-Vélez and Mario Leyton. 2010. A Survey of Algorithmic Skeleton Frameworks: High-Level Structured Parallel Programming Enablers. *Software: Practice and Experience* 40, 12 (2010), 1135–1160. DOI: <https://doi.org/10.1002/spe.1026>
- Google SIG MLIR Open Design Meeting. 2020. *Using MLIR for Multi-Dimensional Homomorphisms*. Retrieved from [https://www.youtube.com/watch?v=RQR\\_9tHscMI](https://www.youtube.com/watch?v=RQR_9tHscMI)
- Sergei Gorlatch. 1999. Extracting and Implementing List Homomorphisms in Parallel Program Development. *Science of Computer Programming* 33, 1 (1999), 1–27. DOI: [https://doi.org/10.1016/S0167-6423\(97\)00014-2](https://doi.org/10.1016/S0167-6423(97)00014-2)
- Sergei Gorlatch and Murray Cole. 2011. Parallel Skeletons. In: David Padua (Ed.), *Encyclopedia of Parallel Computing*. Springer-Verlag GmbH, 1417–1422.
- Sergei Gorlatch and Christian Lengauer. 1997. (De) Composition Rules for Parallel Scan and Reduction. In *Proceedings of the 3rd Working Conference on Massively Parallel Programming Models (Cat. No.97TB100228)*. 23–32. DOI: <https://doi.org/10.1109/MPPM.1997.715958>
- Kazushige Goto and Robert A. van de Geijn. 2008. Anatomy of High-Performance Matrix Multiplication. *ACM Transactions on Mathematical Software* 34, 3, Article 12 (May 2008), 25 pages. DOI: <https://doi.org/10.1145/1356052.1356053>
- Tobias Grosser, Armin Groesslinger, and Christian Lengauer. 2012. Polly - Performing Polyhedral Optimizations on a Low-level Intermediate Representation. *Parallel Processing Letters* 22, 04 (2012), 1250010. DOI: <https://doi.org/10.1142/S0129626412500107>
- Tobias Grosser, Sven Verdoolaege, and Albert Cohen. 2015. Polyhedral AST Generation Is More Than Scanning Polyhedra. *ACM Transactions on Programming Languages and Systems* 37, 4, Article 12 (Jul. 2015), 50 pages. DOI: <https://doi.org/10.1145/2743016>
- John A. Gunnels, Fred G. Gustavson, Greg M. Henry, and Robert A. van de Geijn. 2001. FLAME: Formal Linear Algebra Methods Environment. *ACM Transactions on Mathematical Software* 27, 4 (Dec. 2001), 422–455. DOI: <https://doi.org/10.1145/504210.504213>
- Bastian Hagedorn, Archibald Samuel Elliott, Henrik Barthels, Rastislav Bodik, and Vinod Grover. 2020a. Fireiron: A Data-Movement-Aware Scheduling Language for GPUs. In *Proceedings of the ACM International Conference on Parallel Architectures and Compilation Techniques (PACT '20)*. ACM, New York, NY, 71–82. DOI: <https://doi.org/10.1145/3410463.3414632>
- Bastian Hagedorn, Bin Fan, Hanfeng Chen, Cris Cecka, Michael Garland, and Vinod Grover. 2023. Graphene: An IR for Optimized Tensor Computations on GPUs. In *Proceedings of the 28th ACM International Conference on Architectural Support for Programming Languages and Operating Systems (ASPLOS '23)*, Vol. 3. ACM, New York, NY, 302–313. DOI: <https://doi.org/10.1145/3582016.3582018>
- Bastian Hagedorn, Johannes Lenfers, Thomas Kundendhler, Xueying Qin, Sergei Gorlatch, and Michel Steuwer. 2020b. Achieving High-Performance the Functional Way: A Functional Pearl on Expressing High-Performance Optimizations as Rewrite Strategies. *Proceedings of the ACM on Programming Languages* 4, ICFP, Article 92 (Aug. 2020), 29 pages. DOI: <https://doi.org/10.1145/3408974>
- Bastian Hagedorn, Larisa Stoltzfus, Michel Steuwer, Sergei Gorlatch, and Christophe Dubach. 2018. High Performance Stencil Code Generation with Lift. In *Proceedings of the 2018 International Symposium on Code Generation and Optimization (CGO '18)*. ACM, New York, NY, 100–112. DOI: <https://doi.org/10.1145/3168824>
- Mary Hall. 2020. Research Challenges in Compiler Technology for Sparse Tensors. In *Proceedings of the IEEE/ACM 10th Workshop on Irregular Applications: Architectures and Algorithms (IA3 '20)*. viii–viii. DOI: <https://doi.org/10.1109/IA351965.2020.00006>
- Maurice H. Halstead. 1977. *Elements of Software Science (Operating and Programming Systems Series)*. Elsevier Science Inc.
- Haskell.org. 2022. Haskell: An Advanced, Purely Functional Programming Language. Retrieved from <https://www.haskell.org>
- Kaiming He, Xiangyu Zhang, Shaoqing Ren, and Jian Sun. 2015. Deep Residual Learning for Image Recognition. arXiv:1512.03385. Retrieved from <http://arxiv.org/abs/1512.03385>
- John L. Hennessy and David A. Patterson. 2019. A New Golden Age for Computer Architecture. *Communications of the ACM* 62, 2 (Jan. 2019), 48–60. DOI: <https://doi.org/10.1145/3282307>
- Troels Henriksen, Sune Hellfritsch, Ponnuswamy Sadayappan, and Cosmin Oancea. 2020. Compiling Generalized Histograms for GPU. In *Proceedings of the SC20: International Conference for High Performance Computing, Networking, Storage and Analysis*. 1–14. DOI: <https://doi.org/10.1109/SC41405.2020.00101>
- Troels Henriksen, Niels G. W. Serup, Martin Elsmann, Fritz Henglein, and Cosmin E. Oancea. 2017. Futhark: Purely Functional GPU-Programming with Nested Parallelism and in-Place Array Updates. In *Proceedings of the 38th ACM SIGPLAN Conference on Programming Language Design and Implementation (PLDI '17)*. ACM, New York, NY, 556–571. DOI: <https://doi.org/10.1145/3062341.3062354>
- Troels Henriksen, Frederik Thorøe, Martin Elsmann, and Cosmin Oancea. 2019. Incremental Flattening for Nested Data Parallelism. In *Proceedings of the 24th Symposium on Principles and Practice of Parallel Programming (PPoPP '19)*. ACM, New York, NY, 53–67. DOI: <https://doi.org/10.1145/3293883.3295707>

- Kristian Hentschel. 2008. Das Krebsregister-Manual der Gesellschaft der epidemiologischen Krebsregister in Deutschland e.V. Zuckschwerdt Verlag.
- Geoffrey E. Hinton, Sara Sabour, and Nicholas Frosst. 2018. Matrix Capsules with EM Routing. In *Proceedings of the International Conference on Learning Representations*. Retrieved from <https://openreview.net/forum?id=HJWLFGWrb>
- Torsten Hoeffer and Roberto Belli. 2015. Scientific Benchmarking of Parallel Computing Systems: Twelve Ways to Tell the Masses When Reporting Performance Results. In *Proceedings of the International Conference for High Performance Computing, Networking, Storage and Analysis (SC '15)*. ACM, New York, NY, Article 73, 12 pages. DOI: <https://doi.org/10.1145/2807591.2807644>
- Andrew G. Howard, Menglong Zhu, Bo Chen, Dmitry Kalenichenko, Weijun Wang, Tobias Weyand, Marco Andreetto, and Hartwig Adam. 2017. MobileNets: Efficient Convolutional Neural Networks for Mobile Vision Applications. arXiv:1704.04861. Retrieved from <http://arxiv.org/abs/1704.04861>
- Cristina Hristea, Daniel Lenoski, and John Keen. 1997. Measuring Memory Hierarchy Performance of Cache-Coherent Multiprocessors Using Micro Benchmarks. In *Proceedings of the ACM/IEEE Conference on Supercomputing (SC '97)*. ACM, New York, NY, 1–12. DOI: <https://doi.org/10.1145/509593.509638>
- Intel. 2019. Math Kernel Library Improved Small Matrix Performance Using Just-in-Time (JIT) Code Generation for Matrix Multiplication (GEMM). Retrieved from <https://www.intel.com/content/www/us/en/developer/articles/technical/oneapi-improved-small-matrix-performance-using-just-in-time-jit-code.html>
- Intel. 2022a. oneAPI Math Kernel Library Link Line Advisor. Retrieved from <https://www.intel.com/content/www/us/en/developer/tools/oneapi/oneapi-link-line-advisor.html>
- Intel. 2022b. oneDNN. Retrieved from [https://oneapi-src.github.io/oneDNN/group\\_dnnl\\_api.html](https://oneapi-src.github.io/oneDNN/group_dnnl_api.html)
- Intel. 2022c. oneMKL. Retrieved from <https://www.intel.com/content/www/us/en/develop/documentation/oneapi-programming-guide/top/api-based-programming/intel-oneapi-math-kernel-library-oneapi.html>
- Wayne Kelly and William Pugh. 1998. *A Framework for Unifying Reordering Transformations*. Technical Report UMIACS-TR-92-126.1. Digital Repository at the University of Maryland.
- Malik Khan, Protonu Basu, Gabe Rudy, Mary Hall, Chun Chen, and Jacqueline Chame. 2013. A Script-Based Autotuning Compiler System to Generate High-Performance CUDA Code. *ACM Transactions on Architecture and Code Optimization* 9, 4, Article 31 (Jan. 2013), 25 pages. DOI: <https://doi.org/10.1145/2400682.2400690>
- Khronos. 2022a. Khronos Releases Vulkan SC 1.0 Open Standard for Safety-Critical Accelerated Graphics and Compute. Retrieved from <https://www.khronos.org/news/press/khronos-releases-vulkan-safety-critical-1.0-specification-to-deliver-safety-critical-graphics-compute>
- Khronos. 2022b. OpenCL: Open Standard For Parallel Programming of Heterogeneous Systems. Retrieved from <https://www.khronos.org/opencl/>
- Jinsung Kim, Aravind Sukumaran-Rajam, Vineeth Thumma, Sriram Krishnamoorthy, Ajay Panyala, Louis-Noël Pouchet, Atanas Rountev, and P. Sadayappan. 2019. A Code Generator for High-Performance Tensor Contractions on GPUs. In *Proceedings of the IEEE/ACM International Symposium on Code Generation and Optimization (CGO '19)*. 85–95. DOI: <https://doi.org/10.1109/CGO.2019.8661182>
- Fredrik Kjolstad, Shoaib Kamil, Stephen Chou, David Lugato, and Saman Amarasinghe. 2017. The Tensor Algebra Compiler. *Proceedings of the ACM on Programming Languages* 1, OOPSLA, Article 77 (Oct. 2017), 29 pages. DOI: <https://doi.org/10.1145/3133901>
- Michael Klemm, Alejandro Duran, Xinmin Tian, Hideki Saito, Diego Caballero, and Xavier Martorell. 2012. Extending OpenMP\* with Vector Constructs for Modern Multicore SIMD Architectures. In *Proceedings of the 8th International Conference on OpenMP in a Heterogeneous World (IWOMP '12)*. Springer-Verlag, Berlin, 59–72. DOI: [https://doi.org/10.1007/978-3-642-30961-8\\_5](https://doi.org/10.1007/978-3-642-30961-8_5)
- Alex Krizhevsky, Ilya Sutskever, and Geoffrey E. Hinton. 2012. ImageNet Classification with Deep Convolutional Neural Networks. In *Proceedings of the Advances in Neural Information Processing Systems*. Fernando Pereira, Christopher J. C. Burges, Léon Bottou, and Kilian Q. Weinberger (Eds.), Vol. 25. Curran Associates, Inc. Retrieved from <https://proceedings.neurips.cc/paper/2012/file/c399862d3b9d6b76c8436e924a68c45b-Paper.pdf>
- Junjie Lai and André Seznec. 2013. Performance Upper Bound Analysis and Optimization of SGEMM on Fermi and Kepler GPUs. In *Proceedings of the IEEE/ACM International Symposium on Code Generation and Optimization (CGO '13)*. 1–10. DOI: <https://doi.org/10.1109/CGO.2013.6494986>
- Monica D. Lam, Edward E. Rothberg, and Michael E. Wolf. 1991. The Cache Performance and Optimizations of Blocked Algorithms. In *Proceedings of the 4th International Conference on Architectural Support for Programming Languages and Operating Systems (ASPLOS 'IV)*. ACM, New York, NY, 63–74. DOI: <https://doi.org/10.1145/106972.106981>
- Vikram Lattner and Vikram Adve. 2004. LLVM: A Compilation Framework for Lifelong Program Analysis & Transformation. In *Proceedings of the International Symposium on Code Generation and Optimization (CGO '04)*. 75–86. DOI: <https://doi.org/10.1109/CGO.2004.1281665>

- Chris Lattner, Mehdi Amini, Uday Bondhugula, Albert Cohen, Andy Davis, Jacques Pienaar, River Riddle, Tatiana Shpeisman, Nicolas Vasilache, and Oleksandr Zinenko. 2021. MLIR: Scaling Compiler Infrastructure for Domain Specific Computation. In *Proceedings of the IEEE/ACM International Symposium on Code Generation and Optimization (CGO '21)*. 2–14. DOI: <https://doi.org/10.1109/CGO51591.2021.9370308>
- Hugh Leather, Edwin Bonilla, and Michael O'boyle. 2014. Automatic Feature Generation for Machine Learning–Based Optimising Compilation. *ACM Transactions on Architecture and Code Optimization* 11, 1, Article 14 (Feb. 2014), 32 pages. DOI: <https://doi.org/10.1145/2536688>
- Roland Leißa, Klaas Boesche, Sebastian Hack, Arsène Pérard-Gayot, Richard Membarth, Philipp Slusallek, André Müller, and Bertil Schmidt. 2018. AnyDSL: A Partial Evaluation Framework for Programming High-Performance Libraries. *Proceedings of the ACM on Programming Languages* 2, OOPSLA, Article 119 (Oct. 2018), 30 pages. DOI: <https://doi.org/10.1145/3276489>
- Ao Li, Bojian Zheng, Gennady Pekhimenko, and Fan Long. 2022. Automatic Horizontal Fusion for GPU Kernels. In *Proceedings of the IEEE/ACM International Symposium on Code Generation and Optimization (CGO '22)*. 14–27. DOI: <https://doi.org/10.1109/CGO53902.2022.9741270>
- Rui Li, Yufan Xu, Aravind Sukumaran-Rajam, Atanas Rountev, and P. Sadayappan. 2021. Analytical Characterization and Design Space Exploration for Optimization of CNNs. In *Proceedings of the 26th ACM International Conference on Architectural Support for Programming Languages and Operating Systems (ASPLOS '21)*. ACM, New York, NY, 928–942. DOI: <https://doi.org/10.1145/3445814.3446759>
- Xiaqing Li, Guangyan Zhang, H. Howie Huang, Zhufan Wang, and Weimin Zheng. 2016. Performance Analysis of GPU-Based Convolutional Neural Networks. In *Proceedings of the 45th International Conference on Parallel Processing (ICPP '16)*. 67–76. DOI: <https://doi.org/10.1109/ICPP.2016.15>
- Amanda Liu, Gilbert Louis Bernstein, Adam Chlipala, and Jonathan Ragan-Kelley. 2022. Verified Tensor-Program Optimization via High-Level Scheduling Rewrites. *Proceedings of the ACM on Programming Languages* 6, POPL, Article 55 (Jan. 2022), 28 pages. DOI: <https://doi.org/10.1145/3498717>
- Stefano Markidis, Steven Wei Der Chien, Erwin Laure, Ivy Bo Peng, and Jeffrey S. Vetter. 2018. NVIDIA Tensor Core Programmability, Performance & Precision. In *Proceedings of the IEEE International Parallel and Distributed Processing Symposium Workshops (IPDPSW '18)*. 522–531. DOI: <https://doi.org/10.1109/IPDPSW.2018.00091>
- Thomas J. McCabe. 1976. A Complexity Measure. *IEEE Transactions on Software Engineering* SE-2, 4 (1976), 308–320. DOI: <https://doi.org/10.1109/TSE.1976.233837>
- Kathryn S. McKinley, Steve Carr, and Chau-Wen Tseng. 1996. Improving Data Locality with Loop Transformations. *ACM Transactions on Programming Languages and Systems* 18, 4 (Jul. 1996), 424–453. DOI: <https://doi.org/10.1145/233561.233564>
- MDH Project. 2024. Multi-Dimensional Homomorphisms (MDH): An Algebraic Approach Toward Performance & Portability & Productivity for Data-Parallel Computations. Retrieved from <https://mdh-lang.org>
- Xinxin Mei, Kaiyong Zhao, Chengjian Liu, and Xiaowen Chu. 2014. Benchmarking the Memory Hierarchy of Modern GPUs. In *Network and Parallel Computing*. Ching-Hsien Hsu, Xuanhua Shi, and Valentina Salapura (Eds.), Springer, Berlin, 144–156.
- Benoît Meister, Eric Papenhausen Akai Kaeru, and Benoît Pradelle Silexica. 2019. Polyhedral Tensor Schedulers. In *Proceedings of the International Conference on High Performance Computing & Simulation (HPCS '19)*. 504–512. DOI: <https://doi.org/10.1109/HPCS48598.2019.9188233>
- Massinissa Merouani, Khaled Afif Boudaoud, Iheb Nassim Aouadj, Nassim Tchoulak, Islem Kara Bernou, Hamza Benyamina, Fatima Benbouzid-Si Tayeb, Karima Benatchba, Hugh Leather, and Riyadh Baghdadi. 2024. LOOPer: A Learned Automatic Code Optimizer For Polyhedral Compilers. arXiv:2403.11522.
- Michael Kruse. 2022. Polyhedral Parallel Code Generation. Retrieved from <https://github.com/Meinersbur/ppcg>, commit = 8a74e46, date = 19.11.2020
- Ravi Teja Mullapudi, Andrew Adams, Dillon Sharlet, Jonathan Ragan-Kelley, and Kayvon Fatahalian. 2016. Automatically Scheduling Halide Image Processing Pipelines. *ACM Transactions on Graphics* 35, 4, Article 83 (Jul. 2016), 11 pages. DOI: <https://doi.org/10.1145/2897824.2925952>
- Stefan K. Muller and Jan Hoffmann. 2021. Modeling and Analyzing Evaluation Cost of CUDA Kernels. *Proceedings of the ACM on Programming Languages* 5, POPL, Article 25 (Jan. 2021), 31 pages. DOI: <https://doi.org/10.1145/3434306>
- NVIDIA. 2017. Programming Tensor Cores in CUDA 9. Retrieved from <https://developer.nvidia.com/blog/programming-tensor-cores-cuda-9/>
- NVIDIA. 2018. Warp-Level Primitives. Retrieved from <https://developer.nvidia.com/blog/using-cuda-warp-level-primitives/>
- NVIDIA. 2022a. CUB. Retrieved from <https://docs.nvidia.com/cuda/cub/>
- NVIDIA. 2022b. cuBLAS. Retrieved from <https://developer.nvidia.com/cublas>
- NVIDIA. 2022c. cuBLAS – BLAS-like Extension. Retrieved from <https://docs.nvidia.com/cuda/cublas/index.html#blas-like-extension>



- NVIDIA. 2022d. cuBLAS – Using the cuBLASLt API. Retrieved from <https://docs.nvidia.com/cuda/cublas/index.html#using-the-cublaslt-api>
- NVIDIA. 2022e. CUDA Deep Neural Network library. Retrieved from <https://developer.nvidia.com/cudnn>
- NVIDIA. 2022f. CUDA Programming Guide. Retrieved from <https://docs.nvidia.com/cuda/cuda-c-programming-guide/>
- NVIDIA. 2022g. CUDA Toolkit Documentation. Retrieved from <https://docs.nvidia.com/cuda/>
- NVIDIA. 2022h. NVRTC. Retrieved from <https://docs.nvidia.com/cuda/nvrtc>
- NVIDIA. 2022i. Parallel Thread Execution ISA. Retrieved from <https://docs.nvidia.com/cuda/parallel-thread-execution>
- OctoML. 2022. Accelerated Machine Learning Deployment. Retrieved from <https://octoml.ai>
- Geraldo F. Oliveira, Juan Gómez-Luna, Lois Orosa, Saugata Ghose, Nandita Vijaykumar, Ivan Fernandez, Mohammad Sadrosadati, and Onur Mutlu. 2021. DAMOV: A New Methodology and Benchmark Suite for Evaluating Data Movement Bottlenecks. *IEEE Access* 9 (2021), 134457–134502. DOI: <https://doi.org/10.1109/ACCESS.2021.3110993>
- OpenMP. 2022. The OpenMP API Specification for Parallel Programming. Retrieved from <https://www.openmp.org>
- Adam Paszke, Sam Gross, Francisco Massa, Adam Lerer, James Bradbury, Gregory Chanan, Trevor Killeen, Zeming Lin, Natalia Gimelshein, Luca Antiga, Alban Desmaison, Andreas Kopf, Edward Yang, Zachary DeVito, Martin Raison, Alykhan Tejani, Sasank Chilamkurthy, Benoit Steiner, Lu Fang, Junjie Bai, and Soumith Chintala. 2019. PyTorch: An Imperative Style, High-Performance Deep Learning Library. In *Proceedings of the Advances in Neural Information Processing Systems*. Hanna Wallach, Hanna Larochelle, Hanna Beygelzimer, Hanna d’Alché-Buc, Emily Fox, and Emily Garnett (Eds.), Vol. 32. Curran Associates, Inc. Retrieved from <https://proceedings.neurips.cc/paper/2019/file/bdbca288fee7f92f2bfa9f7012727740-Paper.pdf>
- Adam Paszke, Daniel D. Johnson, David Duvenaud, Dimitrios Vytiniotis, Alexey Radul, Matthew J. Johnson, Jonathan Ragan-Kelley, and Dougal Maclaurin. 2021. Getting to the Point: Index Sets and Parallelism-Preserving Autodiff for Pointful Array Programming. *Proceedings of the ACM on Programming Languages* 5, ICFP, Article 88 (Aug. 2021), 29 pages. DOI: <https://doi.org/10.1145/3473593>
- Simon J. Pennycook, Jason D. Sewall, and Victor W. W. Lee. 2019. Implications of a Metric for Performance Portability. *Future Generation Computer Systems* 92 (2019), 947–958. DOI: <https://doi.org/10.1016/j.future.2017.08.007>
- Phitchaya Mangpo Phothilimthana, Archibald Samuel Elliott, An Wang, Abhinav Jangda, Bastian Hagedorn, Henrik Barthels, Samuel J. Kaufman, Vinod Grover, Emina Torlak, and Rastislav Bodik. 2019. Swizzle Inventor: Data Movement Synthesis for GPU Kernels. In *Proceedings of the 24th International Conference on Architectural Support for Programming Languages and Operating Systems (ASPLOS ’19)*. ACM, New York, NY, 65–78. DOI: <https://doi.org/10.1145/3297858.3304059>
- Federico Pizzuti, Michel Steuwer, and Christophe Dubach. 2020. Generating Fast Sparse Matrix Vector Multiplication from a High Level Generic Functional IR. In *Proceedings of the 29th International Conference on Compiler Construction (CC ’20)*. ACM, New York, NY, 85–95. DOI: <https://doi.org/10.1145/3377555.3377896>
- Victor Podlozhnyuk. 2007. Image Convolution with CUDA. In *NVIDIA Corporation White Paper*.
- Markus Puschel, José M. F. Moura, Jeremy R. Johnson, David Padua, Manuela M. Veloso, Bryan W. Singer, Jianxin Xiong, Franz Franchetti, Aca Gacic, Yevgen Voronenko, Kang Chen, Robert W. Johnson, and Nicholas Rizzolo. 2005. SPIRAL: Code Generation for DSP Transforms. *Proceedings of the IEEE* 93, 2 (2005), 232–275. DOI: <https://doi.org/10.1109/JPROC.2004.840306>
- Jonathan Ragan-Kelley, Connelly Barnes, Andrew Adams, Sylvain Paris, Frédo Durand, and Saman Amarasinghe. 2013. Halide: A Language and Compiler for Optimizing Parallelism, Locality, and Recomputation in Image Processing Pipelines. In *Proceedings of the 34th ACM SIGPLAN Conference on Programming Language Design and Implementation (PLDI ’13)*. ACM, New York, NY, 519–530. DOI: <https://doi.org/10.1145/2491956.2462176>
- Ari Rasch. 2024. Full Version: (De/Re)-Composition of Data-Parallel Computations via Multi-Dimensional Homomorphisms. arXiv:2405.05118.
- Ari Rasch, Julian Bigge, Martin Wrodczyk, Richard Schulze, and Sergei Gorlatch. 2020a. dOCAL: High-Level Distributed Programming with OpenCL and CUDA. *The Journal of Supercomputing* 76, 7 (2020), 5117–5138. DOI: <https://doi.org/10.1007/s11227-019-02829-2>
- Ari Rasch and Sergei Gorlatch. 2016. Multi-Dimensional Homomorphisms and Their Implementation in OpenCL. In *Proceedings of the International Workshop on High-Level Parallel Programming and Applications (HLPP)*. 101–119.
- Ari Rasch, Richard Schulze, and Sergei Gorlatch. 2019a. Generating Portable High-Performance Code via Multi-Dimensional Homomorphisms. In *Proceedings of the 28th International Conference on Parallel Architectures and Compilation Techniques (PACT ’19)*. 354–369. DOI: <https://doi.org/10.1109/PACT.2019.00035>
- Ari Rasch, Richard Schulze, and Sergei Gorlatch. 2020b. md\_poly: A Performance-Portable Polyhedral Compiler Based on Multi-Dimensional Homomorphisms. In *Proceedings of the International Workshop on Polyhedral Compilation Techniques (IMPACT 20)*. 1–4.
- Ari Rasch, Richard Schulze, and Sergei Gorlatch. 2020c. md\_poly: A Performance-Portable Polyhedral Compiler based on Multi-Dimensional Homomorphisms. In *Proceedings of the ACM SRC Grand Finals Candidates*, 2019–2020. 1–5.

- Ari Rasch, Richard Schulze, Waldemar Gorus, Jan Hiller, Sebastian Bartholomäus, and Sergei Gorlatch. 2019b. High-Performance Probabilistic Record Linkage via Multi-Dimensional Homomorphisms. In *Proceedings of the 34th ACM/SI-GAPP Symposium on Applied Computing (SAC '19)*. ACM, New York, NY, 526–533. DOI: <https://doi.org/10.1145/3297280.3297330>
- Ari Rasch, Richard Schulze, Denys Shabalin, Anne Elster, Sergei Gorlatch, and Mary Hall. 2023. (De/Re)-Compositions Expressed Systematically via MDH-Based Schedules. In *Proceedings of the 32nd ACM SIGPLAN International Conference on Compiler Construction (CC '23)*. ACM, New York, NY, 61–72. DOI: <https://doi.org/10.1145/3578360.3580269>
- Ari Rasch, Richard Schulze, Michel Steuwer, and Sergei Gorlatch. 2021. Efficient Auto-Tuning of Parallel Programs with Interdependent Tuning Parameters via Auto-Tuning Framework (ATF). *ACM Transactions on Architecture and Code Optimization* 18, 1, Article 1 (Jan. 2021), 26 pages. DOI: <https://doi.org/10.1145/3427093>
- Ari Rasch, Martin Wrodarczyk, Richard Schulze, and Sergei Gorlatch. 2018. OCAL: An Abstraction for Host-Code Programming with OpenCL and CUDA. In *Proceedings of the IEEE 24th International Conference on Parallel and Distributed Systems (ICPADS '18)*. 408–416. DOI: <https://doi.org/10.1109/PADSW.2018.8644541>
- Chandan Reddy, Michael Kruse, and Albert Cohen. 2016. Reduction Drawing: Language Constructs and Polyhedral Compilation for Reductions on GPU. In *Proceedings of the 2016 International Conference on Parallel Architectures and Compilation (PACT '16)*. ACM, New York, NY, 87–97. DOI: <https://doi.org/10.1145/2967938.2967950>
- Toomas Rimmelg, Thibaut Lutz, Michel Steuwer, and Christophe Dubach. 2016. Performance Portable GPU Code Generation for Matrix Multiplication. In *Proceedings of the 9th Annual Workshop on General Purpose Processing Using Graphics Processing Unit (GPGPU '16)*. ACM, New York, NY, 22–31. DOI: <https://doi.org/10.1145/2884045.2884046>
- Bruce Sagan. 2001. *The Symmetric Group: Representations, Combinatorial Algorithms, and Symmetric Functions*, Vol. 203. Springer Science & Business Media.
- Caio Salvador Rohwedder, Nathan Henderson, João P. L. De Carvalho, Yufei Chen, and José Nelson Amaral. 2023. To Pack or Not to Pack: A Generalized Packing Analysis and Transformation. In *Proceedings of the 21st ACM/IEEE International Symposium on Code Generation and Optimization (CGO '23)*. ACM, New York, NY, 14–27. DOI: <https://doi.org/10.1145/3579990.3580024>
- Karen Simonyan and Andrew Zisserman. 2014. Very Deep Convolutional Networks for Large-Scale Image Recognition. arXiv:1409.1556. DOI: <https://doi.org/10.48550/ARXIV.1409.1556>
- Paul Springer and Paolo Bientinesi. 2016. Design of a High-Performance GEMM-Like Tensor-Tensor Multiplication. Retrieved from <http://arxiv.org/abs/1607.00145>
- Michel Steuwer, Christian Fensch, Sam Lindley, and Christophe Dubach. 2015. Generating Performance Portable Code Using Rewrite Rules: From High-Level Functional Expressions to High-Performance OpenCL Code. In *Proceedings of the 20th ACM SIGPLAN International Conference on Functional Programming (ICFP '15)*. ACM, New York, NY, 205–217. DOI: <https://doi.org/10.1145/2784731.2784754>
- Michel Steuwer, Philipp Kegel, and Sergei Gorlatch. 2011. SkelCL - A Portable Skeleton Library for High-Level GPU Programming. In *Proceedings of the 2011 IEEE International Symposium on Parallel and Distributed Processing Workshops and Phd Forum*. 1176–1182. DOI: <https://doi.org/10.1109/IPDPS.2011.269>
- Michel Steuwer, Thomas Koehler, Bastian Köpcke, and Federico Pizzuti. 2022. RISE & Shine: Language-Oriented Compiler Design. arXiv:2201.03611. Retrieved from <https://arxiv.org/abs/2201.03611>
- Michel Steuwer, Toomas Rimmelg, and Christophe Dubach. 2017. LIFT: A Functional Data-Parallel IR For High-Performance GPU Code Generation. In *Proceedings of the IEEE/ACM International Symposium on Code Generation and Optimization (CGO '17)*. 74–85. DOI: <https://doi.org/10.1109/CGO.2017.7863730>
- StreamHPC. 2016. Comparing Syntax for CUDA, OpenCL and HiP. Retrieved from <https://streamhpc.com/blog/2016-04-05/comparing-syntax-cuda-opencl-hip/>
- Yifan Sun, Nicolas Bohm Agostini, Shi Dong, and David R. Kaeli. 2019. Summarizing CPU and GPU Design Trends with Product Data. arXiv:1911.11313. Retrieved from <http://arxiv.org/abs/1911.11313>
- Adilla Susungi, Norman A. Rink, Albert Cohen, Jeronimo Castrillon, and Claude Tadonki. 2020. Meta-Programming for Cross-Domain Tensor Optimizations. *ACM SIGPLAN Notices* 53, 9 (Apr. 2020), 79–92. DOI: <https://doi.org/10.1145/3393934.3278131>
- Joel Svensson, Mary Sheeran, and Koen Claessen. 2011. Obsidian: A Domain Specific Embedded Language for Parallel Programming of Graphics Processors. In *Implementation and Application of Functional Languages*. Sven-Bodo Scholz and Olaf Chitil (Eds.), Springer, Berlin, 156–173.
- TensorFlow. 2022a. MobileNet v1 Models for Keras. Retrieved from <https://github.com/keras-team/keras/blob/master/keras/applications/mobilenet.py>
- TensorFlow. 2022b. ResNet Models for Keras. Retrieved from <https://github.com/keras-team/keras/blob/master/keras/applications/resnet.py>
- TensorFlow. 2022c. VGG16 Model for Keras. Retrieved from <https://github.com/keras-team/keras/blob/master/keras/applications/vgg16.py>

- Philippe Tillet and David Cox. 2017. Input-Aware Auto-Tuning of Compute-Bound HPC Kernels. In *Proceedings of the International Conference for High Performance Computing, Networking, Storage and Analysis (SC '17)*. ACM, New York, NY, Article 43, 12 pages. DOI: <https://doi.org/10.1145/3126908.3126939>
- Philippe Tillet, H. T. Kung, and David Cox. 2019. Triton: An intermediate language and compiler for tiled neural network computations. In *Proceedings of the 3rd ACM SIGPLAN International Workshop on Machine Learning and Programming Languages (MAPL '19)*. ACM, New York, NY, 10–19. DOI: <https://doi.org/10.1145/3315508.3329973>
- Uday Bondhugula. 2022. Pluto: An Automatic Polyhedral Parallelizer and Locality Optimizer. Retrieved from <https://github.com/bondhugula/pluto>, commit = 12e075a, date = 31.10.2021.
- Nicolas Vasilache, Oleksandr Zinenko, Aart J. C. Bik, Mahesh Ravishankar, Thomas Raoux, Alexander Belyaev, Matthias Springer, Tobias Gysi, Diego Caballero, Stephan Herhut, Stella Laurenzo, and Albert Cohen. 2022. Composable and Modular Code Generation in MLIR: A Structured and Retargetable Approach to Tensor Compiler Construction. arXiv:2202.03293.
- Nicolas Vasilache, Oleksandr Zinenko, Theodoros Theodoridis, Priya Goyal, Zachary Devito, William S. Moses, Sven Verdoolaege, Andrew Adams, and Albert Cohen. 2019. The Next 700 Accelerated Layers: From Mathematical Expressions of Network Computation Graphs to Accelerated GPU Kernels, Automatically. *ACM Transactions on Architecture and Code Optimization* 16, 4, Article 38 (Oct. 2019), 26 pages. DOI: <https://doi.org/10.1145/3355606>
- Sven Verdoolaege, Juan Carlos Juega, Albert Cohen, José Ignacio Gómez, Christian Tenllado, and Francky Catthoor. 2013. Polyhedral Parallel Code Generation for CUDA. *ACM Transactions on Architecture and Code Optimization* 9, 4, Article 54 (Jan. 2013), 23 pages. DOI: <https://doi.org/10.1145/2400682.2400713>
- Sven Verdoolaege and Tobias Grosser. 2012. Polyhedral Extraction Tool. In *Proceedings of the International Workshop on Polyhedral Compilation Techniques (IMPACT '12)*, Vol. 141.
- Mohamed Wahib and Naoya Maruyama. 2014. Scalable Kernel Fusion for Memory-Bound GPU Applications. In *SC '14: Proceedings of the International Conference for High Performance Computing, Networking, Storage and Analysis*. 191–202. DOI: <https://doi.org/10.1109/SC.2014.21>
- Bram Wasti, José Pablo Cambroner, Benoit Steiner, Hugh Leather, and Aleksandar Zlateski. 2022. LoopStack: A Lightweight Tensor Algebra Compiler Stack. arXiv:2205.00618v1. Retrieved from <https://doi.org/10.48550/ARXIV.2205.00618>
- R. Clinton Whaley and Jack J. Dongarra. 1998. Automatically Tuned Linear Algebra Software. In *SC '98: Proceedings of the 1998 ACM/IEEE Conference on Supercomputing*. 38–38. DOI: <https://doi.org/10.1109/SC.1998.10004>
- Maurice V. Wilkes. 2001. The Memory Gap and the Future of High Performance Memories. *ACM SIGARCH Computer Architecture News* 29, 1 (2001), 2–7.
- Michael E. Wolf and Monica S. Lam. 1991. A Loop Transformation Theory and an Algorithm to Maximize Parallelism. *IEEE Transactions on Parallel and Distributed Systems* 2, 4 (1991), 452–471. DOI: <https://doi.org/10.1109/71.97902>
- Rohan Yadav, Alex Aiken, and Fredrik Kjolstad. 2022. DISTAL: The Distributed Tensor Algebra Compiler. In *Proceedings of the 43rd ACM SIGPLAN International Conference on Programming Language Design and Implementation (PLDI '22)*. ACM, New York, NY, 286–300. DOI: <https://doi.org/10.1145/3519939.3523437>
- Cambridge Yang, Eric Atkinson, and Michael Carbin. 2021. Simplifying Dependent Reductions in the Polyhedral Model. *Proceedings of the ACM on Programming Languages* 5, POPL, Article 20 (Jan. 2021), 33 pages. DOI: <https://doi.org/10.1145/3434301>
- Lianmin Zheng, Chengfan Jia, Minmin Sun, Zhao Wu, Cody Hao Yu, Ameer Haj-Ali, Yida Wang, Jun Yang, Danyang Zhuo, Koushik Sen, Joseph E. Gonzalez, and Ion Stoica. 2020a. Ansor: Generating High-Performance Tensor Programs for Deep Learning. In *Proceedings of the 14th USENIX Symposium on Operating Systems Design and Implementation (OSDI '20)*. USENIX Association, 863–879. Retrieved from <https://www.usenix.org/conference/osdi20/presentation/zheng>
- Size Zheng, Renze Chen, Anjiang Wei, Yicheng Jin, Qin Han, Liqiang Lu, Bingyang Wu, Xiuhong Li, Shengen Yan, and Yun Liang. 2022. AMOS: Enabling Automatic Mapping for Tensor Computations on Spatial Accelerators with Hardware Abstraction. In *Proceedings of the 49th Annual International Symposium on Computer Architecture (ISCA '22)*. ACM, New York, NY, 874–887. DOI: <https://doi.org/10.1145/3470496.3527440>
- Size Zheng, Yun Liang, Shuo Wang, Renze Chen, and Kaiwen Sheng. 2020b. FlexTensor: An Automatic Schedule Exploration and Optimization Framework for Tensor Computation on Heterogeneous System. In *Proceedings of the 25th International Conference on Architectural Support for Programming Languages and Operating Systems*. ACM, New York, NY, 859–873. DOI: <https://doi.org/10.1145/3373376.3378508>

Received 17 October 2023; revised 21 February 2024; accepted 16 April 2024